GEOCHEMICAL DISPERSION AT THE MOUNT TORRENS LEAD-ZINC PROSPECT, SOUTH AUSTRALIA, WITH PARTICULAR EMPHASIS ON ACID SULFATE SOILS

M.S. Skwarnecki, R.W. Fitzpatrick and P.J. Davies

CRC LEME REPORT 174

June 2002

Prepared for
Pima Mining NL
CSIRO Mineral Exploration & Mining Sector (Glass Earth – Advanced regolith geochemical technologies)

CRC LEME is an unincorporated joint venture between The Australian National University, Curtin University of Technology, Adelaide University, University of Canberra, Geoscience Australia, CSIRO Exploration & Mining, CSIRO Land & Water, Bureau Of Rural Sciences, Minerals Council Of Australia, Primary Industry & Resources South Australia, and New South Wales Department of Mineral Resources, Geological Survey. Headquarters:- CRC LEME c/o CSIRO Exploration and Mining, P.O. Box 1130, Bentley, Western Australia, 6102.

Addresses and affiliations of authors

M.S. Skwarnecki
Cooperative Research Centre for Landscape
Environments and Mineral Exploration
c/- CSIRO Land & Water
Private Mail Bag 2,
Glen Osmond 5064
South Australia

R.W. Fitzpatrick
Cooperative Research Centre for Landscape
Environments and Mineral Exploration
c/- CSIRO Land & Water
Private Mail Bag 2,
Glen Osmond 5064
South Australia

P.J. Davies
Cooperative Research Centre for Landscape
Environments and Mineral Exploration
c/- CSIRO Land & Water
Private Mail Bag 2,
Glen Osmond 5064
South Australia

PREFACE

The accumulation and oxidation of iron- and sulfur-rich precipitates in acid sulfate soils from rising ground and surface waters (bearing sulfate and Fe^{2+} ions) in the Mt Lofty Ranges are causing less permeable soil layers to form in saline discharge areas. From an exploration viewpoint, the evolution of such conditions carries indications of the presence of blind or concealed ore deposits. The geochemistry and mineralogy of the iron oxide and oxyhydroxysulphate precipitates forming in the saline sulfidic soils indicates that they commonly have anomalous levels of indicator elements, for which, the iron oxides have a high sorptive capacity. The saline scalds with associated acid sulfate soils containing iron precipitates, sulfidic materials and mottled sulfuric horizons provide a geochemical sampling medium for the detection of mineral or ore deposits.

This orientation study examines geochemical dispersion at the Mount Torrens prospect in regolith, including gossans, saprolite, pedogenic materials associated with acid sulfate soils containing sulfuric horizons and sulfidic materials, and Fe- and Al-rich precipitates in saline seeps. The results indicate that concentrations of As, Ba, Bi, Cd, Cu, P, Pb, Sn, Tl and Zn are greatest in those acid sulfate soils proximal to the mineralised zone, and therefore, that acid sulfate soils and their associated pedogenic materials are a valid geochemical sampling medium for mineral exploration.

CONTENTS

LIST OF FIGURES

LIST OF TABLES

LIST OF APPENDICES

ABSTRACT

At the Mount Torrens prospect, minor Pb-Zn-Ag mineralisation in calc-silicate rocks occurs at the base of the Talisker Calc-siltstone. The sulfides (typically pyrite, galena and sphalerite) vary from disseminated (barren) to massive (mineralised) pods comprising 50-70% pyrite, 10-25% galena, and 5-10% sphalerite. Reverse circulation and diamond drilling by CRAE Pty Ltd outlined an inferred resource of 0.7 Mt ore at 6.4% Pb, 1.6% Zn and 41 ppm Ag.

The Talisker Calc-siltstone (including the Nairne Pyrite Member) is underlain by sandstones of the Backstairs Passage Formation and overlain by metasedimentary units of the Tapanappa Formation. The Tapanappa sequences have weathered to produce ferruginous saprolite, which forms low rolling hills in the central part of the area investigated. Weathering of the sulfides has produced gossans, characterised by the occurrence of goethite, hematite, kaolinite, cerussite, barite, jarosite, plumbogummite, plumbojarosite, gorceixite, iodargyrite and native gold.

In fresh rock, the mineralised zones are anomalous in Pb, Zn, Ag, Ca, Mn, Na, As, Cd, In, Mo, Sb, Te and Tl, but are relatively depleted in Ti, REE, V and Zr. Compared to the gossans, fresh sulfides contain more Ca, Mn, Cd, S and Zn (which are strongly leached during weathering), and less Cu, Se, U and W. Ferruginous saprolite along the mineralised zone generally has greater concentrations of As, Cu, Mo, Pb and Tl than that lateral to the mineralised horizon.

Acid sulfate soils in seeps have developed in rising saline groundwater tables and are expanding in response to land clearing. Potential acid sulfate soils (PASS) consist of black sulfidic materials (pyritic, waterlogged mud) and are stable under reducing conditions. However, when they are exposed to air by drainage, they become strongly acidic (pH<4), liberating sulfuric acid, and are termed actual acid sulfate soils (ASS) with sulfuric horizons. The acidic solutions dissolve clay minerals and oxidise Fe sulfides to produce white (hydrated Al oxyhydroxide) and brownish orange Fe oxide (ferrihydrite, goethite and schwertmannite) precipitates, which have high sorptive capacities for trace elements (e.g., As). Bright yellow mottles with plumbojarosite have been recorded in acid sulfate soils where these overlie mineralisation. These seep materials, together with the gossans, ferruginous saprolite and saprolite, were studied to determine whether they have potential as mineral exploration sampling media for base-metal mineralisation.

The Fe- and Al-rich precipitates (gels) locally contain significant concentrations of As, Ba, Cd, P, Pb, Sn and Zn. Black sulfidic materials locally contain anomalous As, Ba, Bi, Cd, Cu, P, Pb, Sn, Tl and Zn, but it is possible that some of these elements may have accumulated through mechanical dispersion from the gossans. These sulfidic materials and associated iron oxide precipitates thus are a geochemical sampling medium for the detection of mineral deposits, particularly where mineralisation is blind.

The black sulfidic materials contain secondary framboidal pyrite. Bright yellow mottles containing plumbojarosite ($PbFe_6(SO_4)_4(OH)_{12}$) and plumbogummite ($PbAl_3(PO_4)_2(OH)_5.H_2O$) occur in the sulfuric horizons, which have developed from the oxidation of the black sulfidic materials. These minerals are absent in similar materials lateral to the mineralised zone. Plumbojarosite and plumbogummite are associated with goethite, jarosite, quartz, clays, mica and detrital monazite.

Sulfuric horizons with secondary Pb minerals are characterised by greater Bi, Cd, Cu, In, Mo, Pb, Tl and Zn concentrations than those lateral to the mineralised zone and reflect the dispersion halo around it. At the prospect scale, a geochemical dispersion halo up to 750 m in width occurs around the mineralisation and is defined by anomalous concentrations of As, Ba, Bi, Cd, Cu, P, Pb, Sn, Tl and Zn in Fe oxide gels and black sulfidic materials.

A mechanistic model, developed to explain the formation of these sulfidic materials, involves saline groundwaters enriched in sulfate (with elements such as Pb and Zn sourced from the mineralised zone) seeping up through soils, concentrating by evaporation and forming various precipitates. The

combination of rising saline sulfate-rich groundwaters, anaerobic conditions associated with saturated soils and organic carbon in soils yielded pyrite-enriched or sulfidic material through anaerobic bacterial reduction of sulfate. Weak and/or incipient oxidation of the sulfidic materials has produced minerals such as jarosite and plumbojarosite in sulfuric horizons overlying mineralisation.

These sulfidic materials, sulfuric horizons and surface Fe-rich precipitates constitute a new sampling medium for mineral exploration and provide broader dispersion haloes around mineralisation than conventional sample types. In addition, sulfidic materials and sulfuric horizons in seeps may be used to locate blind mineralisation in areas of cover.

1. INTRODUCTION

Acid sulfate soils in saline seeps have developed in the Mount Lofty Ranges as a response to land clearing and rising water tables. The seeps form unsightly discharge areas, with eroded “iron ochre scalds” and swampy saline sulfidic soils, which continue to creep up slopes in high rainfall (>500mm) catchments. Recent investigations have found that accumulation and oxidation of iron and sulfur in seasonally rising ground and surface water are causing less permeable soil layers to form in discharge areas. Preliminary data on the composition of the iron oxide precipitates forming in the saline sulfidic soils indicates that they commonly have elevated levels of indicator elements, for which the iron oxides have a high sorptive capacity. These scalds and associated iron oxide precipitates thus have potential as a geochemical sampling medium for the detection of mineral deposits. Consequently, this information has potential to be used to assist in understanding the underlying regolith and develop new tools for mineral exploration. In particular, they have potential to give, or at least enhance, surface expressions of otherwise buried and blind deposits.

In these catchments, the saline groundwater, enriched in sulfate (SO_4^{2-}) and ions such as Na^+, Mg^{2+}, AsO_4^{3-}, I^- and Cl^-, can seep up through the soil and concentrate by evaporation, forming various mineral precipitates within and on top of the soil. The combination of rising sulfate-rich groundwater tables, waterlogging, agricultural activity and fractured lithologies rich in Fe and S can lead to the formation of saline soils with potential and actual acid sulfate (ASS) soil conditions (Fitzpatrick et al., 1996, 2000). If the soil is waterlogged, anaerobic bacteria use the sulfate to promote the degradation of organic matter. This process produces pyrite (FeS_2) and forms "sulfidic materials". The pyrite-enriched soils are termed 'potential' acid sulfate soils (PASS) because they have all the ingredients necessary to produce ASS. ASS result when cattle, drainage works or other disruptions expose the waterlogged soils, and the pyrite within, to air. When this happens, pyrite is oxidised to sulfuric acid and various iron sulfate-rich minerals, and "actual" ASS forms. When sulfuric acid forms, the soil pH can drop from neutral (pH 7) to below 4, with values as low as 2, to form a "sulfuric horizon". The sulfuric acid dissolves the soil, causing ions (e.g., Na^+, Mg^{2+}, Ca^{2+}, Ba^{2+}, Cl^-, SO_4^{2-}, SiO_4^{4-}) to be mobilised on the soil surface and in stream waters.

This orientation study at the Mount Torrens Pb-Zn prospect is part of a larger national project whose principal objective is to determine whether saline acid sulfate seeps and soils can be used as exploration sampling media. This project is to address this objective by establishing the type of information (geochemical dispersion patterns and processes) needed to develop regolith-landform based models from the Herrmanns and Dairy Creek catchments in the Mount Lofty Ranges, South Australia, by:

- quantifying the chemical and mineralogical composition of saline acid sulfate seepages within a key area to determine whether they have characteristics that can be related to the nearby presence of base metal mineralisation;
- developing more accurate process models for developing local (catchment) and regional guidelines for geochemical mineral exploration models;
- ultimately, applying this knowledge to geochemical exploration for massive sulfide deposits in the Kanmantoo Trough.

1.1 Location, landscape, climate and land use

The Mt Torrens prospect is situated at 34°53’15’’S 139°00’18’’E, about 45 km east of Adelaide (Figure 1.1) in the eastern Mount Lofty Ranges.

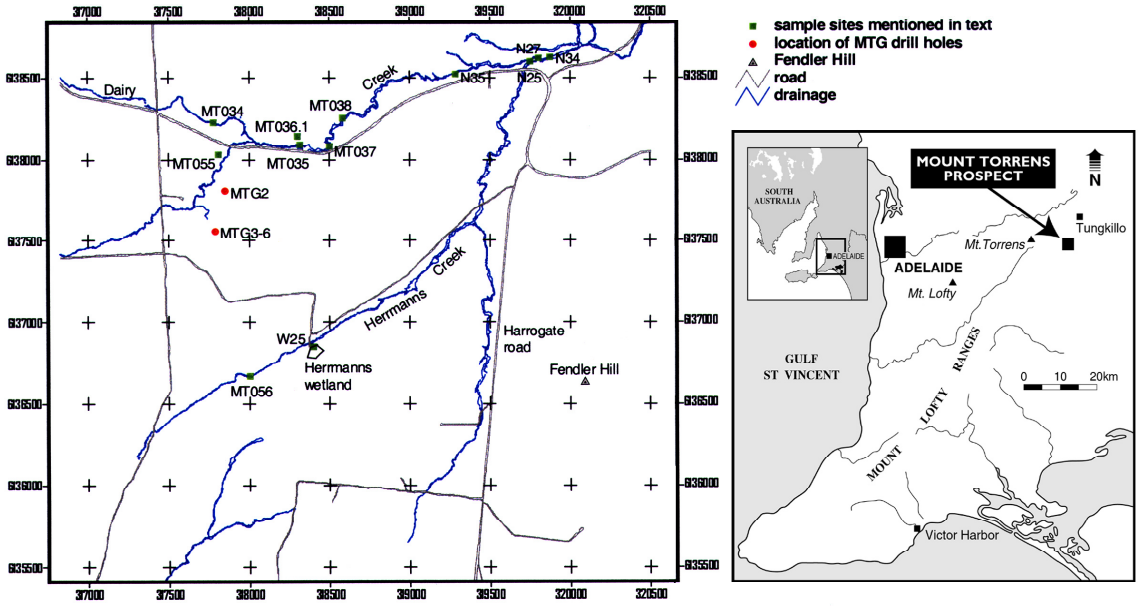

Figure 1.1. Location of the Mount Torrens prospect, South Australia, showing localities and sample sites mentioned in the text.

The landscape is undulating low hills with altitudes between 400 to 500m and local relief of about 30 to 50m. The climate of the area is Mediterranean, with a pronounced maximum of rainfall in winter (May to August) and hot, dry summers (December to February). Annual rainfall is topographically controlled, with a mean average annual rainfall of 680 mm. The land cover of the area is predominantly pasture, most native tree vegetation having been cleared by the end of the 19th century. The remaining areas of remnant vegetation are associated mainly with topographic high points, roadways and watercourses. Land use is predominantly pastures grazed by sheep or cattle. Increasingly, land is being used for more intensive purposes such as viticulture, commercial forestry and some cereal cropping. The catchments drain to the east and into the Murray River system. Stream channels have a normal tributary pattern and are mostly eroding soils, bedrock or the alluvial soils and sediments of valley floors, sometimes to depths of two to three metres.

1.2 Regional geology

The Kanmantoo Group (Figure 1.2) occurs in a fault-controlled basin that developed in the early Cambrian by extensional tectonism along the southeastern flank of the Neoproterozoic Adelaide Geosyncline, following initial stable platform carbonate sedimentation (Normanville Group). The marine clastic flyschoid sediments of the basin (together with the Neoproterozoic succession to the west) were deformed, metamorphosed and intruded by granites during the Delamerian Orogeny (middle to late Cambrian), and are now exposed in an arcuate zone over 300 km in length in the eastern and southern Mount Lofty Ranges. At least two main phases of deformation have been recognised. Metamorphism at low pressure and high temperature locally attained amphibolite facies, and appears to have coincided with a major period of granite emplacement.

The apparent thickness of the Kanmantoo Group is up to 15 km, and may consist of a stack of thrust sheets. The main rock types are sandstones, siltstones and phyllites, with intercalated pelites and minor carbonates. The lowermost sequence comprises muddy sandstone and siltstone (Carrickalinga Head Formation), which passes up into cleaner, cross-bedded, feldspathic sandstone (Backstairs Passage Formation). A disconformity separates the Backstairs Passage Formation from the overlying upper parts of the sequence, which comprises interbedded muddy sandstone and siltstone (Tapanappa and Balquhidder Formations), and dominantly fine-grained clastic rocks of the Talisker Calc-siltstone, and Tunkalilla Formation.

Most of the significant base-metal syn-sedimentary mineralisation in the Kanmantoo Group is confined to the Tapanappa Formation. It may be spatially associated with exhalites, such as garnetiferous lithologies (including BIF) and gahnite-bearing rocks, and unusual metamorphic mineral assemblages interpreted to be metamorphosed alteration zones. Sulfide mineralisation has been classified into four commodity-based categories:

(i) Cu±Au (e.g., Kanmantoo, Breadalbane, Bremer);
(ii) Pb-Zn-Ag±Au (e.g., Aclare, Wheal Ellen);
(iii) Cu-As±Au (e.g., Preamimma, Glenalbyn);
(iv) Fe (pyrite, pyrrhotite) at various stratigraphic levels (e.g., Brukunga).

The Talisker Calc-siltstone, a regionally extensive siltstone unit with minor calc-silicate, incorporates the laterally extensive Fe sulfide-rich Nairne Pyrite Member. Minor Pb-Zn-Ag mineralisation in carbonates and calc-silicates occurs at the base of this unit at the Mount Torrens prospect.

1.3 Previous mineral exploration investigations

Regional stream-sediment sampling (<180 µm fraction) by the South Australian Department of Mines and Energy (SADME) of the Mannum A 1:25 000 sheet (Sibenaler, 1975) yielded anomalous samples east of Tungkillo. Re-sampling of these stream sediments by Peter Dunn (on behalf of CRAE) and extension of stream sediment sampling to those areas not previously sampled yielded an anomalous sample with 2100 ppm Pb in Dairy Creek (English, 1977; Figure 1.3). Subsequent rock-chip sampling (27.7 % Pb) upstream of the stream-sediment anomaly led to the discovery of the gossans.

Reverse circulation and diamond drilling outlined an inferred resource of 0.7 Mt ore at 6.4% Pb, 1.6% Zn and 41 ppm Ag (Belperio et al., 1998). The mineralisation occurs at the base of the Talisker Calc-siltstone, stratigraphically below the base of the Nairne Pyrite Member. The sulfides (typically pyrite, galena and sphalerite) vary from disseminated (barren) to massive (mineralised) pods comprising 50-70% pyrite, 10-25% galena, and 5-10% sphalerite. Subsequently, the region has been explored by ESSO Minerals, Aberfoyle, and Pima Mining (since 1996).

The mineralised horizon is defined by a zone 1.5 km long and up to 100 m wide of soils anomalous in Pb (up to 1.61%; Figure 1.4), Zn (up to 1900 ppm), Cu (up to 750 ppm) and As (up to 150 ppm). Reverse circulation and diamond drilling has intersected mineralisation at depth in the area south of Dairy Creek. Soil sampling to the east of the Harrogate road (Figure 1.4) was carried out on the eastern limb of the regional syncline along the presumed repetition of the Talisker Calc-siltstone. Although no repetition of this unit was recognised from the mapping, prominent Pb-Zn soil anomalies occur. They may be related to pyritic cherts in the basal Tapanappa Formation and do not appear to have been tested by drilling.

Scott et al. (1979) investigated the mineralogy and geochemistry of the gossans as part of a broader CRAE-sponsored gossan project. Reconnaissance hydrogeochemical sampling (Giblin et al., 1994) suggested that the groundwaters were anomalous in Cu, Mo, Pb and Zn and these may have been derived from a mineralised source. At Guthries, to the northeast of the Mount Torrens prospect,

groundwaters are relatively enriched in Cu, Pb, Zn and Tl, which may have been sourced from weathering sulfides in bedrock. These conclusions are supported by the $\delta^{34}S$ (-15 - +5 per mil) and $^{206}Pb/^{204}Pb$ (~17.8) ore signatures of the groundwaters at the Mount Torrens prospect and Guthries.

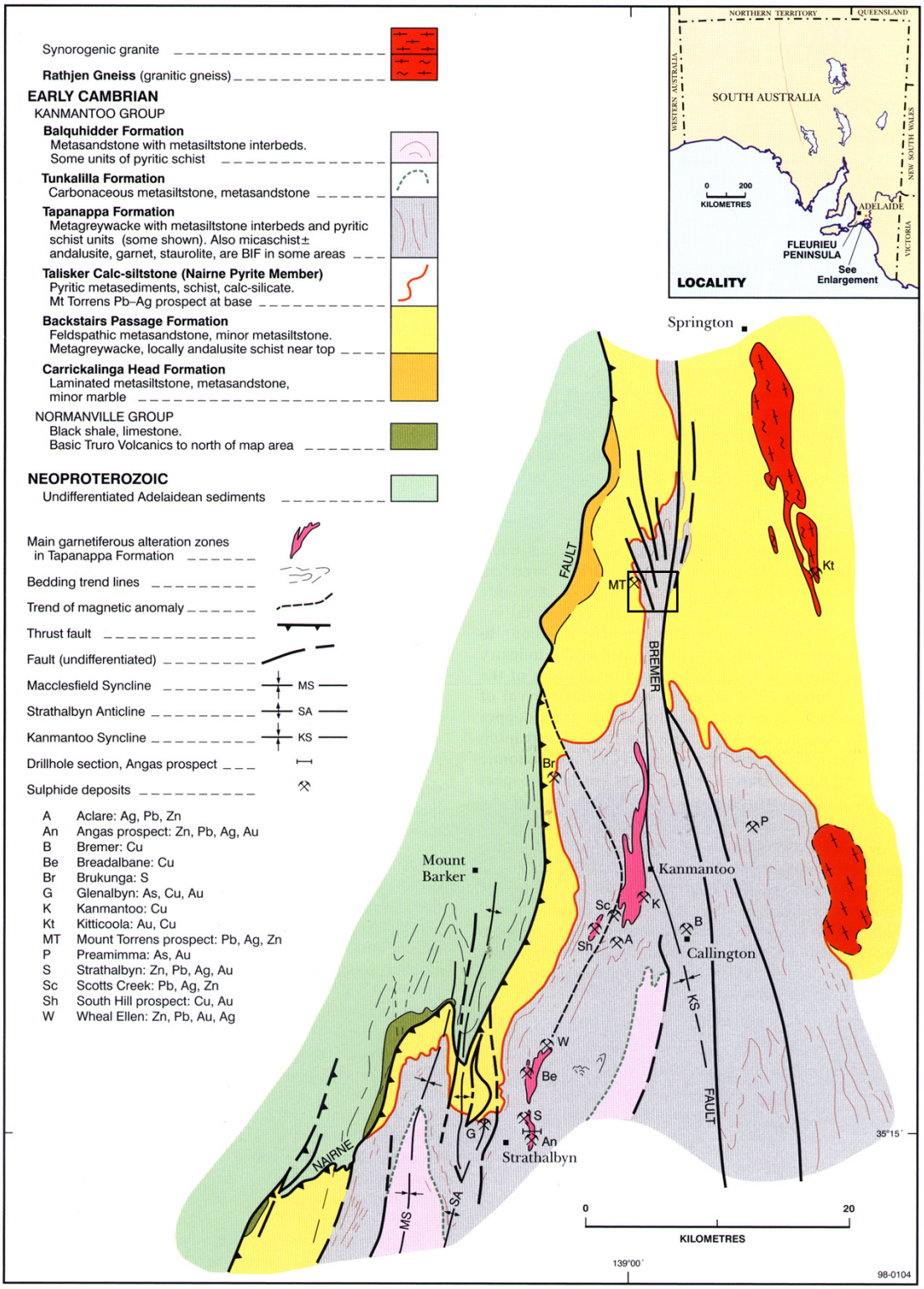

Figure 1.2. Regional geological setting of mineral deposits in the Kanmantoo Group (from Toteff, 1999). The black rectangle indicates the area of study.

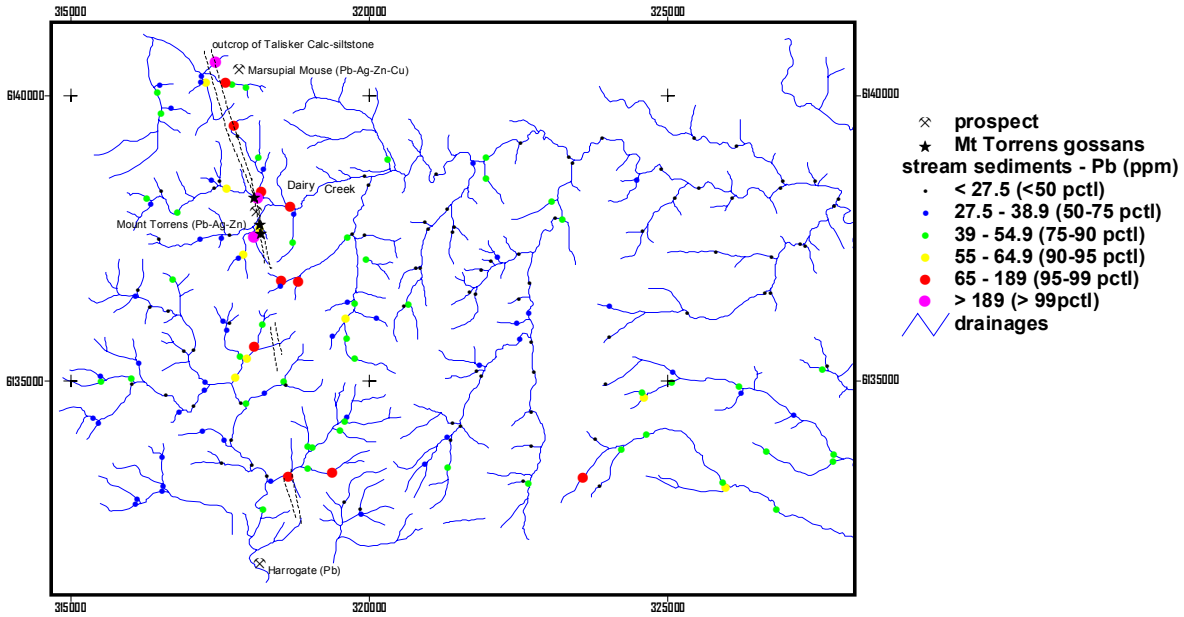

Figure 1.3. Distribution of Pb (ppm) in <180µm stream sediments, Mount Torrens area. The outcrop of the Talisker Calc-siltstone is denoted by the dotted lines. These analyses have been classified on percentile (pctl) ranges.

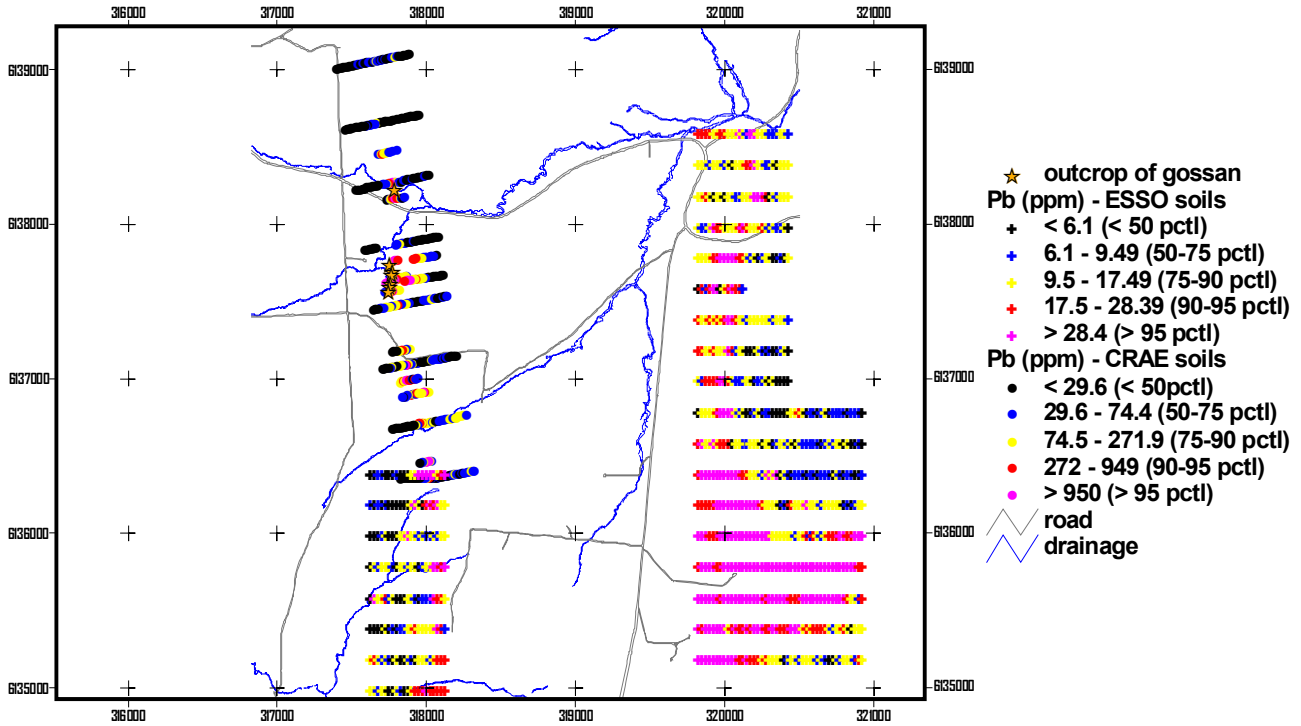

Figure 1.4. Distribution of Pb (ppm) in <180 μm soils, Mount Torrens prospect. Note that the CRAE and ESSO soils were analysed by different methods, which are not described in the open-file reports. These analyses have been classified on percentile (pctl) ranges.

1.4 Objectives and work programme

The principal objective was to determine whether pedogenic features associated with saline acid sulfate seeps and regolith have potential as exploration sampling media for base metal mineralisation. Specific objectives included:

(i) determination of the geological setting of the Mount Torrens prospect;
(ii) determination of the distribution of regolith materials and their morphological, geochemical and mineralogical properties;
(iii) development of regolith model(s) to explain formation of acid sulfate soil properties;
(iv) evaluation of the effectiveness of various regolith materials as sampling media for mineral exploration.

The prospect was mapped at 1:5000 scale in May and June, 2000. Sampling of regolith was carried out during the mapping and in September, 2000. Old CRAE Pty Ltd diamond drill core (Scott et al., 1979) was inspected and sampled in Sydney in late May 2001.

2. STUDY METHODS

2.1 Mapping

Geological and regolith mapping was carried out using an aerial photograph enlarged to nominal 1:5000 scale. All polygons were transferred onto an orthophotographic base and the resultant map was scanned by AGSO. The various layers were separated and compiled within ArcInfo, and exported to ArcView. The maps are shown in Appendices 1 and 2.

2.2 Sample collection

Three hundred and eighteen samples were collected from outcrops, creek sections, augered holes and diamond drill core:

(i) 56 samples of **ferruginous saprolite** from outcrops and diamond drill core;
(ii) 4 samples of **ferricrete** from outcrops;
(iii) 69 samples of **saprolite** from creek sections and diamond drill core;
(iv) 10 samples of **gossan** from outcrop and diamond drill core;
(v) 8 samples of **gossanous siltstone** from diamond drill core;
(vi) 13 samples of **fresh siltstone** (Nairne Pyrite Member) from diamond drill core;
(vii) 3 samples of fresh **sulfide-rich rock** from mineralised zones in diamond drill core;
(viii) 20 samples of **black sulfidic material** from creek sections and shallow pits, including 4 samples of admixtures of sulfidic mud and gravel;
(ix) 9 samples of **Fe- and Al-oxide precipitates (gels)**, mainly from creek sections;
(x) 9 samples of **layered crusts** from shallow pits;
(xi) 35 samples of **clay** from augered holes and creek sections;
(xii) 17 samples samples of **black (carbonaceous) mud** from creek sections;
(xiii) 24 samples of **sand** (11) and **alluvium** (13) from creek sections;
(xiv) 27 samples of **loam** (21), **loam/sand** (5), and **loam/clay** (2) from augered holes and stream sections;
(xv) 13 miscellaneous samples, comprising **soil** (4), **gravel** (7) and **carbonate** (2), from creek sections.

2.3 Sample preparation

In the laboratory, a 250g aliquot of sample was crushed in a jaw crusher (rock-chip samples only). Samples were oven-dried and about 100 g was milled in a Cr-free disc mill to a nominal 90% passing through 106 μm.

2.4 Analysis

The milled aliquots were analysed by atomic absorption spectrophotometry (AAS), inductively coupled plasma optical emission spectrometry (ICP-OES) and inductively coupled plasma spectrometry (ICP-MS) by AMDEL in Adelaide. The digestions, methods and respective element suites were:

(i) Au – aqua regia digest (a mixture of nitric and hydrochloric acids) of sample (up to 50 g), extraction into di-isobutyl ketone (DIBK), and analysis on a graphite furnace AAS;
(ii) ICP-OES suite (Al, Ba, Ca, Cr, Cu, Fe, K, Mg, Mn, Na, Nb, Ni, P, Pb, S, Ti, V, Zn); sample digestion with hydrochloric, nitric and hydrofluoric acids, with a final dissolution in hydrochloric acid (mixed acid digest);
(iii) ICP-MS suite (Ag, As, Bi, Cd, Co, Cs, Ga, In, Mo, Rb, Sb, Se, Sn, Sr, Te, Th, Tl, U, W, Y, Hf, Ce, Dy, Er, Eu, Gd, Ho, La, Lu, Nd, Pr, Sm, Tb, Tm, Yb); mixed acid digest;
(iv) Hg – aqua regia digest followed by generation of cold vapour and analysis by AAS.

One hundred and twenty-three samples were also analysed by X-ray fluorescence spectrometry (XRF) at CSIRO for SiO_2, Al_2O_3, Fe_2O_3, MnO, MgO, CaO, Na_2O, K_2O, TiO_2, P_2O_5, Cl and Zr on fused borate glass discs. The ICP and XRF analyses are listed in Appendix 3.

2.5 Standards and statistical treatment of data

Pulped in-house rock standards (CRC LEME Standards 7, 9 and 10) were placed in the analytical stream to monitor precision. Results are given in Appendix 4. The recommended values were obtained from XRF and instrumental neutron activation analysis (INAA) data (reliable total analyses). The results obtained by ICP should not be compared too closely in absolute terms, since the mixed acid digests do not provide total element extractions and consequently element abundances are understated.

Statistical summaries are provided Appendices 7-8. Most data sets are relatively small (<50 samples) and there was generally little difference in the results of the statistical treatment of the data using either cumulative frequencies or probability plots. Consequently, the geochemical data was processed using the former method. For the purposes of this report, the 'background' value was taken as the 50^{th} percentile, whereas 'anomalous' values are those above the 90^{th} percentile. Spearman Rank correlation coefficients were computed using DataDesk (version 6).

3. GEOLOGICAL SETTING AND MINERALISATION

3.1 Talisker Calc-siltstone

Base metal mineralisation is hosted by metasedimentary rocks at the base of the Talisker Calc-siltstone (as shown in the geological map for the Cambrian Kanmantoo Group; Appendix 1), which incorporates pyritic metasedimentary rocks of the Nairne Pyrite Member. From an analysis of the drill cores, there are three main units within the Talisker Calc-siltstone:

(i) interbedded biotite-muscovite schists and biotitic quartzites (Nairne Pyrite Member); these are typically pyritic;
(ii) garnetiferous, pyritic quartzite with biotite, muscovite, calcite, microcline and plagioclase, locally with minor, generally remobilised galena and sphalerite; and
(iii) a basal finely-bedded calc-silicate unit with massive to disseminated pyrite, sphalerite and galena, and colourless spessartite, scapolite, epidote/clinozoisite, hyalophane, microcline, plagioclase, biotite and calcite (Figures 3.5-3.6); chloritic selvedges occur along sulfidic zones.

Scapolite is closely associated with pyrite, sphalerite, feldspars, biotite and spessartite (Figure 3.3). Scapolite in sulfide-rich zones is the Ca-rich end-member (mizzonite; Figure 3.1), whereas in sulfide-poor domains the Na- and Cl-rich end-member (marialite) predominates.

Mineralisation occurs at the base of the Talisker Calc-siltstone in a zone 10 m thick and 450 m long, and varies from disseminated (barren) to massive (mineralised) pods comprising pyrite (50-70%), galena (10-25%) and sphalerite (5-10%; Figure 3.3C & D).

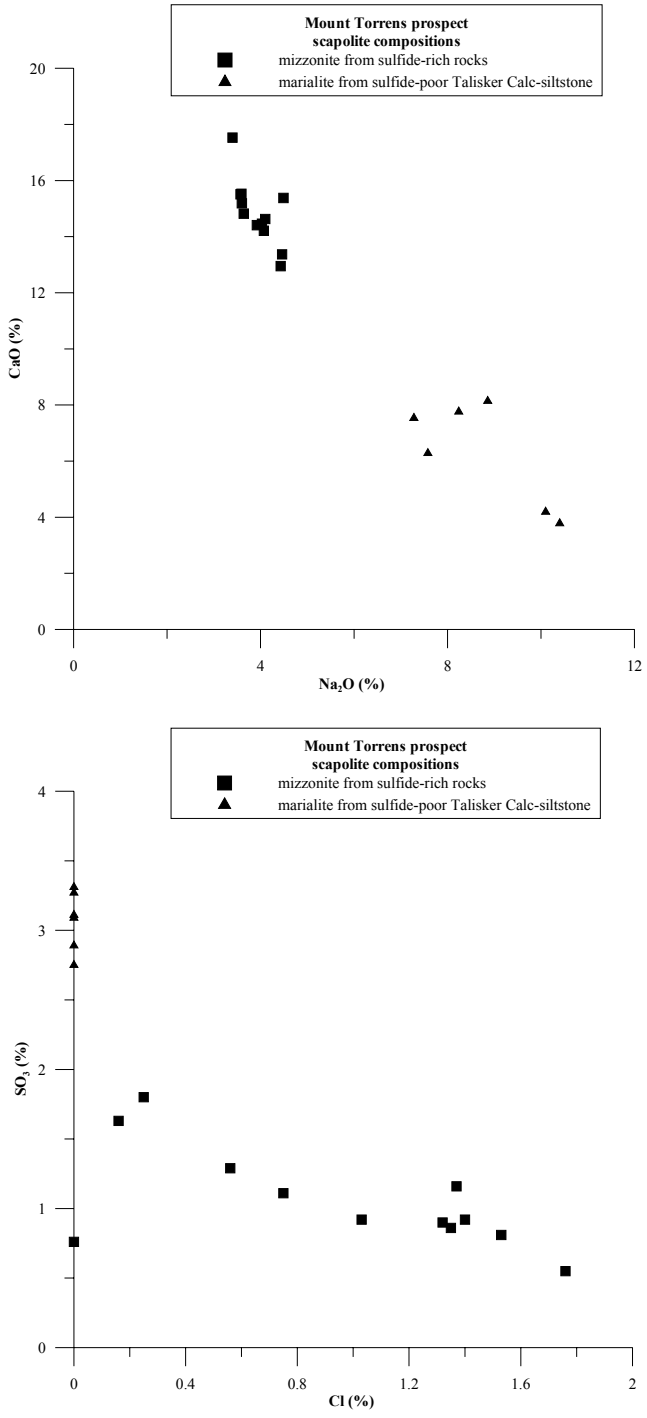

Figure 3.1. The CaO, Na_2O, SO_3 and Cl contents of scapolite group minerals from sulfide-rich and sulfide-poor domains of the Talisker Calc-siltstone.

3.2 Backstairs Passage Formation

To the west, biotitic sandstones of the Backstairs Passage Formation crop out, and locally contain cross-cutting tremolite lenses and quartz-feldspar-mica pegmatites. The sandstones are lepidoblastic quartz-rich rocks with disseminated biotite (locally retrogressed to chlorite), plagioclase (commonly strongly sericitised), and rare muscovite, epidote (locally chloritised) and pyrite (Figure 3.2A & B). Scapolite occurs rarely in basal sections of the formation.

The sandstones to the east on Fendler Hill belong to the Backstairs Passage Formation and occur on the eastern limb of a regional syncline (Figure 1.2). They are quartz-rich, lepidoblastic and contain minor biotite (locally with pleochroic haloes and zircon), feldspar and muscovite. In the north, concordant, discontinuous lenses of mafic amphibolite consist of abundant fine-grained hornblende, feldspar and, more rarely, epidote, and contain corona textures (Figure 3.2C & D)

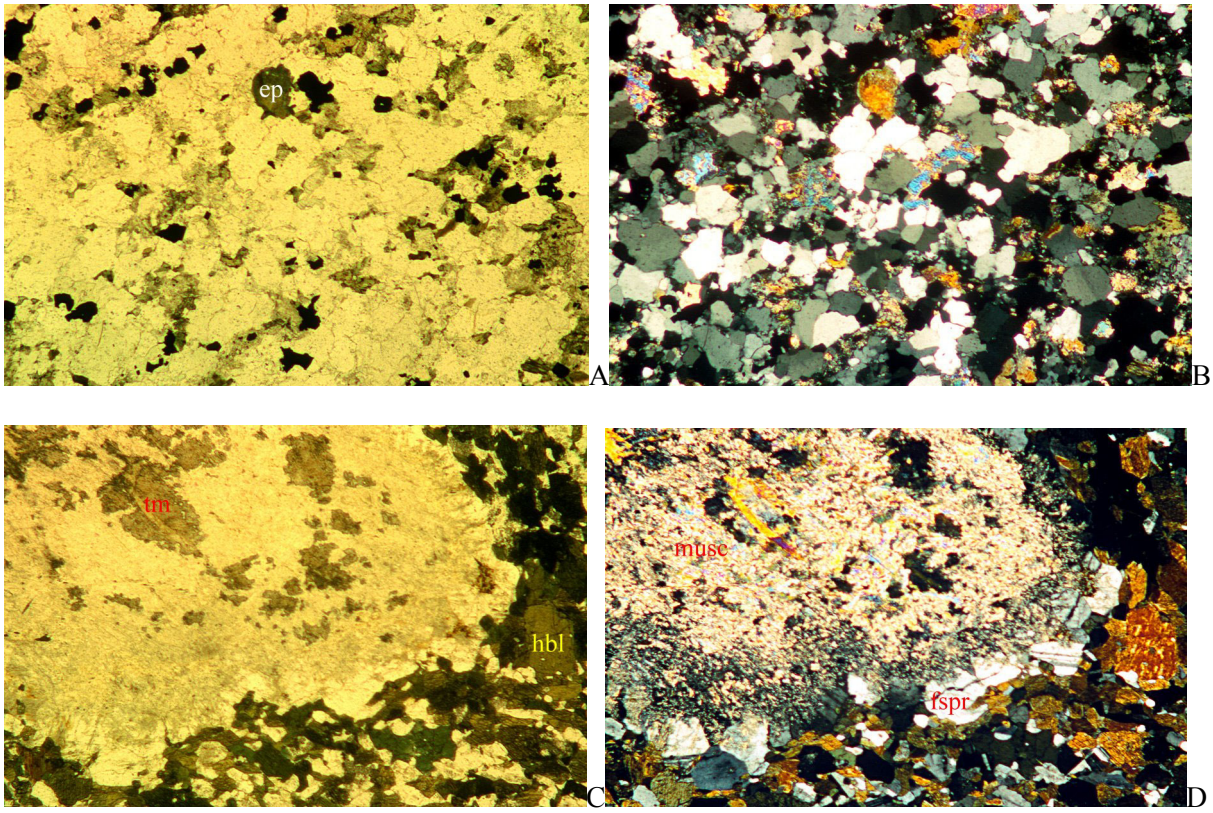

Figure 3.2. Backstairs Passage Formation sandstone and mafic amphibolite.

A. Backstairs Passage Formation sandstone comprising quartz and feldspar with disseminated biotite and epidote (ep). Plane polarised light, sample 16 (317403E, 6138342N), magnification x310.

B. As above, crossed polars.

C. Corona texture in mafic amphibolite within Backstairs Passage Formation sandstones, comprising hornblende and relatively minor feldspar. A former coarse-grained feldspar grain with tourmaline (tm) inclusions has been replaced by a felted mass of muscovite (musc) flakes. The symplectitic intergrowths along the margin of the corona are fringed by feldspar (fspr). Plane polarised light, sample 160 (320365E, 6138267N), magnification x100.

D. As above, crossed polars.

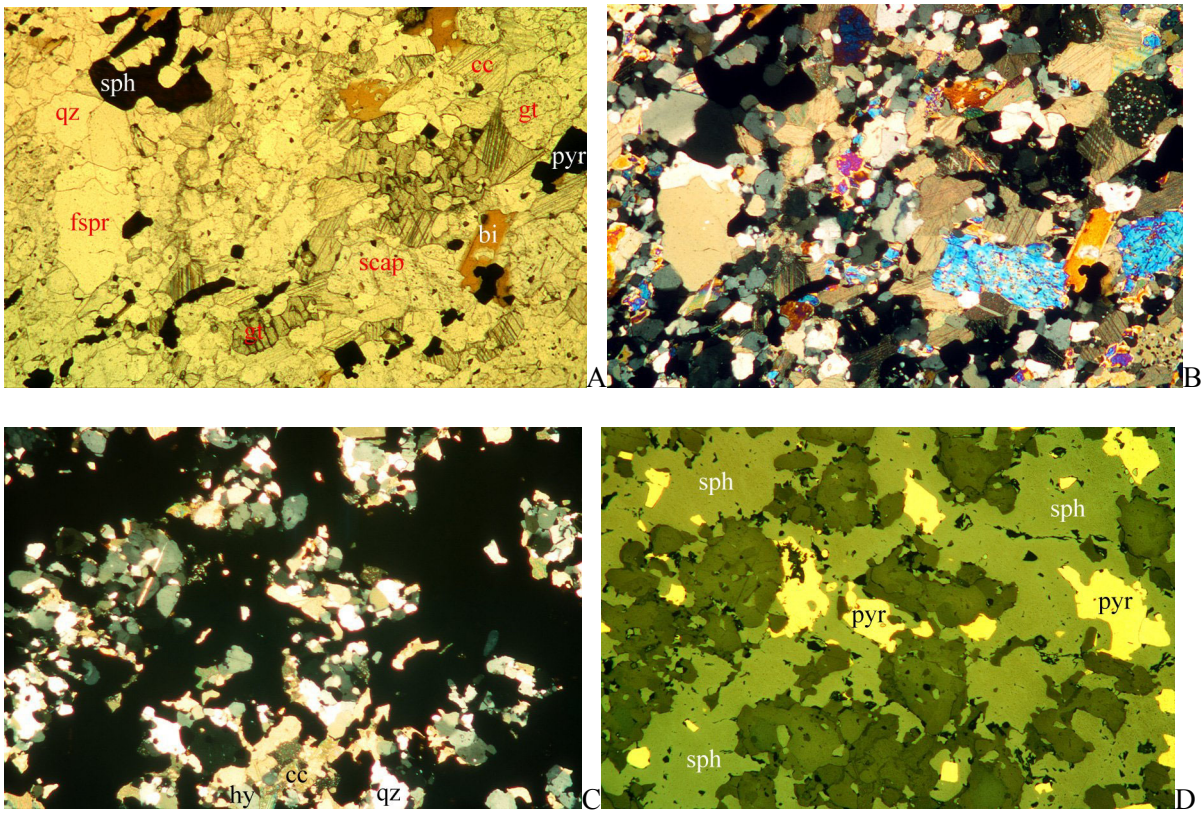

Figure 3.3. Talisker Calc-siltstone lithologies.

A. Talisker Calc-siltstone, comprising quartz (qz), feldspar (fspr), biotite (bi), spessartite (gt), scapolite (scap) and calcite (cc), with disseminated sphalerite (sph) and pyrite (pyr). Plane polarised light, MT77DD1, 166.7-167 m depth, magnification x250.

B. As above, crossed polars.

C. Sphalerite-rich domain (sph) with disseminated pyrite (pyr), with intergrown quartz (qz), hyalophane (hy) and calcite (cc). Crossed polars, DD84KA1, 310.95-311.5 m depth, magnification x250.

D. As above, reflected light.

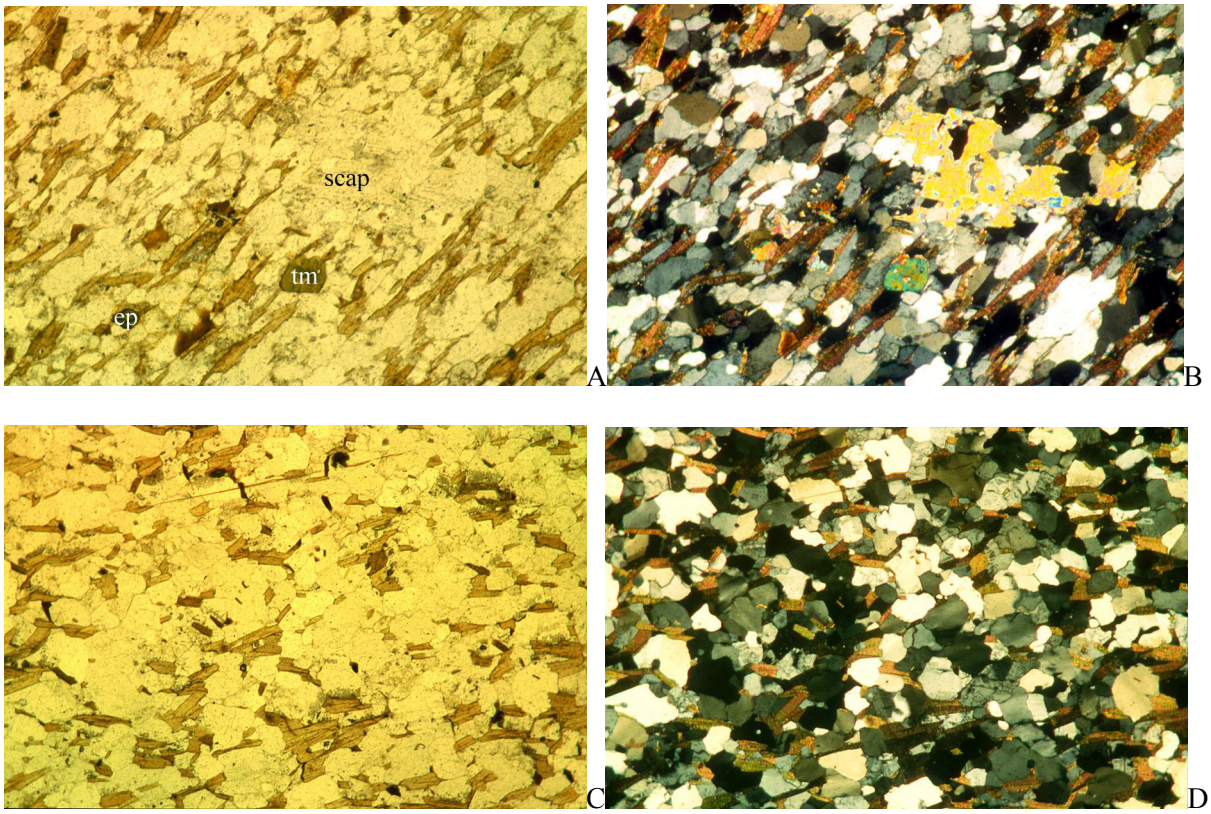

Figure 3.4. Tapanappa Formation lithologies.

A. Quartz-feldspar-biotite rock, basal section of the Tapanappa Formation, with rare poikiloblastic scapolite (scap) and disseminated tourmaline (tm) and epidote (ep). Plane polarised light, sample 14 (317901E, 6138660N), magnification x400.

B. As above, crossed polars.

C. Quartz-feldspar-biotite rock, upper Tapanappa Formation, exhibiting a more typical mineralogical composition. Plane polarised light, sample 177 (319936E, 6136071N), magnification x250.

D. As above, crossed polars.

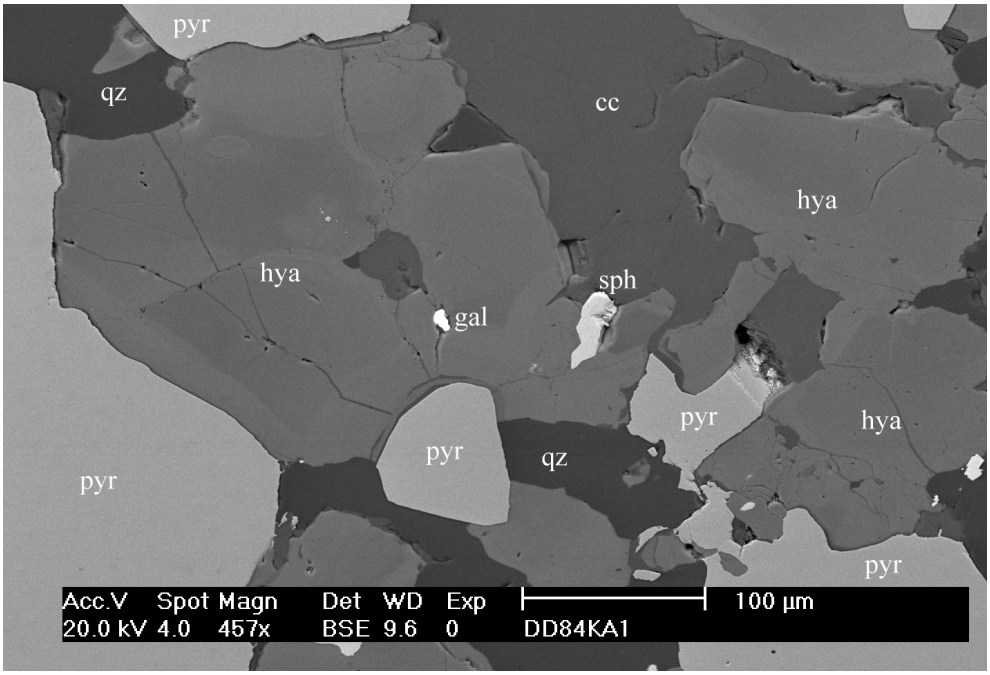

Figure 3.5. Irregular zoning in hyalophane (hya) due to minor variations of Ba content. The hyalophane is intergrown with relatively fine-grained galena (gal), sphalerite (sph), pyrite (pyr) and calcite (cc). Diamond drill hole DD84KA2, 235.75-236 m depth. Back-scattered electron image (SEM) of polished section.

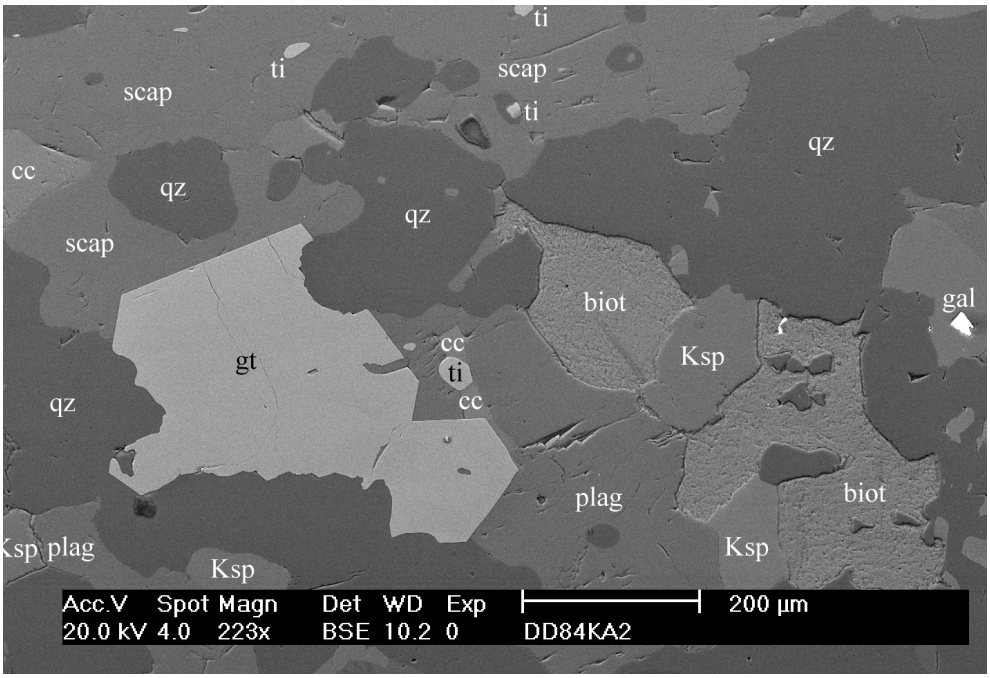

Figure 3.6. Spessartite (gt) grains intergrown with scapolite (scap), plagioclase (plag), microcline (Ksp), quartz (qz), and biotite (biot). Disseminated titanite (ti) and galena (gal) also occur. The spessartite is anomalously colourless. Diamond drill hole DD84KA2, 235.75-236 m depth. Back-scattered electron image (SEM) of polished section.

3.3 Tapanappa Formation

To the east of the Talisker Calc-siltstone (Appendix 1), relatively coarse-grained, lepidoblastic quartz-plagioclase-microcline-biotite-muscovite rocks of the Tapanappa Formation crop out (Figure 3.4A & B). Microcline contains only minor Ba (<0.2%). Fine-grained zircon and monazite, commonly as inclusions in biotite, also occur. Colourless spessartite occurs locally in basal zones of the Tapanappa Formation and may signify a Mn halo around the mineralised zone.

East of the Harrogate road, weathered (saprolitic) quartz-feldspar-biotite schists (sheared Tapanappa Formation lithologies; Figure 3.4C & D) occur on the western slopes of the hills and become progressively more abundant to the south (Appendix 1). Prominent linear outcrops of coarse-grained muscovite schist are probably shear zones within these quartz-feldspar-biotite schists (or possibly, strongly deformed Talisker Calc-siltstone) and have locally been intruded by quartz-feldspar-mica pegmatites. In the south, outcrops of weathered pyritic chert occur.

3.4 Structural trends

Structural trends are dominantly north-south (Appendix 1), except for a small area in the extreme south-east of the area mapped where the dominant strike is east-west and there appears to be a fold closure. The change in strike appears to be related, in part, to upright folds plunging about 30^{o} to the south-east.

Numerous quartz veins occur (Appendix 1). Discernible trends are rare, but most veins tend to trend parallel to strike, or orthogonal to it.

4. REGOLITH

4.1 Regolith-landform units

4.1.1. Erosional regime

Units of the erosional regime (Appendix 2) occur on rolling hills, where thin soils overlie bedrock, saprock or ferruginous saprolite. Outcrops of bedrock are common. Ferruginous saprolite, derived from Tapanappa Formation and Talisker Calc-siltstone rocks, crops out on low hills in central parts of the area. It also crops out locally on the western slopes of the hills to the east of the Harrogate road. Gossans occur very locally at the base of slope of steep low hills (ferruginous saprolite derived from the Talisker Calc-siltstone) and superficially resemble ferruginous saprolite on weathered surfaces. There is generally no saprolite preserved over sandstones of the Backstairs Passage Formation in the west or east.

4.1.2. Depositional regime

Alluvium and colluvium occur along the valleys of Dairy and Herrmanns creeks and their tributaries. Saprolite derived from Tapanappa Formation rocks is exposed where the creeks are deeply incised. A typical section from Dairy Creek (Figure 4.30) comprises:

surface soil (A1 horizon; loamy)	0-5 cm
stratified alluvium - sandy	5-30 cm
stratified alluvium – clayey - with sand and gravel bands	30-80cm
sulfidic materials and/or black muds	80-100 cm
C horizon - mottled saprolite	100+ cm

Ferricrete occurs along the valley floor to the east of the Harrogate road and has cemented alluvium, colluvium and lag derived from quartz veins and ferruginous saprolite. It is likely that the Fe oxides

were derived from erosion of ferruginous material from the hills to the east and south, where patches of ferruginous saprolite are still preserved (Appendix 2).

4.2 Previous soil-landscape investigations in the study area

4.2.1. Soil-landscape investigations

Initial soil-landscape investigations were conducted by Fritsch & Fitzpatrick (1994). Soils of the area are typical of the eastern Mount Lofty Ranges: they are derived from strongly weathered micaceous sandstones and schists of the underlying metasedimentary rocks. Relationships between landform elements, soil types, drainage, waterlogging, salinity and acidity are summarised in Table 4.1. The soils are characterised by abrupt textural boundaries between sandy- and loamy-textured surface horizons (A and E horizons) and clayey subsurface horizons (B horizons) with mottled and/or sodic properties (Fritsch & Fitzpatrick, 1994) and classify mostly as Xeralfs according to soil taxonomy (Soil Survey Staff, 1999). Waterlogging frequently develops during winter in many of the soils, particularly those in the lower slopes to flats. Studies also provided evidence for the formation of upland freshwater acid sulfate soils (ASS) with sulfidic materials and Fe-rich precipitates by saline ground water discharge, which have resulted from land clearing, excess discharge of groundwater and soil erosion (Fitzpatrick et al., 1996; Fitzpatrick & Self, 1997).

Soil data at point sites, and hydrology and elevation data were used with structural analysis to construct the principal toposequence types (Fritsch & Fitzpatrick 1994; Fitzpatrick et al., 1996). Soils of the lower slopes, terraces and valley floors frequently have sodic (Natrixeralfs) and alluvial soils (Entisols), and wet soils (Aquents) in saline groundwater discharge areas with perched wetlands (Table 4.1). Soils of the groundwater discharge areas are commonly saline and sulfidic (potential acid sulfate soils, PASS; Fitzpatrick et al., 1996). They contribute to degraded water quality through leakage of salts and acid weathering products following oxidation of the sulfidic materials (acid sulfate soils, ASS). The clayey B horizons of sodic soils, developed in areas where saline groundwater discharge has occurred, commonly disperse and erode. Soils of the mid and upper slopes in the study area principally have sandy and loamy A horizons overlying red and yellow clayey B horizons (Palexeralfs).

Table 4.1. Landform element, soil types, drainage, waterlogging, salinity and acidity classes.

Landform Element	**Soil Descriptions**	**Drainage/ *Waterlogging***	**Salinity and acidity**
Flat/ stream channel	Gully, tunnel and rill erosion with salt efflorescence (halite & gypsum) on soils with grey sandy loam surface over yellow-grey clay or sulfidic material or sulfuric horizons	Very poorly drained *Strongly waterlogged*	Extremely saline Mostly alkaline (pH >7.5) with sporadic occurrences of acidic (pH <5.5) near-surface layers (<5cm), due to oxidation of sulfidic material
Flat – saline seepages	Salt efflorescence (halite & gypsum) on surface with grey sandy loam surface over yellow-grey clay	Poorly drained *Strongly waterlogged*	Very saline
Flat – freshwater seepages	Grey sandy loam surface layer over yellow-grey mottled clay	Poorly drained *Strongly waterlogged*	Slightly saline
Lower slope seepages	Salt efflorescence (halite and gypsum) on surface with loamy black sulfidic material overlying over yellow-grey clay	Very poorly drained *Strongly waterlogged*	Extremely saline. Mostly alkaline (pH >7.5) with sporadic occurrences of highly acidic (pH <5.5) layers near-surface (<5cm), due to oxidation of sulfidic material
Lower slope, open depressions	Grey sandy loam surface layer over yellow-red-grey mottled clay	Poorly drained *Periodic waterlogging*	Slightly saline
Mid-slope	Brown loam over red and yellow uniform coloured clay; deep	Freely drained *Infrequently waterlogged*	Non saline
Crest or upper-slopes	Deep and shallow well drained red and yellow soils with quartz and ferricrete fragments	Freely drained *Infrequently waterlogged*	Non saline

4.3 Gossans and saprolite

The gossans crop out locally in a zone 200 m long along a fence-line at the base of low hills formed of Nairne Pyrite Member. The gossans are superficially very similar in appearance to ferruginous saprolite. However, on fractured surfaces, bright yellow mottles or patches (dominantly plumbojarosite, minor plumbogummite) occur in a reddish-purple matrix (mainly hematite; Figure 4.1). Gossans with boxworks after pyrite occur only along the old costean (at 6137561N 317745E) and are probably weathered equivalents of barren pyrite-rich mineralisation. In Dairy Creek, a galena-rich vein outcropping in the creek bed has been weathered to cerussite (Figure 4.2).

Figure 4.1. Fractured surface of an outcrop of the Mount Torrens gossan showing reddish-purple matrix (hematite and quartz with minor plumbogummite and plumbojarosite) and bright yellow mottles (dominantly plumbojarosite and jarosite with minor goethite and plumbogummite).

Figure 4.2. Cerussite-rich veinlet in the bed of Dairy Creek. The loose specimen of the vein shows ovoid quartz- and feldspar-rich domains within a grey matrix of cerussite with relict, fine-grained, unreplaced galena.

4.3.1. Regolith profiles through the gossans

The mineralogical variations through the gossan and weathered metasiltstones in diamond drill holes MTG3-4 are shown in Figures 4.3 and 4.4. Although the abundances of the minerals are based on peak heights determined from XRD patterns, the relative distributions of the minerals are in good agreement with visual observations made on the drill core. Both holes were collared at the same point (at inclinations of 85^{o} and 80^{o} respectively) and were intended to drill down-dip along the gossan. However, these holes (and also MTG5-6) indicate that the gossan represents the weathered keel of a sulfidic lens and does not persist down-dip for more than 7.5 m. Fresh rock was not intersected by either MTG3 or 4, although the presence of minor pyrite at the base of MTG4 suggests that drill hole was terminated close to the base of weathering.

Goethite and hematite are present throughout the profile, but are relatively concentrated in the gossan. Hematite appears to be more abundant than in MTG2, and hematite-rich zones occur in the gossan. The gossans contain relatively minor quartz, kaolinite/halloysite and mica. Jarosite, barite, plumbogummite and plumbojarosite appear to be largely absent from the gossans (although SEM investigations have demonstrated that these minerals can occur in the cavities of boxworks) and are most abundant disseminated through weathered metasiltstones (Figure 4.5). In MTG3, jarosite and plumbojarosite extend to shallower depths than plumbogummite. Scott et al. (1979) interpreted the general absence of secondary Pb minerals from the gossan as being due to relatively low pH conditions during gossan formation, and suggested that the leached Pb was precipitated in the immediate hangingwall (in metasiltstones), or was derived laterally, from groundwaters flowing downslope (Sylvester, 1978a). An alternative explanation is that the gossan represents a pod of relatively barren massive pyrite and that the disseminated secondary Pb minerals in the metasiltstones are the weathering products of disseminated sulfides such as galena.

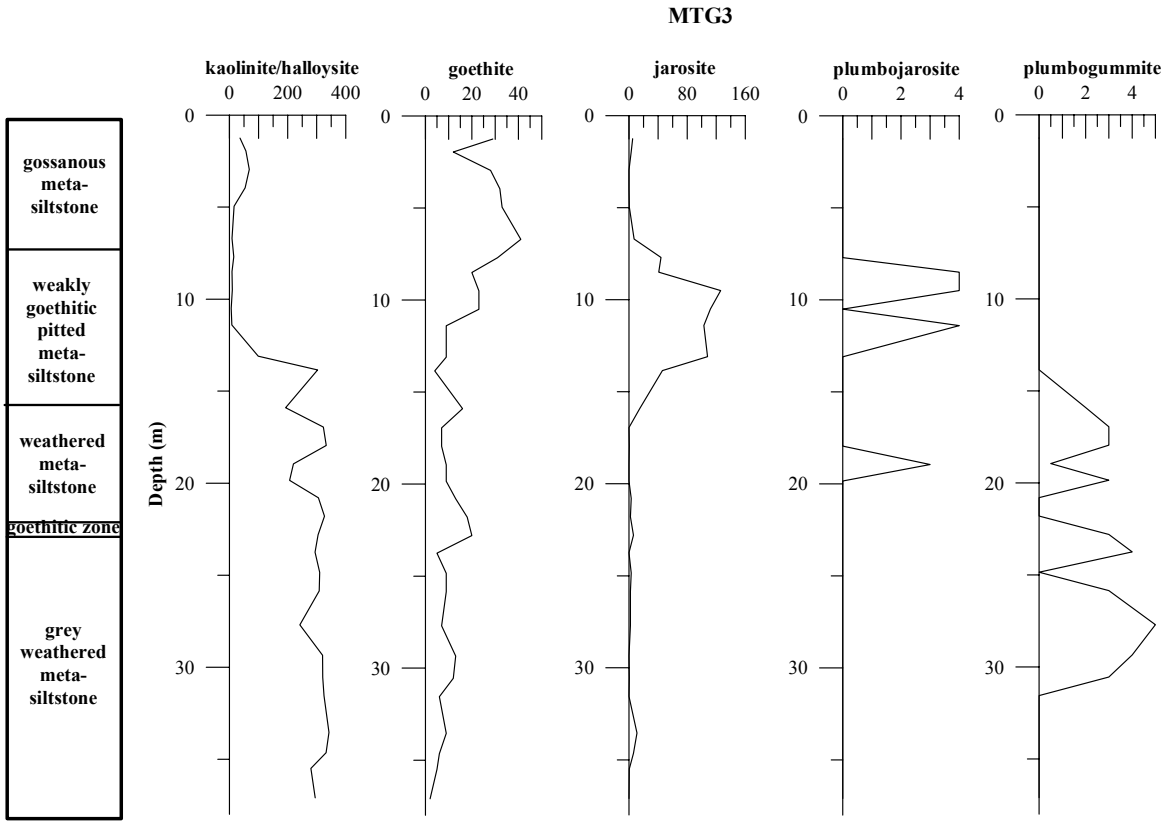

Figure 4.3. Qualitative mineralogical profiles for selected minerals through gossan and weathered metasiltstones (Talisker Calc-siltstone), diamond drill hole MTG3 (data from Scott et al., 1979). Profiles for the other minerals are shown in Appendix 10.

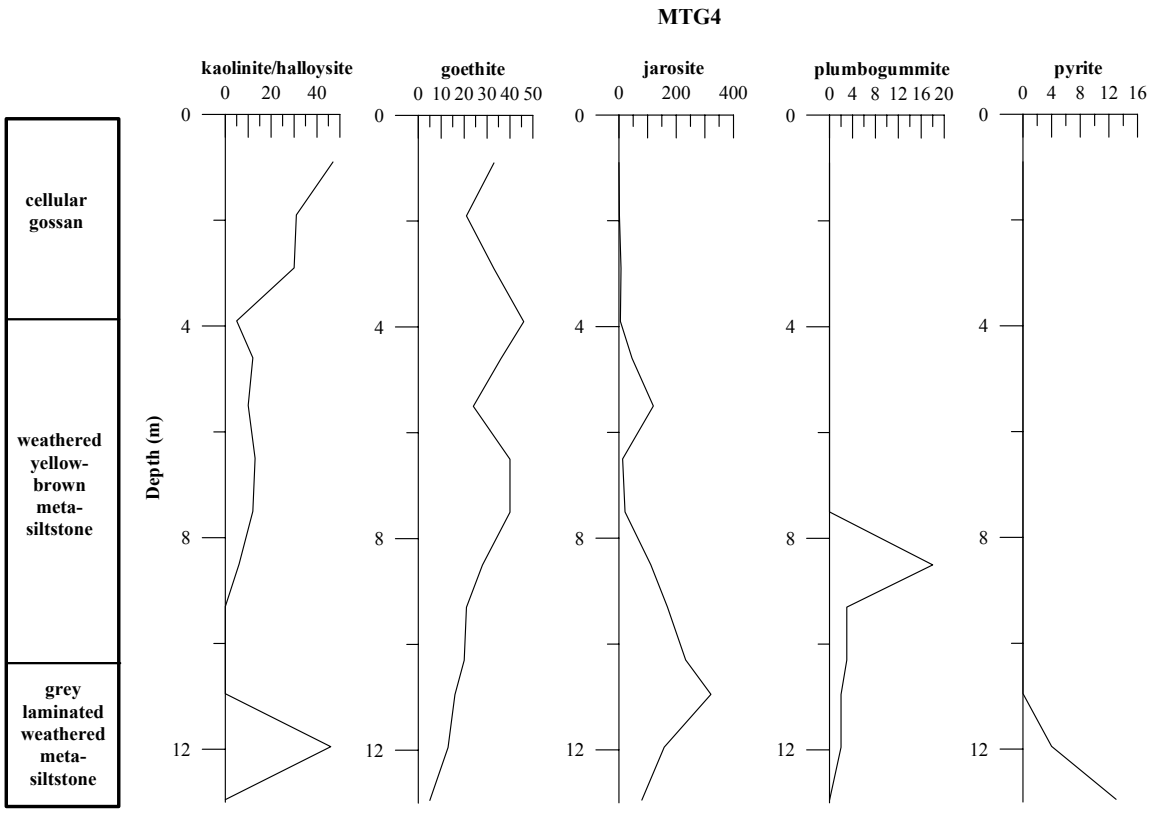

Figure 4.4. Qualitative mineralogical profiles for selected minerals through gossan and weathered siltstones (Talisker Calc-siltstone), diamond drill hole MTG4 (data from Scott et al., 1979). Profiles for the other minerals are shown in Appendix 10.

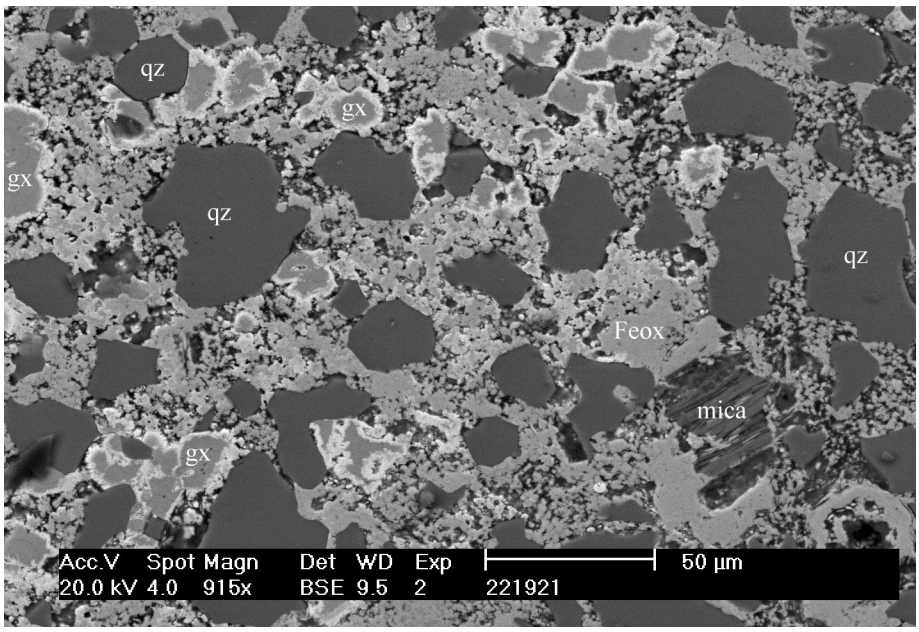

Figure 4.5. Disseminated gorceixite (gx) with bright rims of plumbogummite disseminated through weathered metasiltstone, comprising quartz (qz), hematite (Feox) and minor mica, in a goethite-dominated matrix. Sample 221921, MTG5, 0.2 m depth. Back-scattered electron image (SEM).

4.3.2. Mineralogy of the regolith profile through the gossans

Previous SEM investigations (Sylvester, 1978b) have revealed the presence of alunite, barite, kaolinite/halloysite, jarosite, Fe oxides with adsorbed Pb, anglesite, iodargyrite, cerussite, plumbojarosite, plumbogummite, native silver, cerargyrite, witherite, molybdite and Ag-Ni-Cu alloys in the gossans and associated saprolite.

This study of samples from regolith profiles intersected by drill holes MTG2-4 and from surface exposures has confirmed the occurrence of many of these minerals (except for alunite, cerargyrite, witherite and molybdite). Additional minerals identified in the gossans include gorceixite, anatase, native gold, natrojarosite and Al-substituted goethite (10-20 mole % Al).

Sulfates

The most abundant sulfates are barite, jarosite group minerals and anglesite.

Barite

Barite is restricted to the regolith. It occurs in the following general associations:

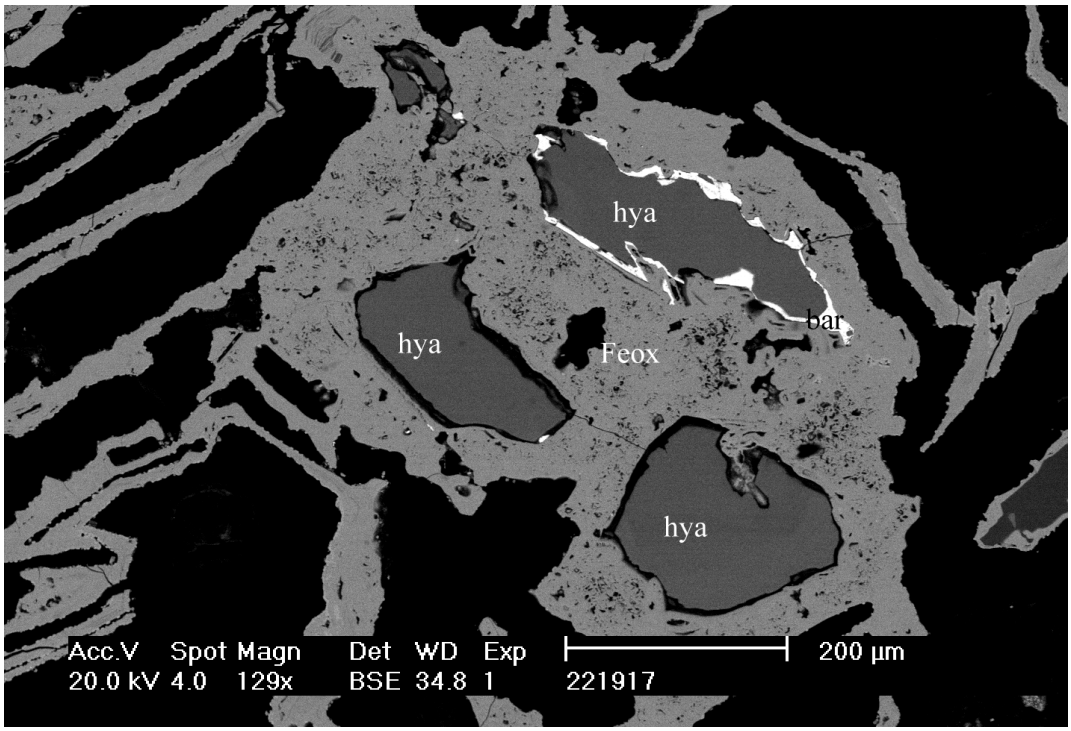

Figure 4.6. Barite (bar) coating a corroded, relict grain of hyalophane, enclosed by Fe oxides (Feox) forming a boxwork after pyrite. The hyalophane contains about 10% Ba. As the hyalophane grain weathered, barite was precipitated as an insoluble coating on the surface of the grain. Sample 221917, MTG4, 6.35 m depth. Back-scattered electron image (SEM).

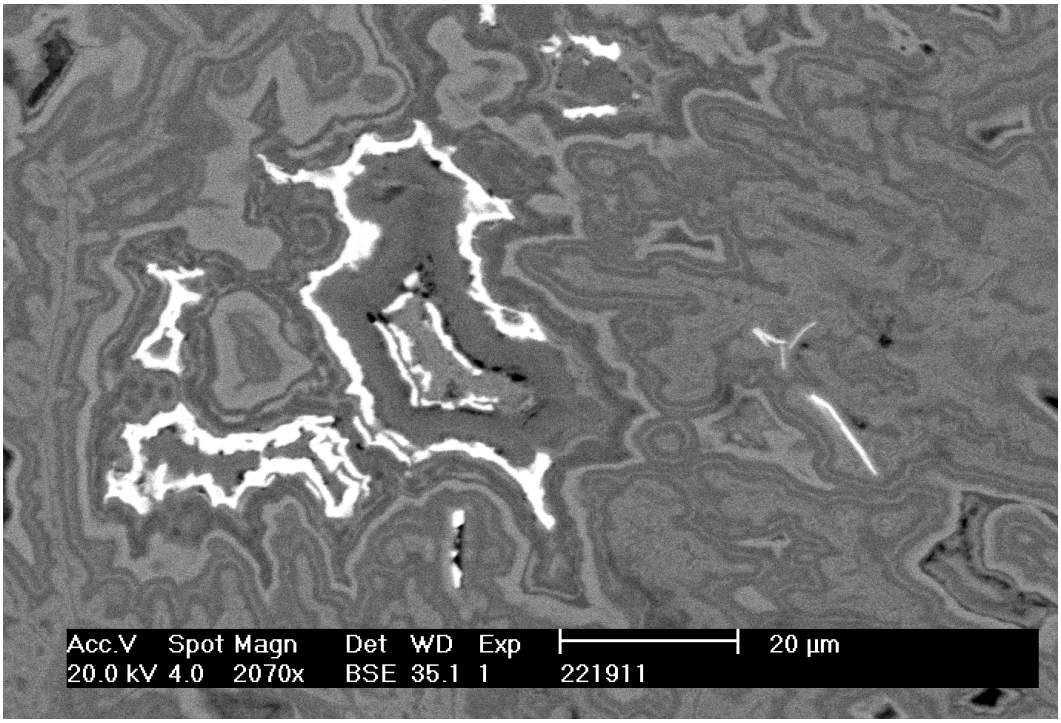

Figure 4.7. Colloform barite (white) intergrown with colloform goethite. The darker colloform banding in the goethite is due to a greater proportion of admixed kaolinite/halloysite. Sample 221911, MTG4, 0.90 m depth. Back-scattered electron image (SEM).

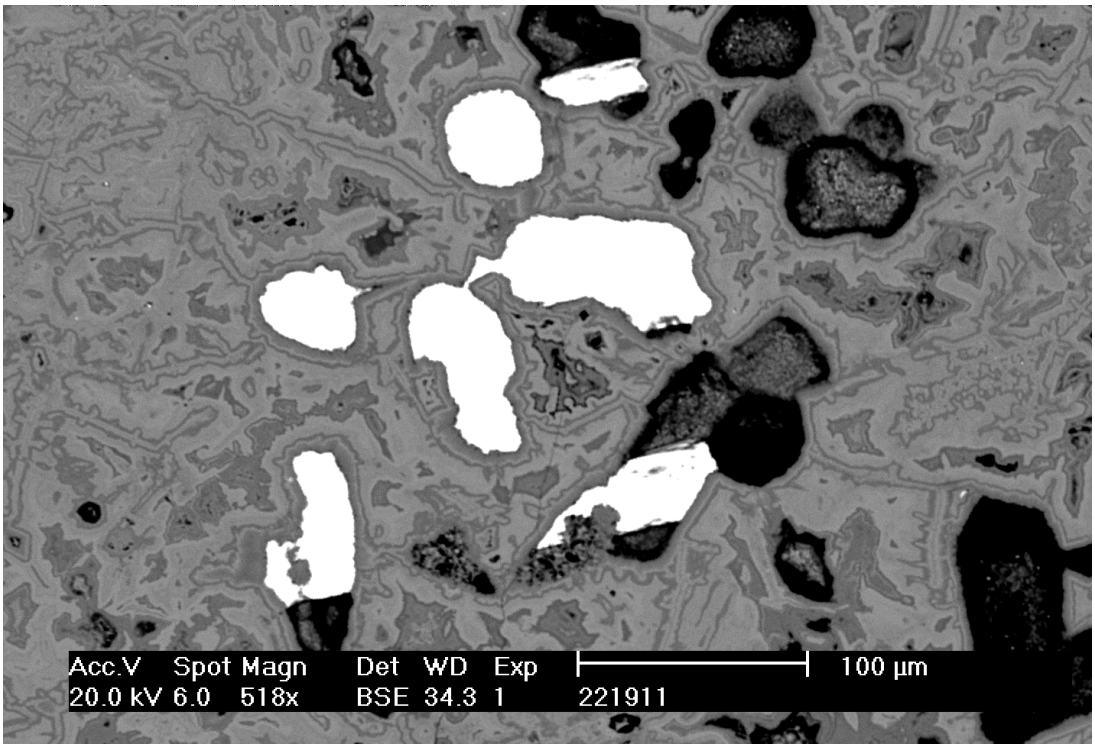

Figure 4.8. Barite (white) in cavities in boxworks after pyrite. The alternate lighter and darker banding is due to the slighter higher proportion of kaolinite/halloysite to goethite in the darker bands. Sample 221911, MTG4, 0.90 m depth. Back-scattered electron image (SEM).

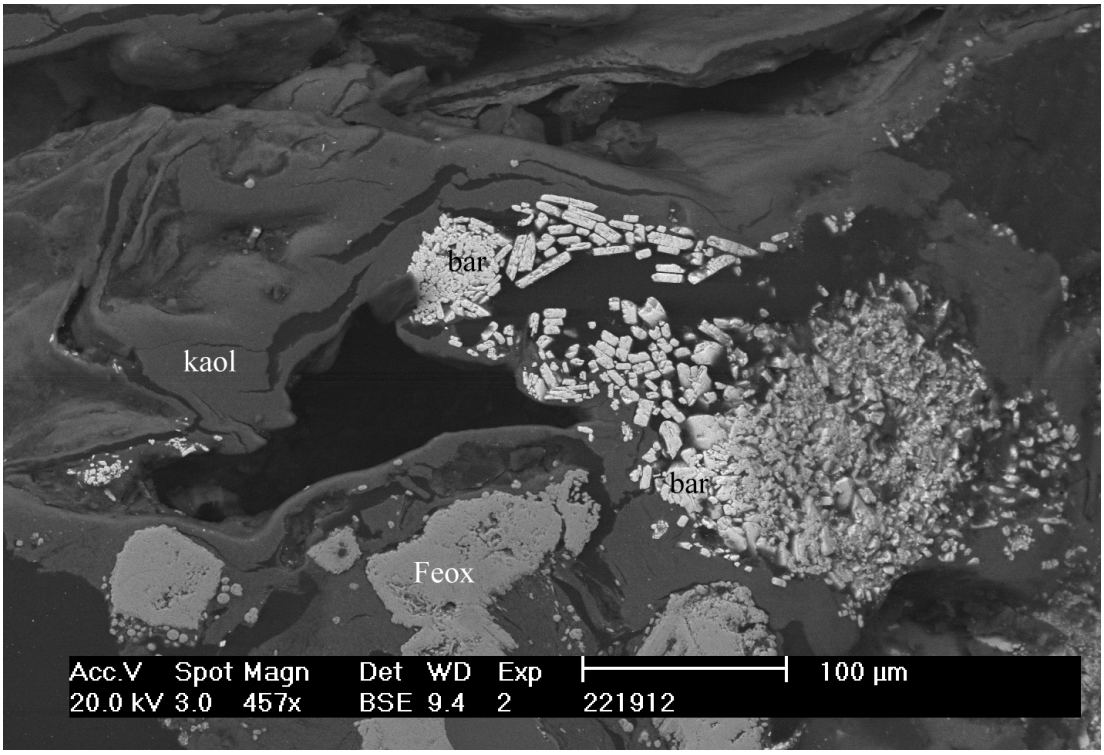

Figure 4.9. An aggregate of euhedral barite (bar) crystals in kaolinite/halloysite (kaol) associated with Fe oxide (Feox) pseudomorphs after pyrite. Sample 221912, MTG4, 1.75 m depth. Back-scattered electron image (SEM).

(i) as rims to relict hyalophane grains (Figure 4.6), associated with boxworks after pyrite;

(ii) in goethite, either within the colloform banding (Figure 4.7), suggesting co-precipitation with the goethite, or in cavities in boxworks after pyrite (Figure 4.8), locally associated with iodargyrite (Figure 4.19);

(iii) disseminated, in saprolite (Figure 4.9) or gossan, associated with silicates (quartz, kaolinite/halloysite, goethite-kaolinite/halloysite pseudomorphs after biotite) and plumbogummite.

Jarosite group

The occurrence of jarosite group minerals is restricted to the regolith. The chemical composition of jarosite group minerals (Figure 4.10) is somewhat variable, even in the same sample. This in part is due to grain size: finer grains are generally natrojarosite, whereas coarser grains are jarosite and are more easily recognised and analysed. Apart from jarosites in weathered pyritic cherts, Pb is a significant component of most types, with compositions trending towards plumbojarosite.

In general terms, jarosite (*s.s.*) appears to be dominant over natrojarosite. Plumbojarosite appears to be relatively abundant in surface gossan exposures, but is relatively rare at depth; in sulfuric horizons of acid sulfate soils (Figure 4.34), it occurs in one locality above the mineralised zone in the Herrmanns creek.

Jarosite occurs disseminated in gossan and saprolite, as an weathering product of pyrite, and may occur associated with boxworks after pyrite (Figure 4.11) associated with plumbogummite. Less commonly, jarosite pseudomorphs after pyrite occur (Figure 4.12). One occurrence of plumbojarosite was noted in the Dairy Creek gossan (Figure 4.13), where it is associated with cerussite and partially replaced by plumbogummite.

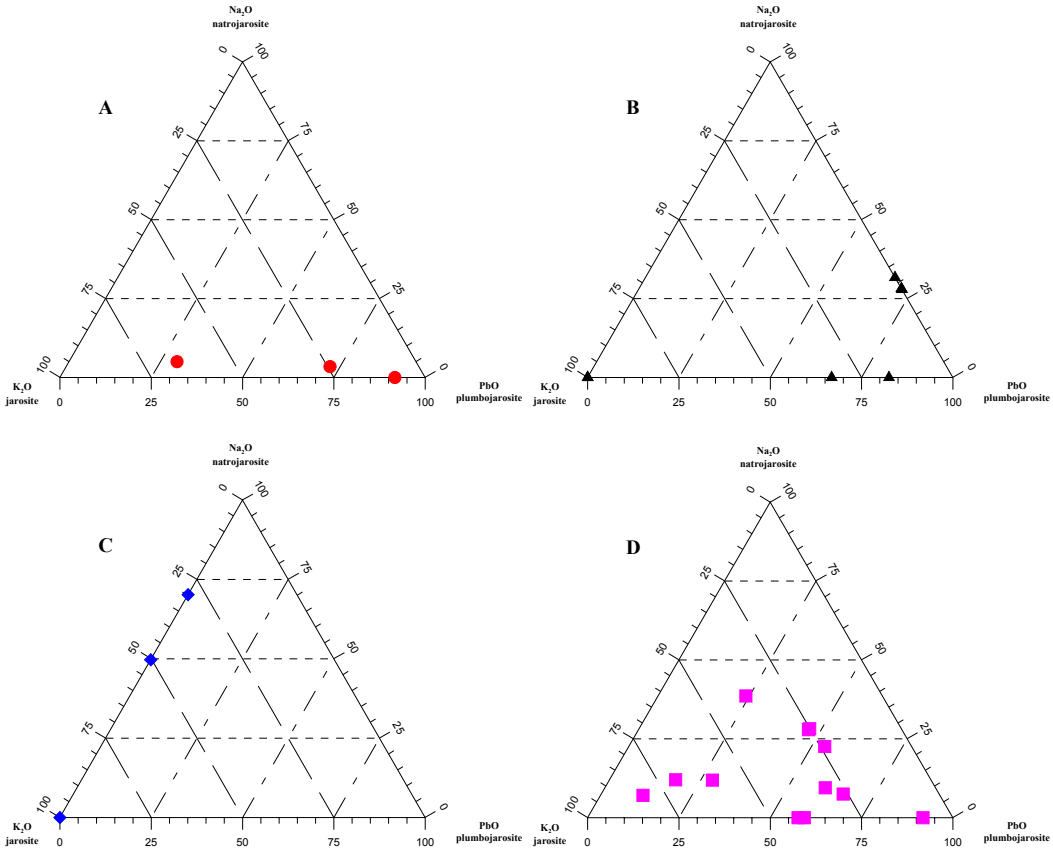

Figure 4.10. Compositional variations in jarosite group minerals. A. acid sulfate soils. B. gossans. C. weathered pyritic cherts. D. weathered metasiltstones.

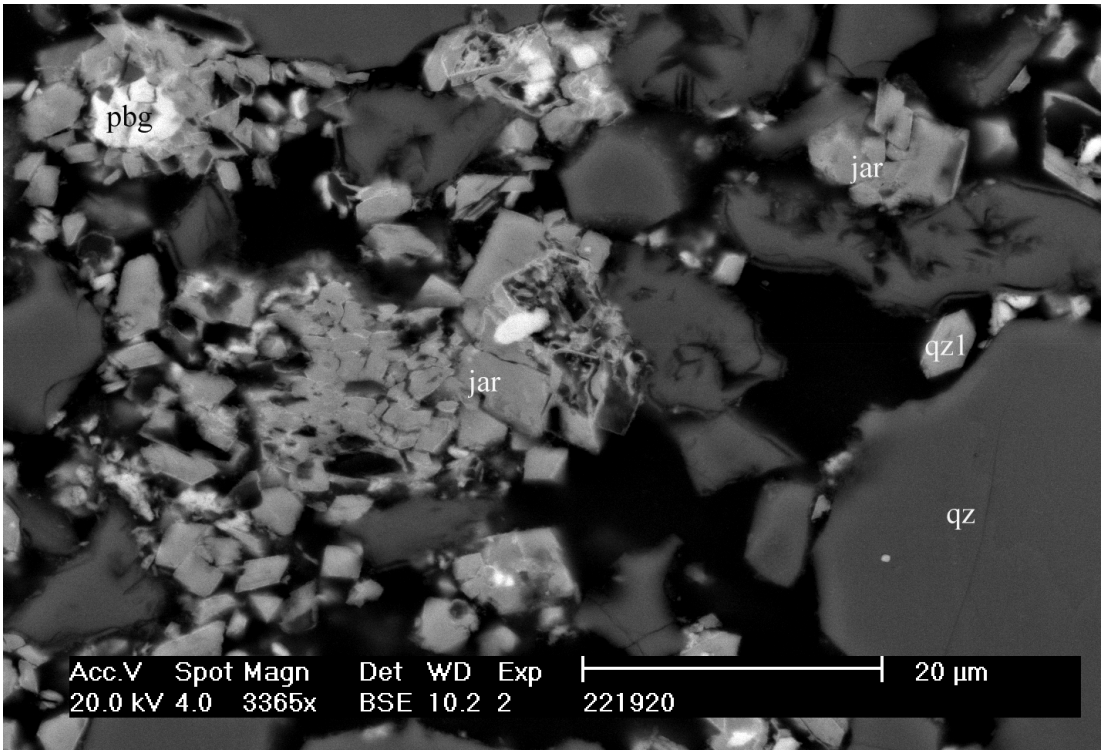

Figure 4.11. Jarosite (jar) grains associated with boxworks after pyrite and plumbogummite (pbg) and quartz grains (qz). The euhedral quartz grain (qz1) is coated by jarosite. Sample 221920, MTG4, 9.40 m depth. Back-scattered electron image (SEM).

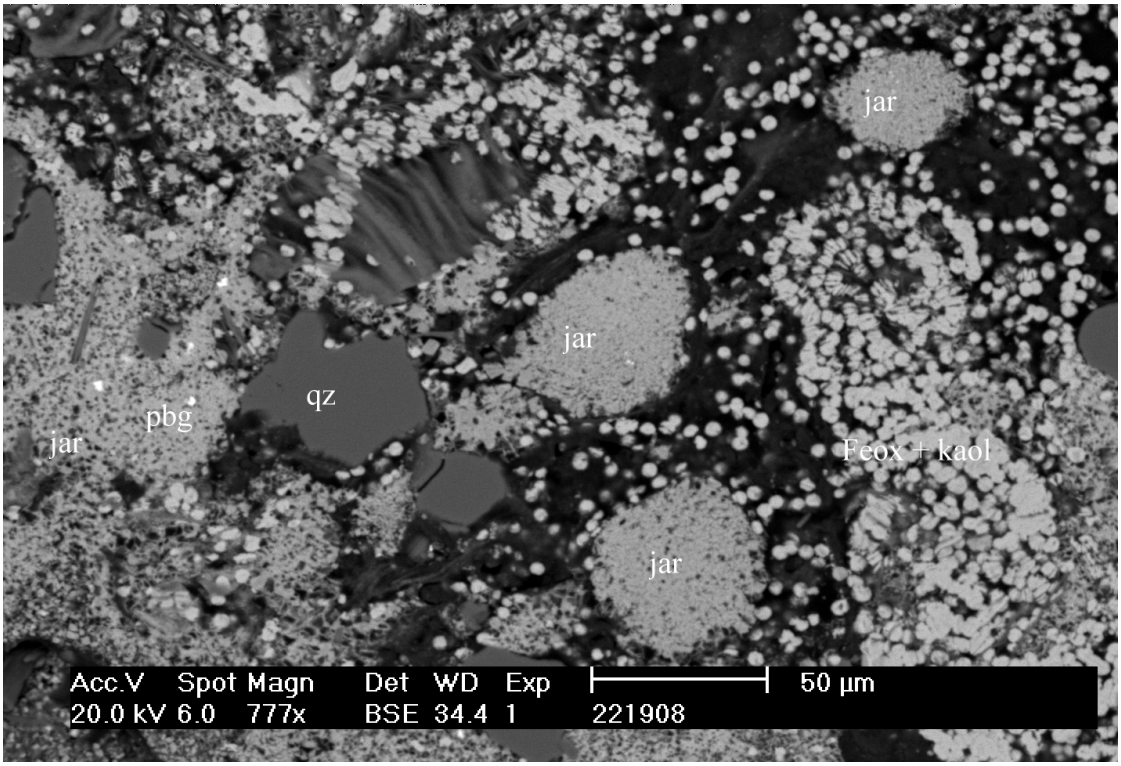

Figure 4.12. Jarosite (jar) pseudomorphs after pyrite framboids, associated with fine-grained disseminated plumbogummite (pbg), Fe oxides (Feox), kaolinite/halloysite (kaol), quartz (qz) and weathered biotite. Sample 221908, MTG3, 6.40 m depth. Back-scattered electron image (SEM).

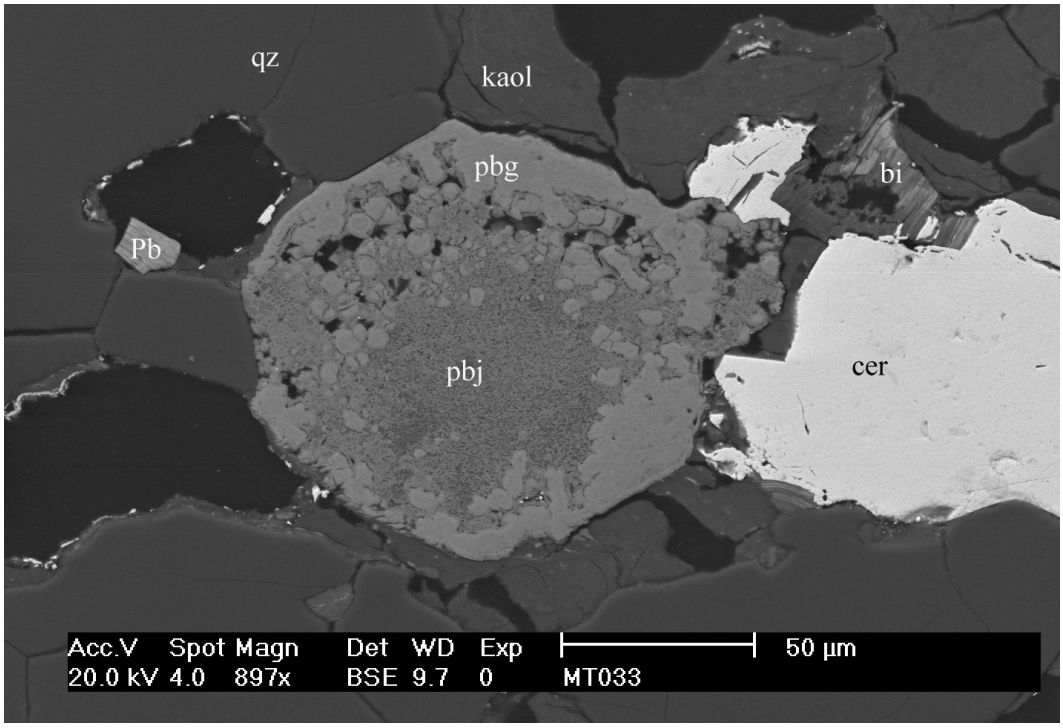

Figure 4.13. Partial replacement of plumbojarosite (pbj) by plumbogummite (pbg), associated with quartz (qz), kaolinite/halloysite (kaol), cerussite (cer), weathered biotite (bi) and a kaolinite/halloysite pseudomorph (Pb) of mica with adsorbed Pb. Sample MT033, outcrop in Dairy Creek. Back-scattered electron image (SEM).

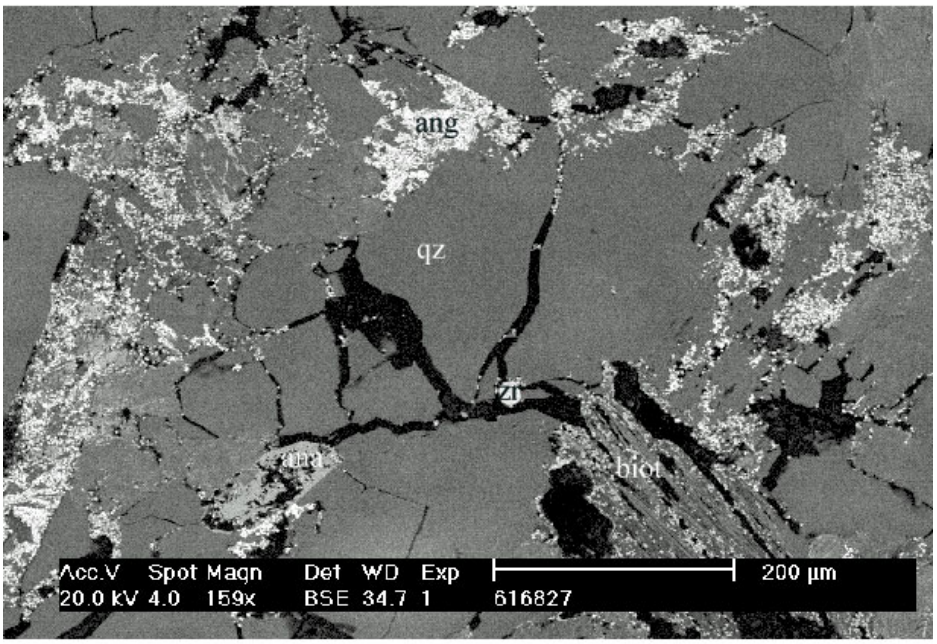

Figure 4.14. Fine-grained anglesite (white; ang) along quartz (qz) and anatase (ana) grain boundaries. Minor disseminated zircon (zr) and weathered biotite (biot) also occur. The fine-grained grey material locally associated with anglesite (brighter, white) is a mixture of goethite and kaolinite/halloysite. Sample 616827, MTG1, 1.82 m depth. Back-scattered electron image (SEM).

Anglesite

Anglesite is relatively rare and was detected in only one sample (Figure 4.14), where it occurs along quartz and kaolinite/halloysite grain boundaries associated with goethite and anatase.

Phosphates

Plumbogummite is the most common phosphate mineral. Gorceixite is relatively rare. Accessory amounts of primary relict monazite occur in the regolith.

Plumbogummite

Plumbogummite ($PbAl_3(PO_4)_2(OH)_5.H_2O$) is restricted to the regolith and occurs as subhedral grains, aggregates of subhedral grains or grains with colloform structure (Figure 4.15) in the following associations:

(i) disseminated, in saprolite, associated with quartz, Fe oxides, kaolinite/halloysite and barite (Figure 4.16);

(ii) associated with jarosite (from the weathering of pyrite; Figure 4.11);

(iii) rarely, in composite grains with gorceixite, as rims (?replacement) on gorceixite (Figure 4.18);

(iv) disseminated in Fe oxides;

(v) rarely, replacing plumbojarosite (Figure 4.13);

(vi) in boxworks, after pyrite (Figure 4.17).

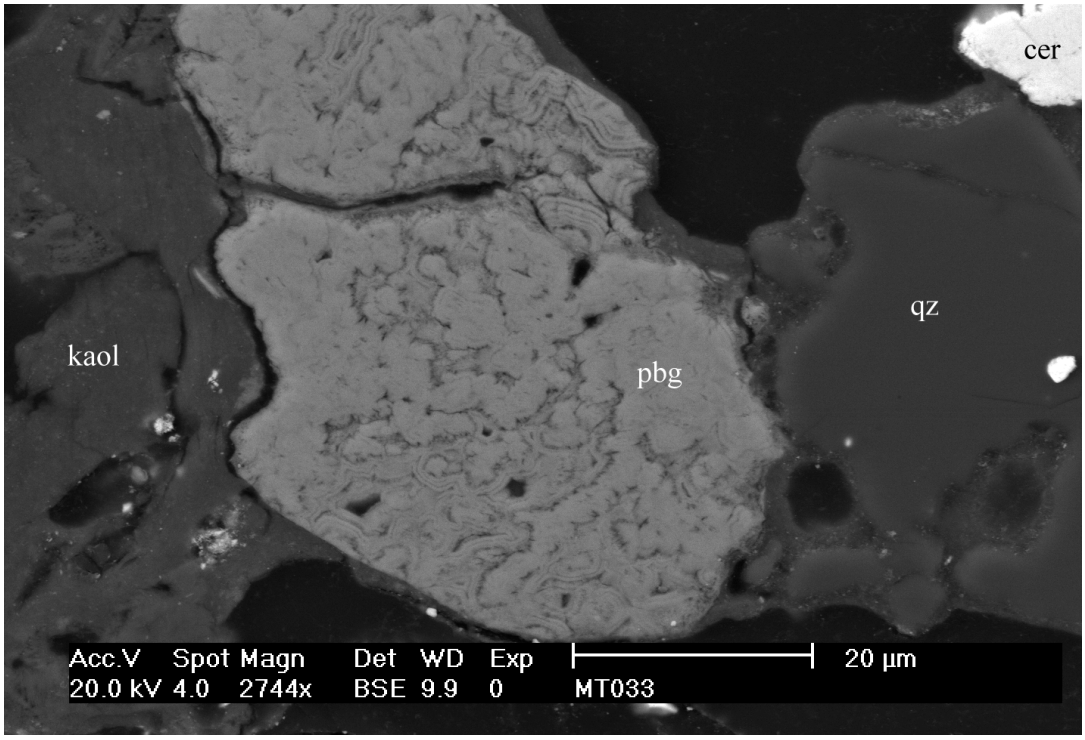

Figure 4.15. Colloform banding in plumbogummite (pbg), associated with quartz (qz), kaolinite/halloysite (kaol) and cerussite (cer). The bright small grain along the right-hand margin of the photograph is galena. Sample MT033, outcrop in Dairy Creek. Back-scattered electron image (SEM).

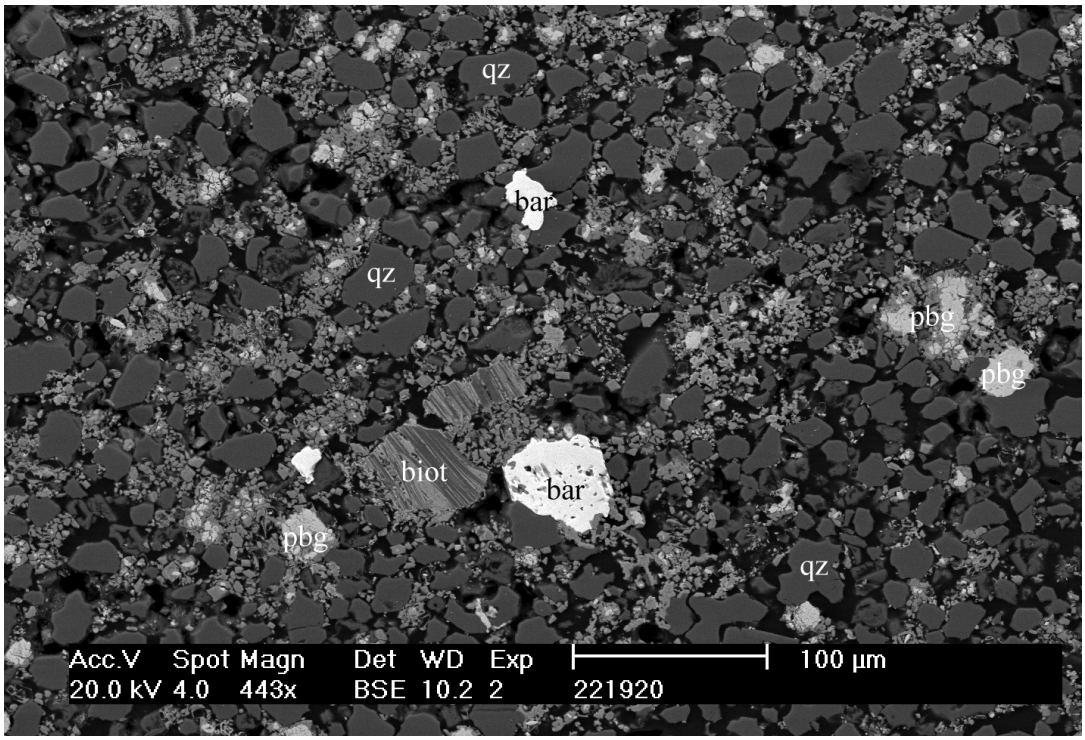

Figure 4.16. Disseminated plumbogummite (pbg) and barite (bar) in weathered siltstone comprising quartz (qz) grains, minor weathered biotite (biot) and interstitial goethite and kaolinite/halloysite (darker grey). Sample 221920, MTG4, 9.40 m depth. Back-scattered electron image (SEM).

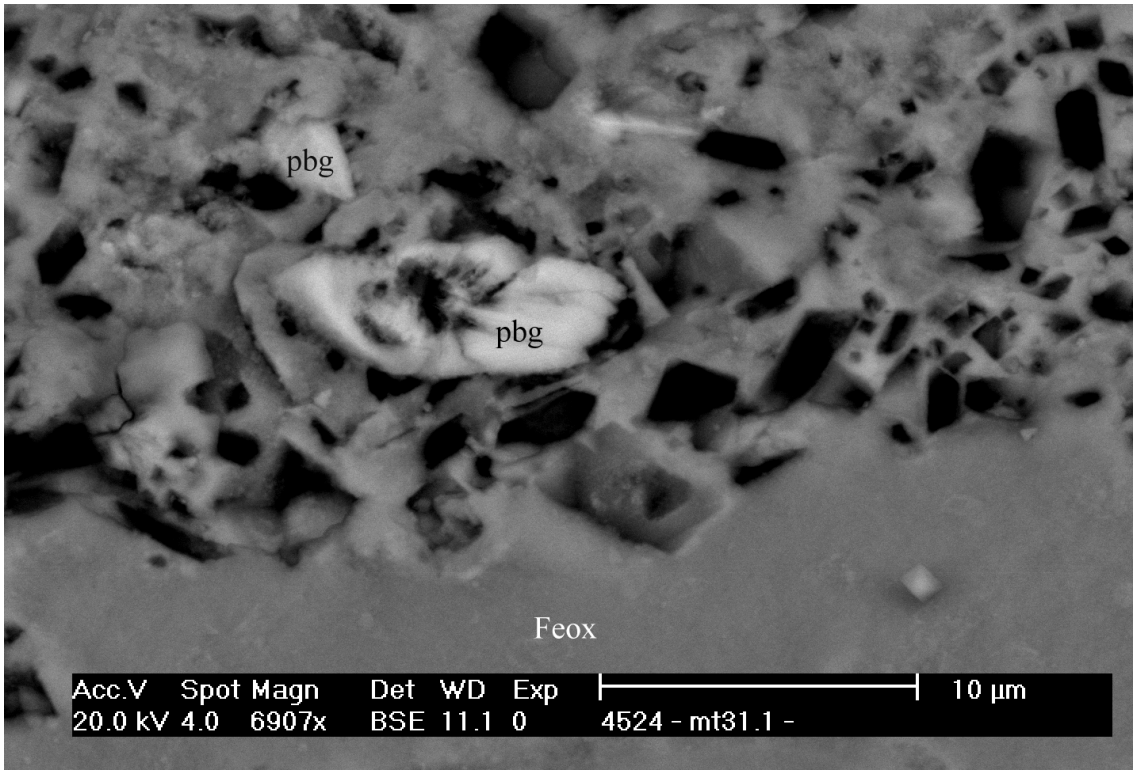

Figure 4.17. Plumbogummite (pbg) in boxworks after pyrite, associated with Fe oxides (Feox). Sample MT031, outcrop of gossan. Back-scattered electron image (SEM).

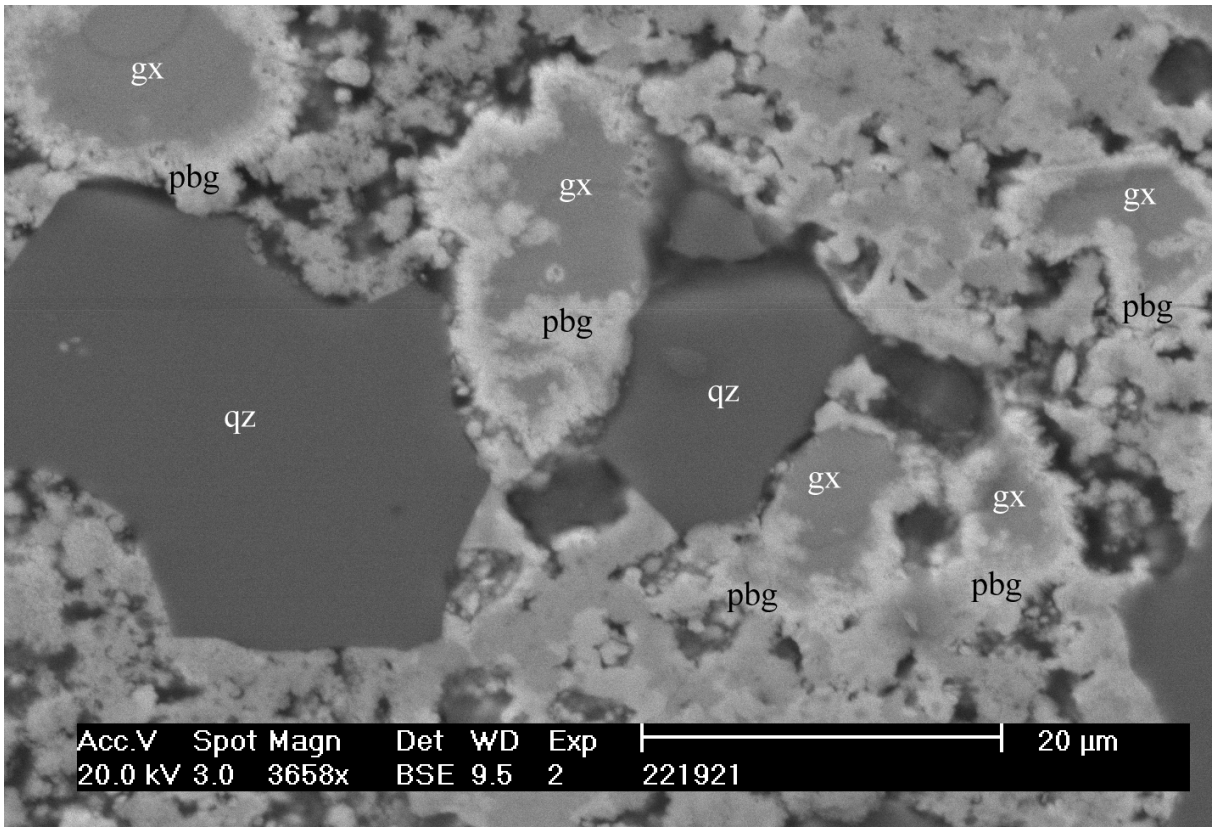

Figure 4.18. Plumbogummite (pbg) rims around cores of gorceixite (gx), associated with quartz (qz) and goethite. Sample 221921, MTG5, 0.20 m depth. Back-scattered electron image (SEM).

Gorceixite

Gorceixite ($(Ba,Ca,Ce)Al_3(PO_4)_2(OH)_5.H_2O$) is rare and occurs as composite grains with plumbogummite rims (Figure 4.18).

Carbonates

Cerussite

Carbonates are generally rare or absent in the regolith. The only significant occurrence is that of cerussite, as a weathering product of a galena vein in outcrop in the bed of Dairy Creek (Figure 4.2). The cerussite occurs as relatively coarse laths (Figure 4.19) associated with quartz, microcline, plumbian kaolinite/halloysite, plumbian Fe oxides (in boxworks after sulfides), and minor plumbogummite and plumbojarosite. Fine-grained relict galena grains are commonly disseminated through the cerussite.

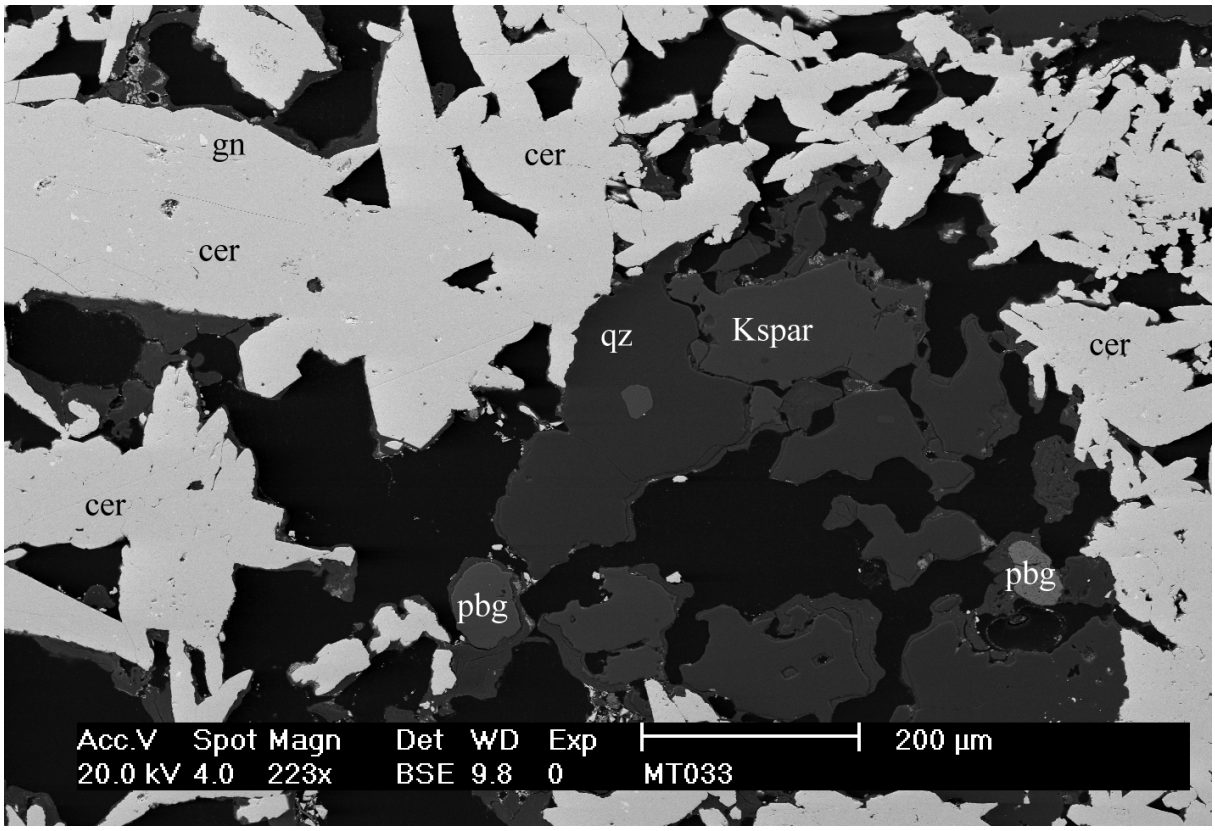

Figure 4.19. Cerussite (cer) laths (locally with fine-grained galena (gn) inclusions) associated with quartz (qz), microcline (Kspar) and minor plumbogummite (pbg). Sample MT033, outcrop in Dairy Creek. Back-scattered electron image (SEM).

Native elements

Native gold

The following small (<1 µm diameter) grains were found: (a) occluded on the margin of a quartz grain, associated with Fe oxides and disseminated plumbogummite (Figure 4.20); and (b) an irregular grain in a cavity in Fe oxides with colloform banding (Figure 4.21).

Grain (a) contains minor amounts of Fe and Hg, but no detectable Ag (a 'secondary' signature). However, grain (b) contains about 10 % Ag (a 'primary' signature) and minor Cu and Fe. The reasons for the disparate chemistry are not clear. It is possible that the quartz grain containing the occluded particle is of detrital origin and unrelated to the base metal mineralisation, whereas the other is possibly the result of contamination from the polishing process.

Halides

Iodargyrite

Iodargyrite (AgI) is widely distributed in small amounts. It typically occurs in cavities in Fe oxides, locally associated with barite (Figure 4.22) or jarosite. Less commonly, it forms relatively coarse grains along grain boundaries of Fe oxides and/or kaolinite/halloysite, associated with disseminated barite, or in goethite-kaolinite/halloysite veinlets (Figure 4.23).

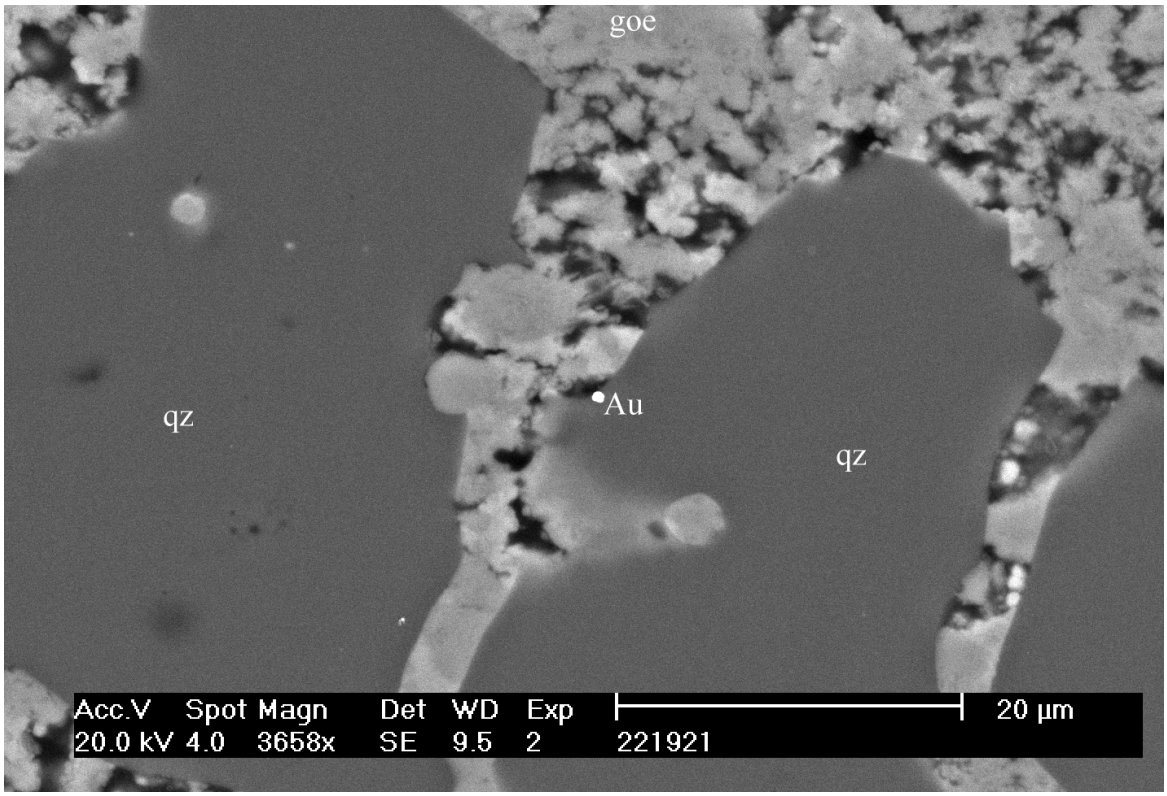

Figure 4.20. A small grain of native gold (Au), about 0.5 µm in diameter, at the edge of a quartz (qz) grain. Goethite (goe) and a minor amount of plumbogummite (small bright grains) occur along quartz grain boundaries. Sample 221921, MTG5, 0.20 m depth. Back-scattered electron image (SEM).

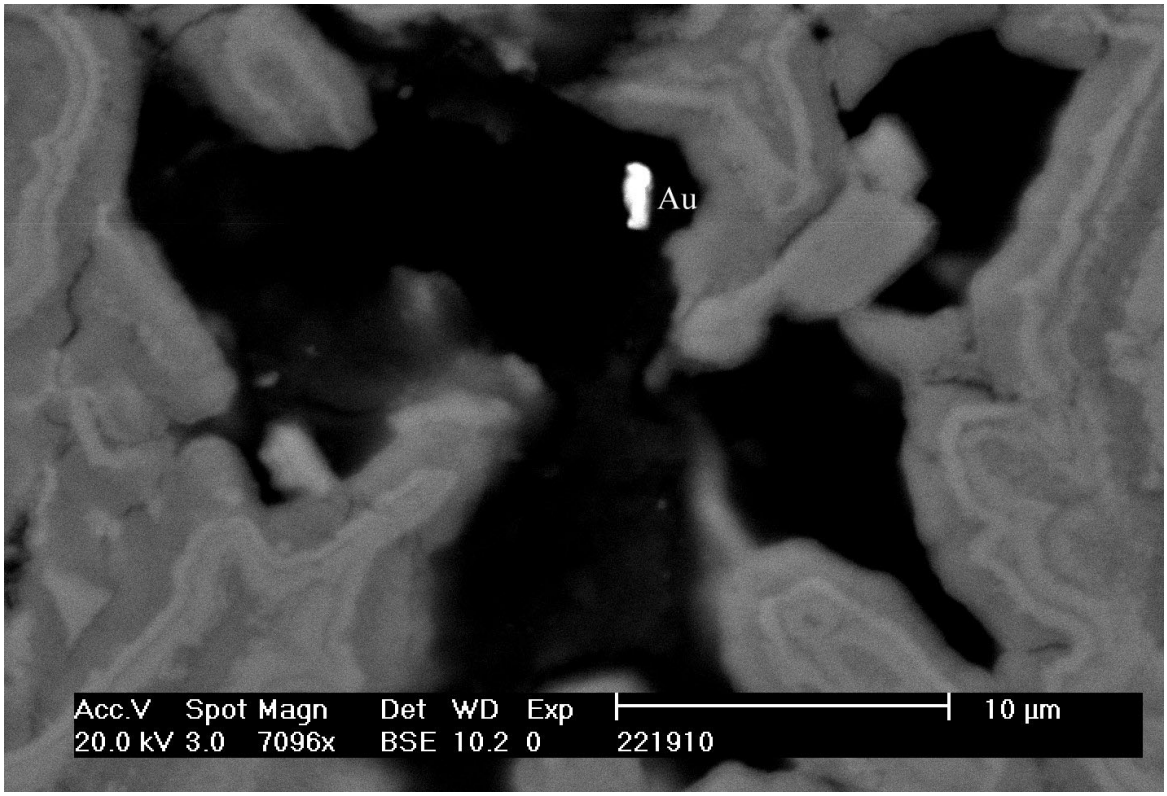

Figure 4.21. A small grain of native gold (Au) containing 10% Ag in a cavity in goethite with colloform banding. Sample 221910, MTG4, 0.30 m depth. Back-scattered electron image (SEM).

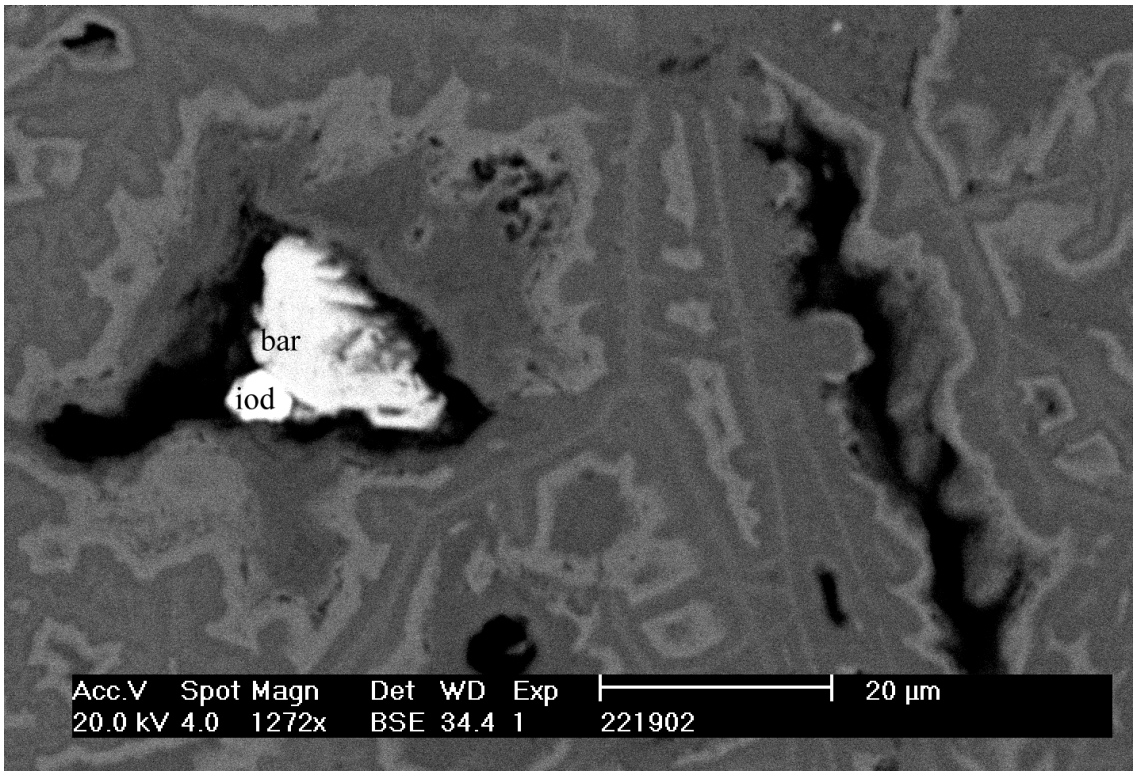

Figure 4.22. Iodragyrite (iod) and barite (bar) grains in a cavity in Fe oxides with colloform banding. The darker bands contain more kaolinite/halloysite. Sample 221902, MTG3, 1.00 m depth. Back-scattered electron image (SEM).

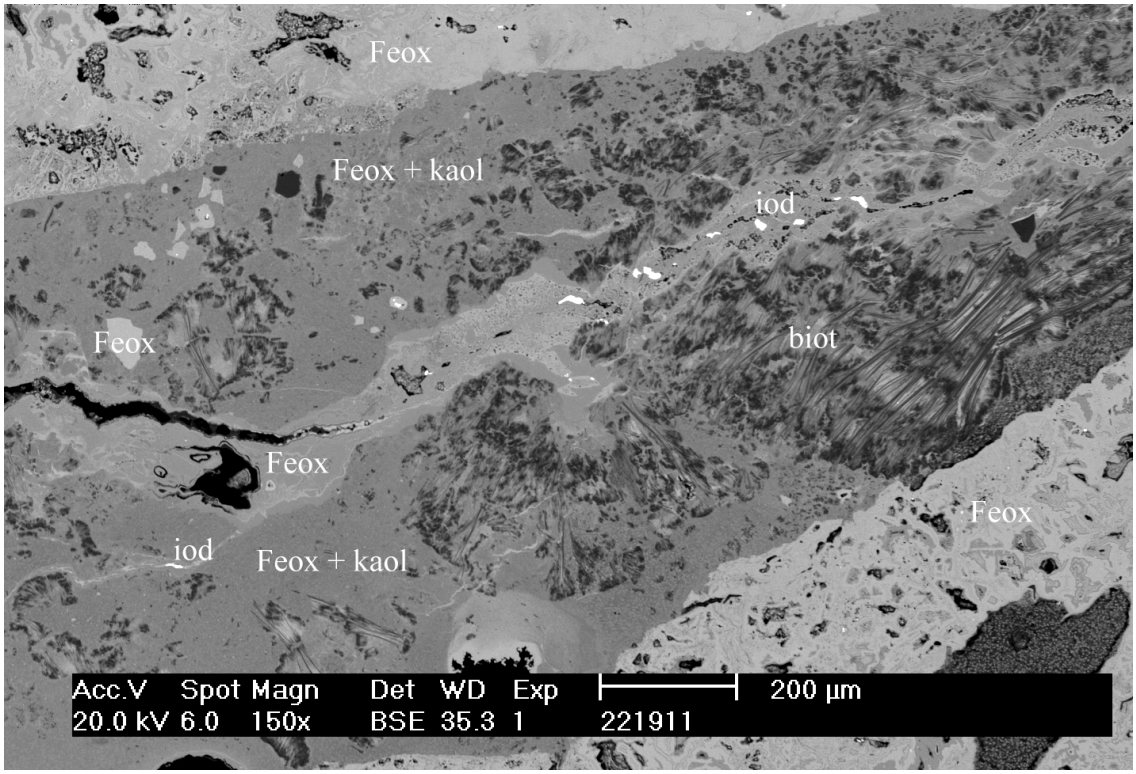

Figure 4.23. Iodargyrite (iod; white) disseminated along a goethite (Feox) veinlet in a domain composed of Fe oxides and kaolinite/halloysite (Feox+kaol) and weathered biotite (biot). Sample 221911, MTG4, 0.90 m depth. Back-scattered electron image (SEM).

Oxides

Anatase

Anatase occurs as:

(i) complex intergrowths with goethite (Figure 4.24), typically in weathered metasiltstones, associated with silicates (kaolinite/halloysite, quartz, weathered biotite) and rarely associated with disseminated plumbogummite and gorceixite;

(ii) coatings on quartz grains (Figure 4.25) in cavities, associated with disseminated plumbogummite and opaline silica; this suggests that Ti was mobile during weathering;

(iii) disseminated subhedral grains, in weathered metasiltstones (Figure 4.14).

SEM analyses suggest that the anatase is essentially TiO_2, with minor amounts of Fe (possibly due to admixed goethite). Microprobe analyses also suggest some Fe is present, together with ZrO_2 (up 1 %), PbO (up to 2.48 %) and V_2O_5 (up to 0.73 %). The minor amounts of Zr substitution in anatase suggest some mobility of Zr during weathering.

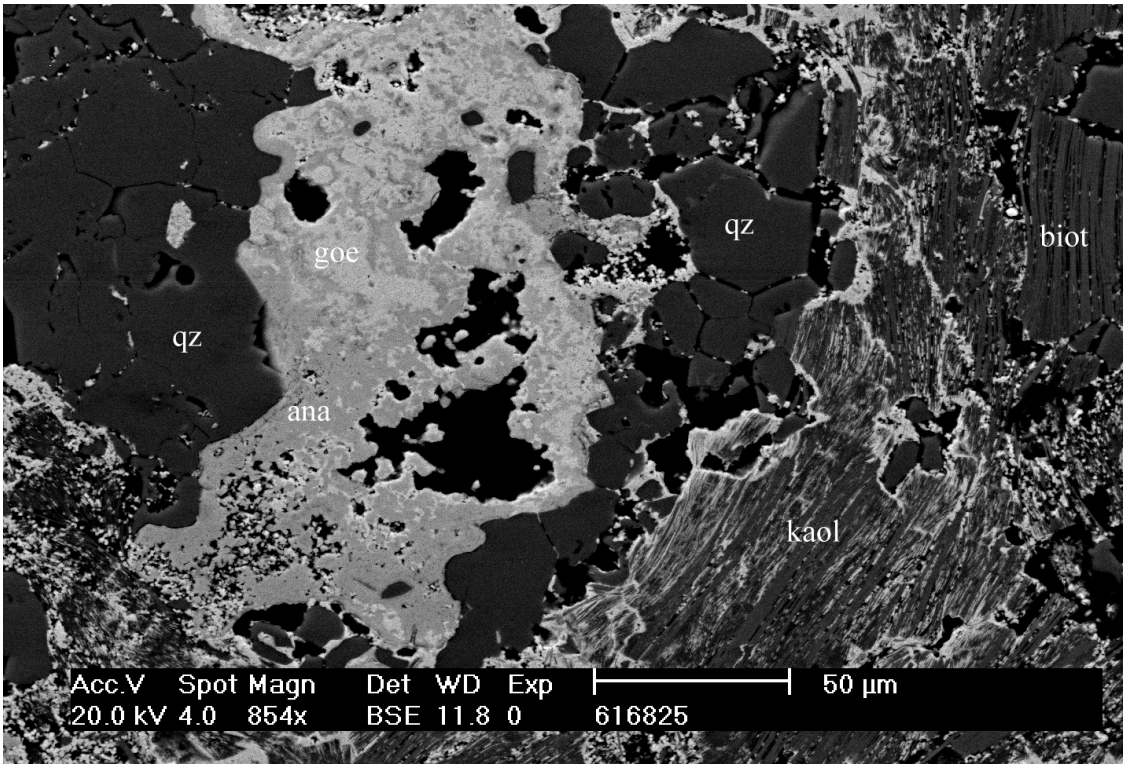

Figure 4.24. Fine-grained intergrowths between anatase (ana) and goethite (goe), associated with kaolinite/halloysite (kaol), quartz (qz) and weathered biotite (biot). Sample 616825, MTG1, 0.50 m depth. Back-scattered electron image (SEM).

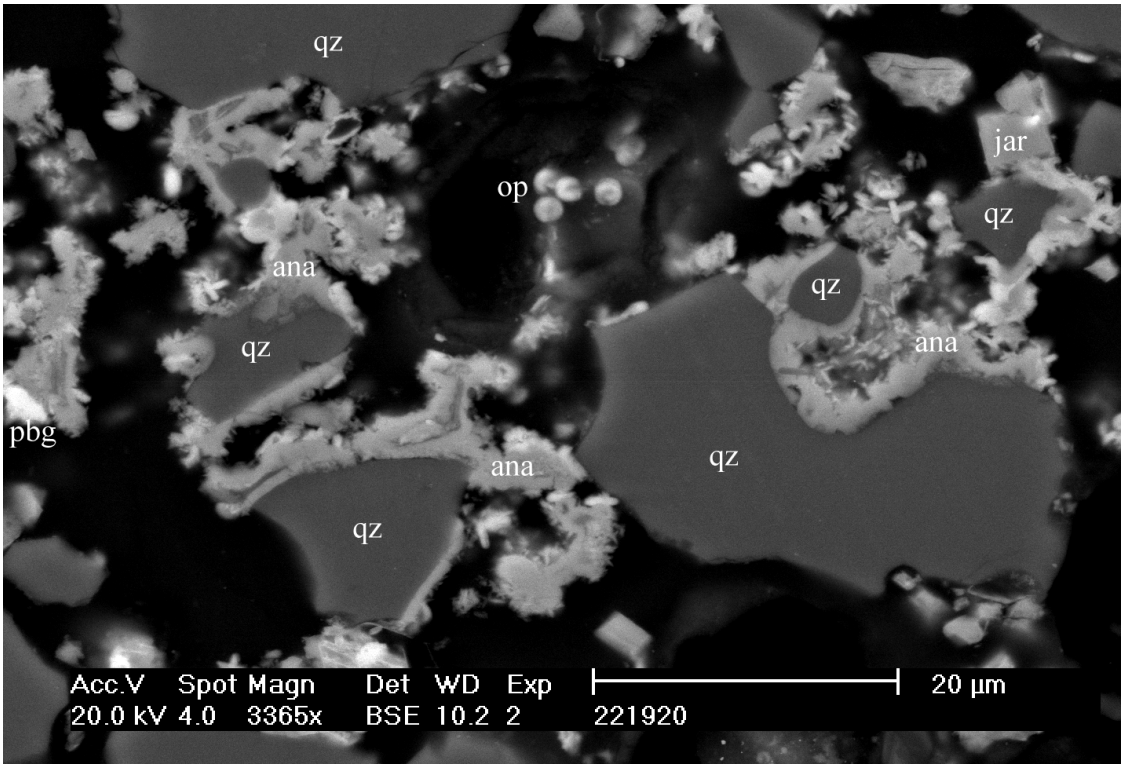

Figure 4.25. Anatase (ana) coatings and aggregates of acicular grains on quartz (qz) grains; note that the quartz exhibits partial dissolution and/or replacement. Minor amounts of jarosite (jar), plumbogummite (pbg) and opaline silica (op) also occur. Sample 221920, MTG4, 9.40 m depth. Back-scattered electron image (SEM).

Fe oxides

Goethite and hematite (with some substituted Al) are relatively abundant in gossan and saprolite. They occur as:

(i) concentrically zoned or banded boxworks after sulfides (dominantly pyrite; Figure 4.26), comprising alternating bands of Fe oxides with minor kaolinite/halloysite, and kaolinite/halloysite-rich bands with relatively minor Fe oxides;

(ii) boxworks after sulfides, forming lattices (Figure 4.27), locally filled in by barite, iodargyrite and mixtures of goethite and kaolinite/halloysite;

(iii) weathering product of mafic minerals (e.g., biotite; Figure 4.28);

(iv) complex intergrowths of goethite with anatase (Figure 4.24);

(v) goethite-kaolinite/halloysite mixtures, typically in weathered metasiltstones (e.g., Figures 4.16 and 4.23), or filling boxworks in gossans (Figure 4.26).

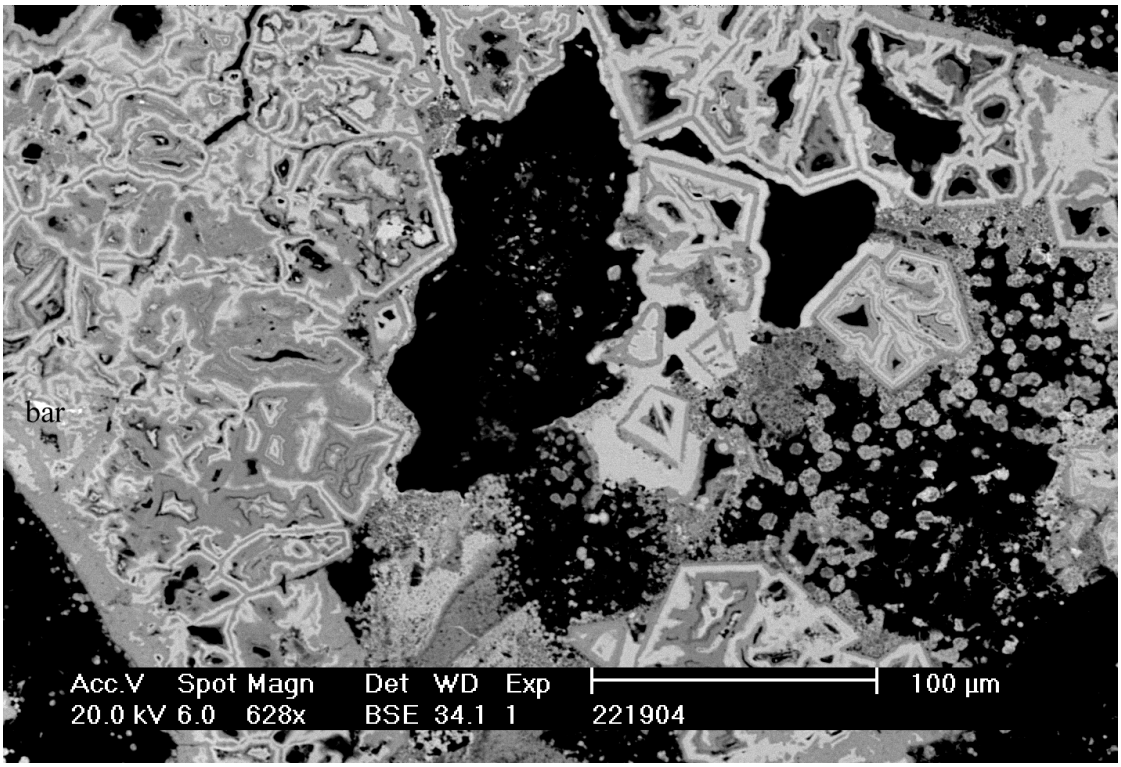

Figure 4.26. Concentrically zoned boxworks after pyrite, comprising alternating zones of goethite (brighter) and goethite with kaolinite/halloysite (darker). A small grain of barite (bar) fills a small cavity. Sample 221904, MTG3, 2.95 m depth. Back-scattered electron image (SEM).

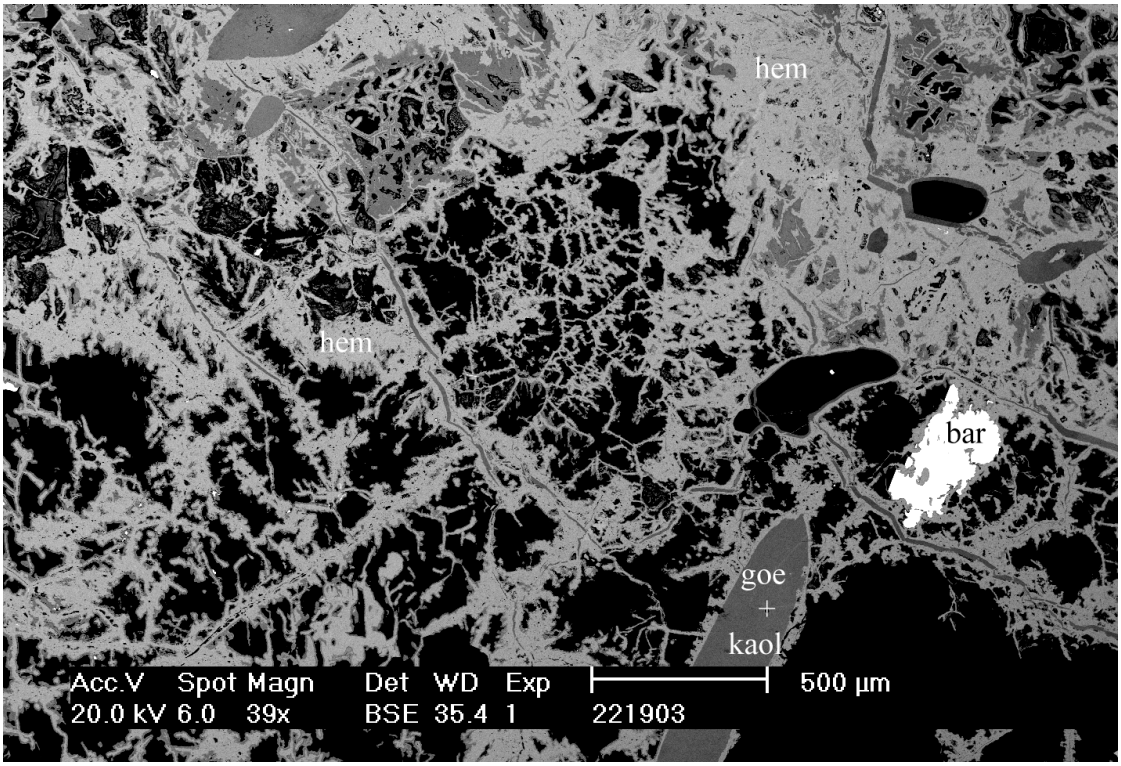

Figure 4.27. Boxworks after pyrite, comprising a latticework of hematite (hem), locally filled by barite (bar) or goethite and kaolinite/halloysite (goe+kaol). Sample 221903, MTG3, 1.95 m depth. Back-scattered electron image (SEM).

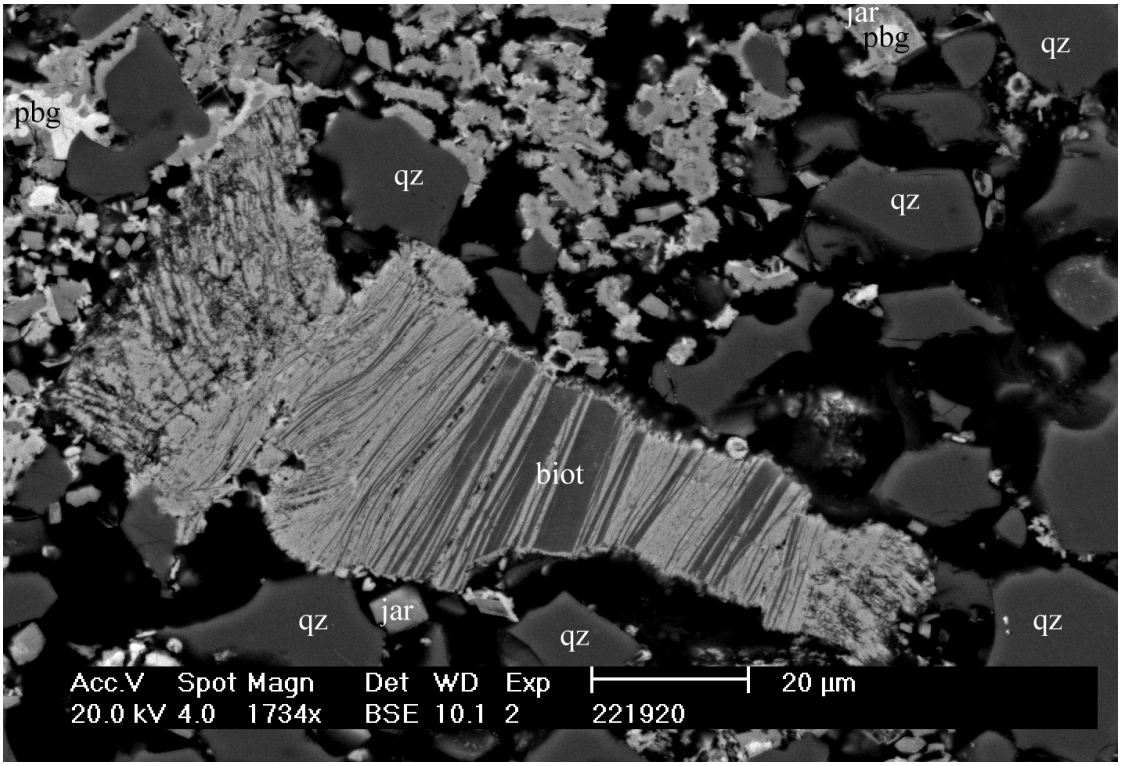

Figure 4.28. Weathered biotite (biot) grain, comprising alternating lamellae that are kaolinite/halloysite-rich (darker) and Fe oxide-rich (brighter), associated with quartz (qz) and minor jarosite (jar) and plumbogummite (pbg). Sample 221920, MTG4, 9.40 m depth. Back-scattered electron image (SEM).

Relict minerals

In rare instances, relict minerals occur in the gossan and saprolite, where they have been protected from weathering by inclusion within quartz grains (e.g., galena, molybdenite) or within Fe oxides (e.g., hyalophane; Figure 4.6).

4.3.3. Regolith profile through the Nairne Pyrite Member

Selected mineralogical variations in the regolith profile through the Nairne Pyrite Member in diamond drill hole MTG2 are shown in Figure 4.29. Although the abundances of the minerals are based on peak heights determined from XRD patterns, the relative distributions of the minerals are in reasonable agreement with visual observations made on the drill core. The weathered section of metasiltstone comprises white kaolinitic/halloysitic saprolite to saprock with ferruginous staining and common boxworks after pyrite. The contact with fresh rock is very sharp and is marked by the presence of pyrite and lack of orange-brown staining in the fresh material.

Quartz occurs in relatively constant amounts throughout the regolith and fresh rock. Pyrite, scapolite and biotite are restricted to fresh rock, although the feldspars, particularly microcline, persist into the regolith (possibly through armouring by Fe oxides; Figure 4.6). The alteration of scapolite to kaolinite/halloysite (Scott et al., 1979) associated with the occurrence of iodargyrite and cerargyrite (Sylvester, 1978b) is consistent with the release of halides from the breakdown of scapolite. The alteration of biotite to kaolinite/halloysite rather than vermiculite or montmorillonite may be indicative of relatively low pH (Scott et al., 1979).

Goethite, hematite, kaolinite/halloysite and jarosite occur only in the regolith. Jarosite is restricted to lower portions of the regolith, presumably where relatively acidic conditions prevailed due to oxidising pyrite.

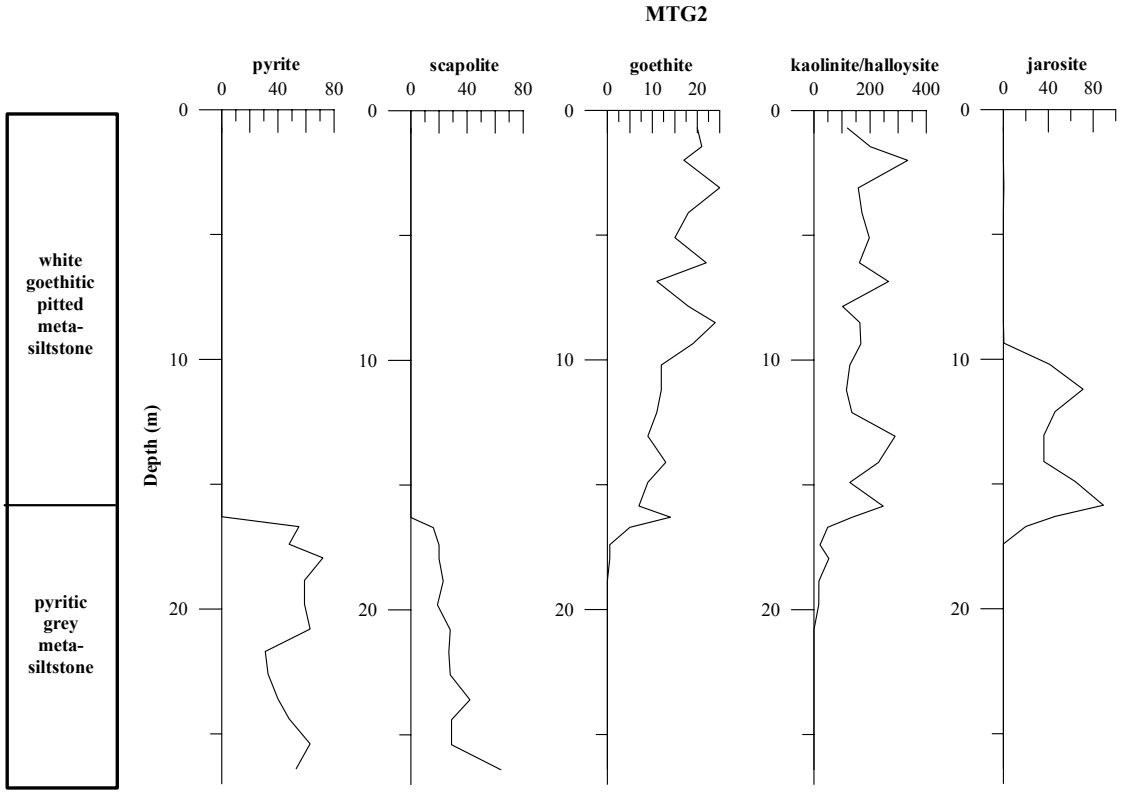

Figure 4.29. Qualitative mineralogical profiles for selected minerals through the Nairne Pyrite Member, diamond drill hole MTG2 (data from Scott et al., 1979). Profiles for the other minerals are shown in Appendix 10.

4.4 Acid sulfate soils with Fe- and Al-rich surface precipitates and crusts

4.4.1. Acid sulfate soils

In their natural state, acid sulfate soils (also termed potential acid sulfate soils (PASS)): (a) contain black sulfidic materials, are waterlogged, anaerobic and exist under reducing conditions at near-neutral pH; (b) have high organic content (up to 2.71 % organic C in the Herrmanns-Dairy Creek materials; Bonifacio et al., 2002); and (c) contain pyrite (typically framboidal; Figure 4.32; Fitzpatrick et al., 1996). They occur at the surface in wetlands or seeps, or are buried beneath alluvium (Figures 4.30 and 4.31). They consist of fine-grained quartz with variable amounts of pyrite, kaolinite/halloysite, albite, microcline, muscovite and monazite.

However, when these sulfidic materials are exposed to air by drainage or excavation, they become strongly acidic (pH <4) and are called actual acid sulfate soils (ASS) and contain sulfuric horizons (Fitzpatrick et al., 1996). The source of acid sulfate conditions is pyrite, which when oxidised generates sulfuric acid, thereby decreasing the pH to less than 3.5 (Table 4.2; Fitzpatrick et al., 1996). Acid sulfate soils generally have bright yellow or straw-coloured mottles of jarosite/natrojarosite and sideronatrite (Figures 4.35 and 4.36). In rare instances, they also contain plumbojarosite (Figure 4.34) and plumbogummite where they overlie mineralised zones in bedrock. Sulfuric acid may leak into drainage and floodwaters, corrode steel and concrete, and attack clay, liberating soluble aluminium, which is toxic to vegetation and aquatic life. Heavy metal contaminants (e.g., As), soluble at low pH, are transported off-site and impact on water and soils.

Figure 4.30. An exposure of black sulfidic material in buried acid sulfate soil in a bank section in Dairy Creek. The regolith sequence comprises relatively young sandy alluvium (with a thin soil horizon) overlying older relatively-clay-rich alluvium with thin gravel layers, which may contain fragments of bright yellow oxidised sulfidic materials containing sideronatrite and jarosite (pH <3.5). The sulfuric horizon overlies the black sulfidic materials and saprolite (derived from Tapanappa Formation lithologies). Note the white salt efflorescences (halite, gypsum) just above the water line.

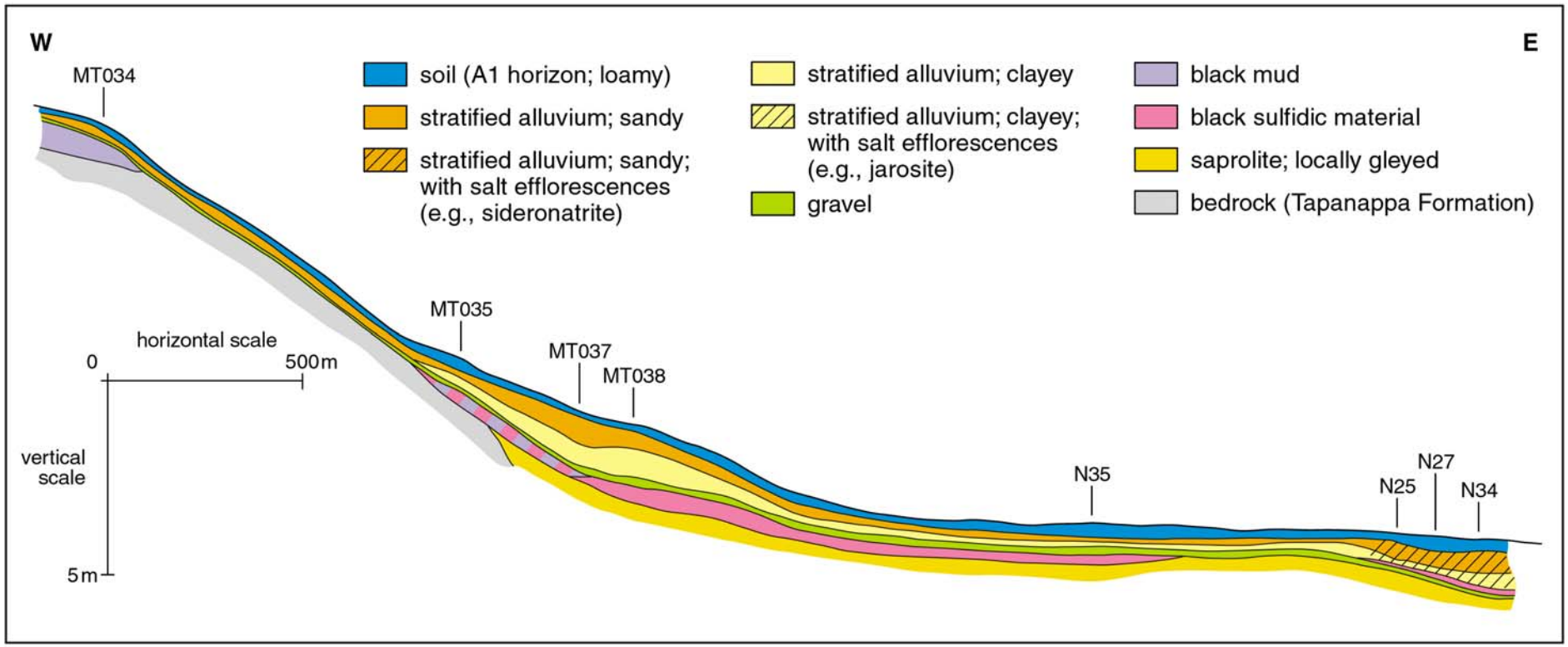

Figure 4.31. Schematic cross-section along Dairy Creek showing distribution of black sulfidic materials and/or black muds and location of sampling sites.

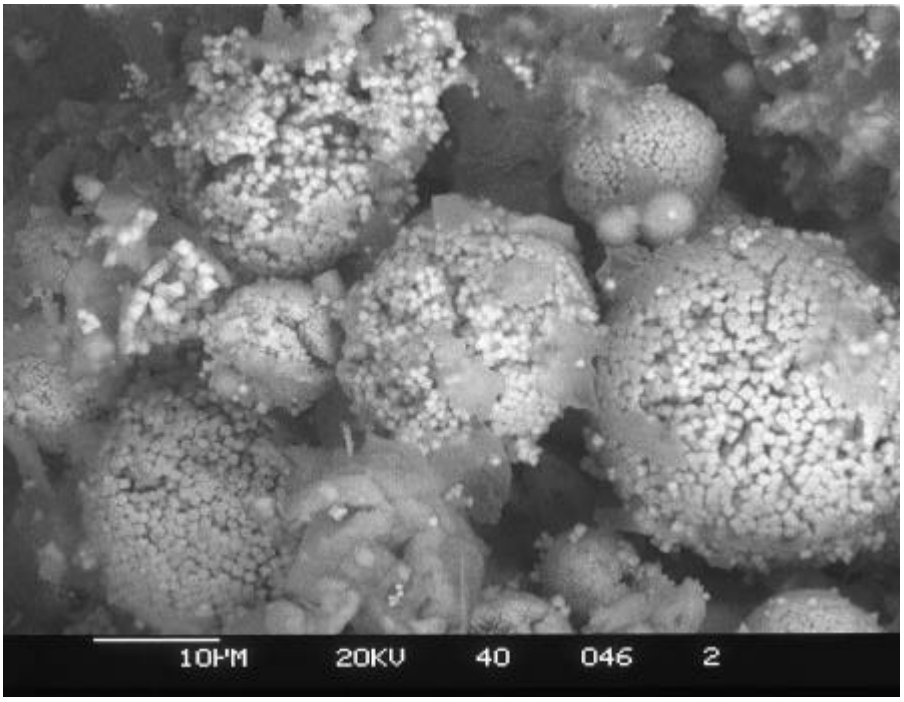

Figure 4.32. Back-scattered electron image (SEM) of sulfide framboids (spheroidal aggregates of pyrite crystals) in sulfidic material (i.e., potential acid sulfate soil or PASS; pH 7-8) in the southern bank of Dairy Creek shown in Figure 4.30.

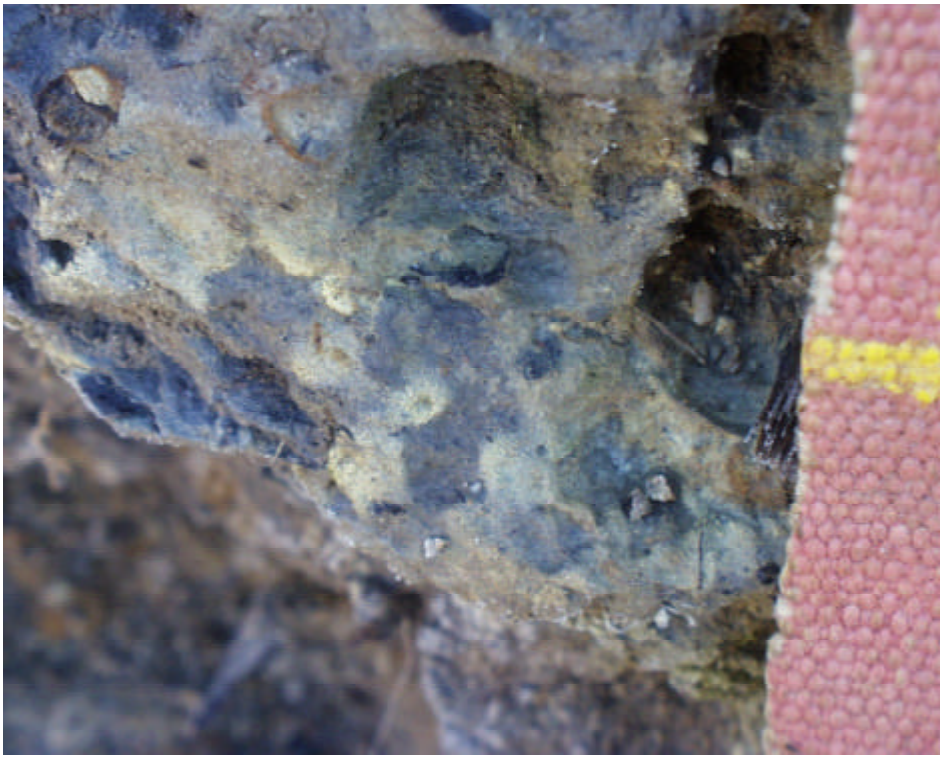

Figure 4.33. Pale yellow jarosite mottling (developed from the weathering of pyrite) in a sulfuric horizon overlying sulfidic materials, Dairy Creek. Profile N27 (see Figure 4.31).

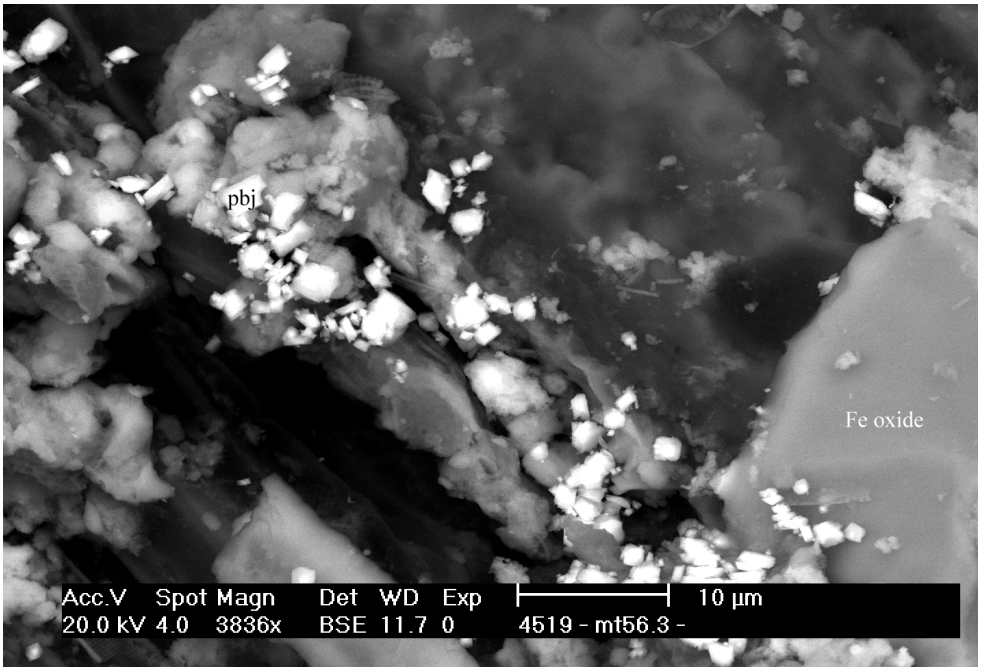

Figure 4.34. Plumbojarosite (pbj) crystals associated with Fe oxides in partially oxidised sulfidic material (sulfuric horizon), Herrmanns Creek. Sample MT056.3. Back-scattered electron image (SEM).

4.4.2. Iron - and Aluminium -rich surface precipitates

Acid leachate from acid sulfate soils dissolves clay minerals and oxidises Fe sulfides to produce hydrated white and red-brown precipitates via biogeochemical reactions (Fitzpatrick et al., 1992) depending upon pH (Figure 4.35). The white precipitate in Figure 4.35 is composed dominantly of Al_2O_3 (42%), SiO_2 (8.283%), SO_3 (7.16%), As (<5ppm) and Na_2O (1.074%). Transmission electron analyses (TEM) and XRD suggest that it is an amorphous hydrated aluminium oxyhydroxide (with some evidence for pseudoboehmite-like characteristics). The red-brown precipitates (ferrihydrite, goethite and schwertmannite) are rich in Fe (35.6%), Mn (0.5%) and As (135ppm). It appears that As is preferentially scavenged by iron oxides.

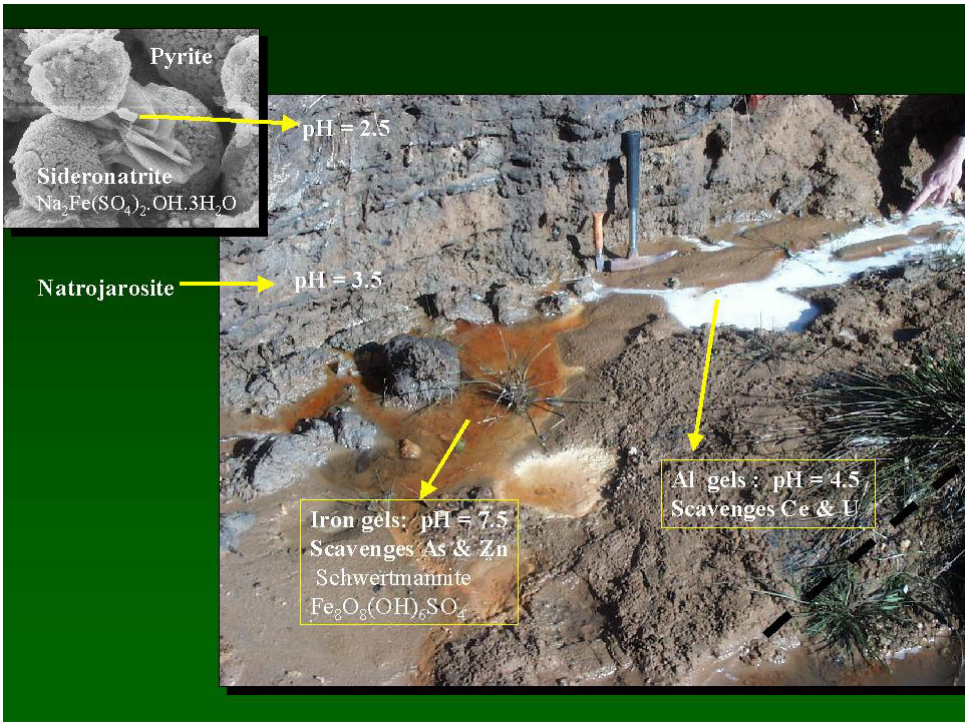

Figure 4.35. A highly saline actual acid sulfate soil (ASS) exposed along upper Dairy Creek and consisting of a sulfuric horizon (pH 2.5-3.5) overlying sulfidic material (potential acid sulfate soil or PASS; pH 7-8) beneath the exposed horizons in the bank. The white precipitate is Al-rich and preferentially forms in sandy layers (pH 4.5), whereas the red-brown precipitates are Fe-rich and preferentially form in clay-rich materials (pH 7.5). The inset shows a SEM image of sideronatrite [$Na_2Fe(SO_4)_2.OH.H_2O$] (large platelets) derived from the oxidation and dissolution of the sulfide framboids in an acid sulfate soil. Adjacent to profile N27 (see Figure 4.31).

Figure 4.36. A highly saline actual acid sulfate soil (ASS) exposed along upper Dairy Creek and consisting of a sulfuric horizon (pH 2.5-3.5) showing green crystals of sideronatrite [$Na_2Fe(SO_4)_2.OH.H_2O$] formed in sandy layers and derived from the oxidation and dissolution of the sulfide framboids. Profile N25 (see Figure 4.31).

Table 4.2. Redox reactions in potential and actual acid sulfate soils.

If potential acid sulfate soils (PASS) are drained, or otherwise exposed to aerobic conditions (earthwork excavations), the sulfides in these materials will oxidise to form reactive sulfuric acid and Fe^{2+} will undergo hydrolysis, as follows:

$FeS_2 + 7/2\ O_2 + H_2O \rightarrow Fe^{2+} + 2SO_4^{2-} + 2H^+$ .....[1]

$FeS_2 + 15/4\ O_2 + 7/2\ H_2O \rightarrow Fe(OH)_3 + 2SO_4^{2-} + 4H^+$ ...[2]

However, these reactions greatly simplify the description of pyrite oxidation, which includes several redox reactions, hydrolysis and complex ion formation, solubility controls, as well as kinetic effects. The initial oxidant of pyrite is O_2 and elemental sulfur is produced:

$FeS_2 + 3/4\ O_2 + 3/2\ H_2O \rightarrow Fe(OH)_3 + 2S$ .....[3]

the oxidation of elemental sulfur produces acidity:

$2S + 3O_2 + 2H_2O \rightarrow 2SO_4^{2-} + 4H^+$ .....[4]

As the pH decreases to below 3.5, which allows Fe^{3+} to remain in solution, Fe^{3+} becomes the dominant oxidant:

$FeS_2 + 14Fe^{3+} + 8H_2O \rightarrow 15Fe^{2+} + 2SO_4^{2-} + 16H^+$ .....[5]

This reaction is biologically mediated by some thiobacilli, such as *Thiobacillus ferroxidans*, which functions well under highly acidic conditions to oxidise most reduced forms of sulfur, including sulfides. *Thiobacillus ferroxidans* can also grow by oxidation of Fe^{2+}. The activity of such organisms results in an acceleration of the rate of pyrite oxidation. It is possible that the supply of Fe^{3+} had to build up to a certain level before the bacteria became active.

4.4.3. Iron-rich surface (hardened) crusts

The compositions of the thin (2-5 mm thick) iron oxide-rich crusts (Figure 4.37), which form on soil surfaces as a consequence of wetting-drying cycles, are variable. In general, they are composed of schwertmannite, ferrihydrite and goethite and are derived from the oxidation and dissolution of the sulfide framboids in the acid sulfate soils (Fitzpatrick et al., 1992, 1996). Compared to background soils, these crusts have higher concentrations of Fe, S, P, As, Ba, Na, Pb, Zn (locally) and REE.

Figure 4.37. Iron-rich crust composed of schwertmannite, ferrihydrite and goethite derived from the oxidation and dissolution of the sulfide framboids in an acid sulfate soil from Guthries. The layers are described in Figure 5.18.

5. GEOCHEMISTRY

5.1 Sampling

A variety of regolith types was sampled (see section 2.2). Except for ferruginous saprolite, saprolite, black sulfidic mud, clays, sand and loam, most sample populations are small, owing to the relatively restricted distribution of some regolith types. For the purposes of determining geochemical dispersion around the Mount Torrens mineralisation, ferruginous saprolite, gossans, black sulfidic mud, and Fe- and Al-oxide precipitates (gels) were deemed to be the most useful, on the basis of their spatial distribution with respect to the mineralised zone and element distributions in box plots (Appendix 8).

5.2 The ore zone in bedrock

The compositions of three samples of fresh sulfidic calc-silicate rock (two containing sphalerite, the other galena-rich) are shown in Appendix 5 (element plots) and Appendix 8 (box plots). These samples generally have relatively large concentrations of Ca, Mn, Na, Ag, As, Cd, In, Mo, Pb, Sb, Te, Tl and Zn, and relatively minor Ti, REE, V and Zr contents. Relative to the galena-rich sample, the sphalerite-bearing samples are enriched in Ca, Mn, As, Au, Cd, Cu, In, Mo, Ni, S, Se, Sr and Zn, and depleted in Si, Al, Na, Ba, Zr, Ag, Sb and Pb. Compared to most gossans and ferruginous saprolites along the ore horizon, the fresh sulfides generally contain greater concentrations of Ca, Mn, Cd (Figure 5.1), S and Zn (Figure 5.2), but lower concentrations of Cu, Se, U and W (Appendix 8).

5.3 Geochemistry of regolith units

5.3.1 Regolith materials along the ore horizons (gossan, ferruginous saprolite, saprolite, weathered metasiltstone with gossanous zones)

The compositions of these regolith materials are somewhat variable. Compared to most regolith types away from the mineralised horizon, the ferruginous saprolite and saprolite generally have greater concentrations of As, Cu, Mo, Pb and Zn (Figures 5.3-5.5). Saprolite is generally richer in Ba, K and Al than ferruginous saprolite and gossan, but contains lesser Fe, Mo and Cu.

5.3.2 Other regolith materials

The compositions of the other regolith (saprolite and ferruginous saprolite away from the mineralised horizon, ferricrete, sulfidic mud, gravel, black mud, crusts, Fe- and Al-oxide precipitates (gels)) show considerable overlap (see box plots, Appendix 8). There are, however, some exceptions to this:

(i) some gels contain significant concentrations of As, Cd, Tl and Zn;
(ii) saprolites show a bimodal distribution of Ba, Co, Cu, K, Mo, Na, Ni, S, Sn, Ti and Tl; for some elements (Co, Cu, Mo, Ni, S and Tl) this is related to lithology; Co and Ni have greater concentrations in saprolite derived from Tapanappa Formation lithologies than from the Talisker Calc-siltstone, whereas concentrations of Cu, Mo, S and Tl are greater in saprolite derived from the Talisker Calc-silicate.

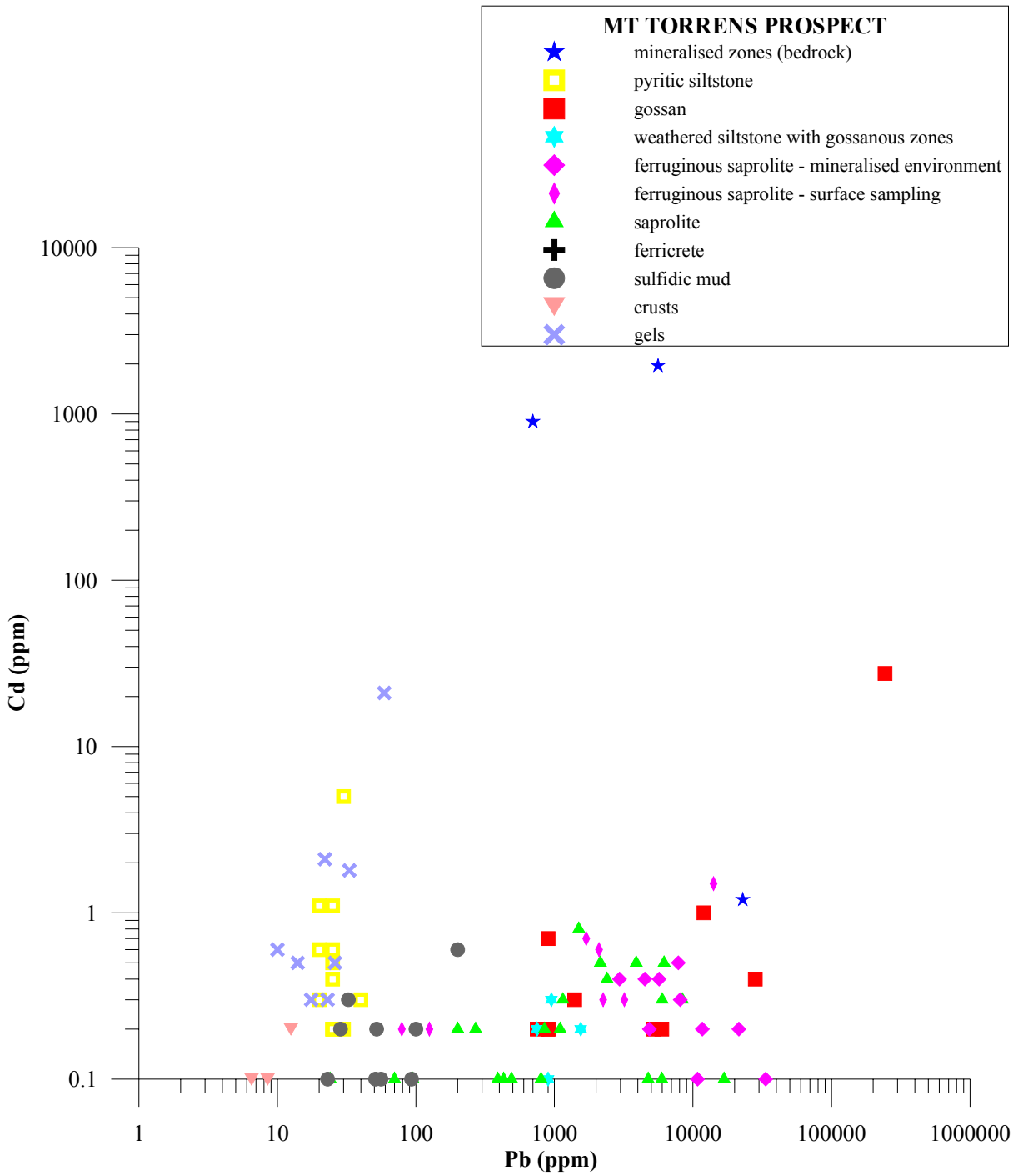

Figure 5.1. Plot of Pb versus Cd.

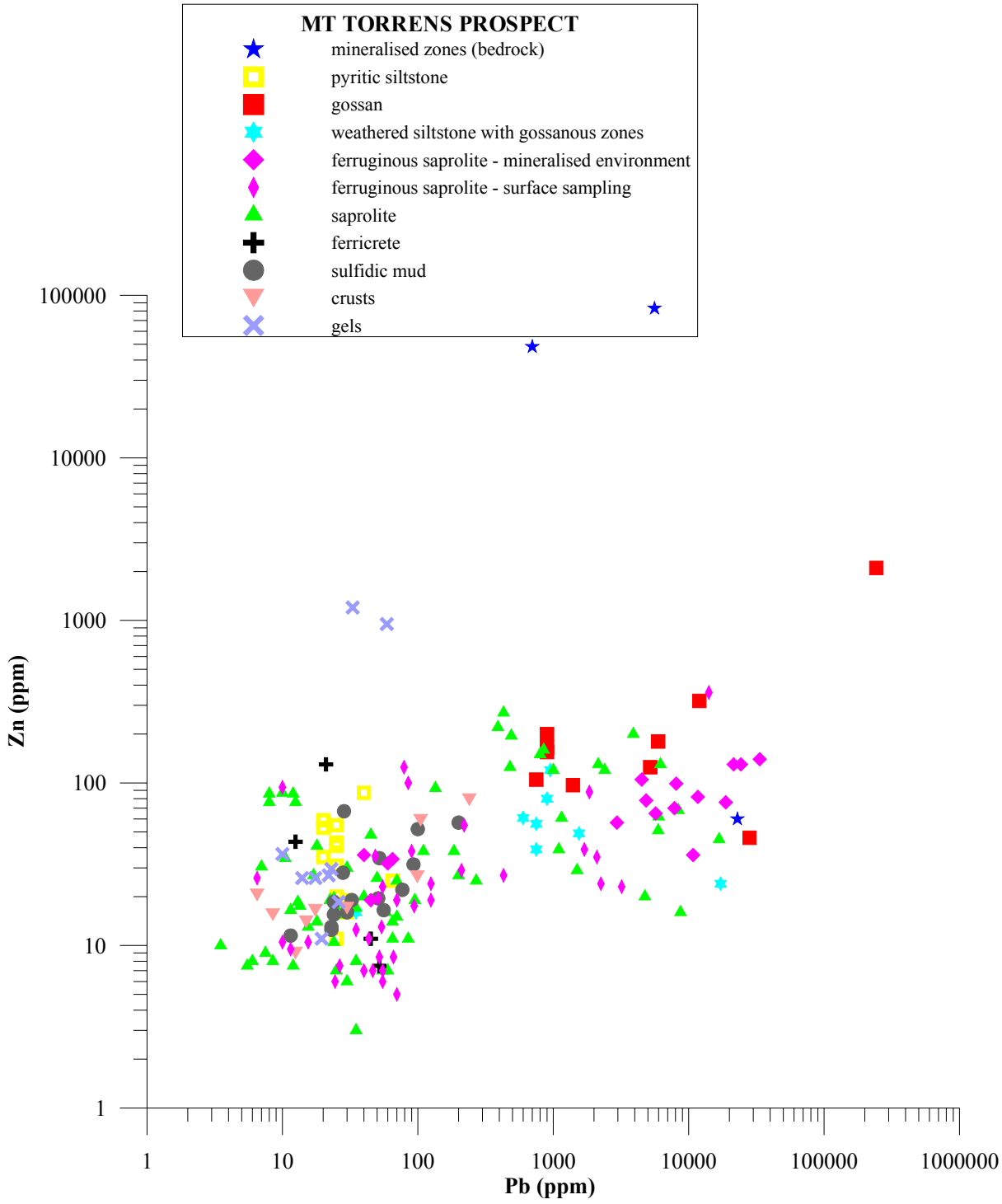

Figure 5.2. Plot of Pb versus Zn.

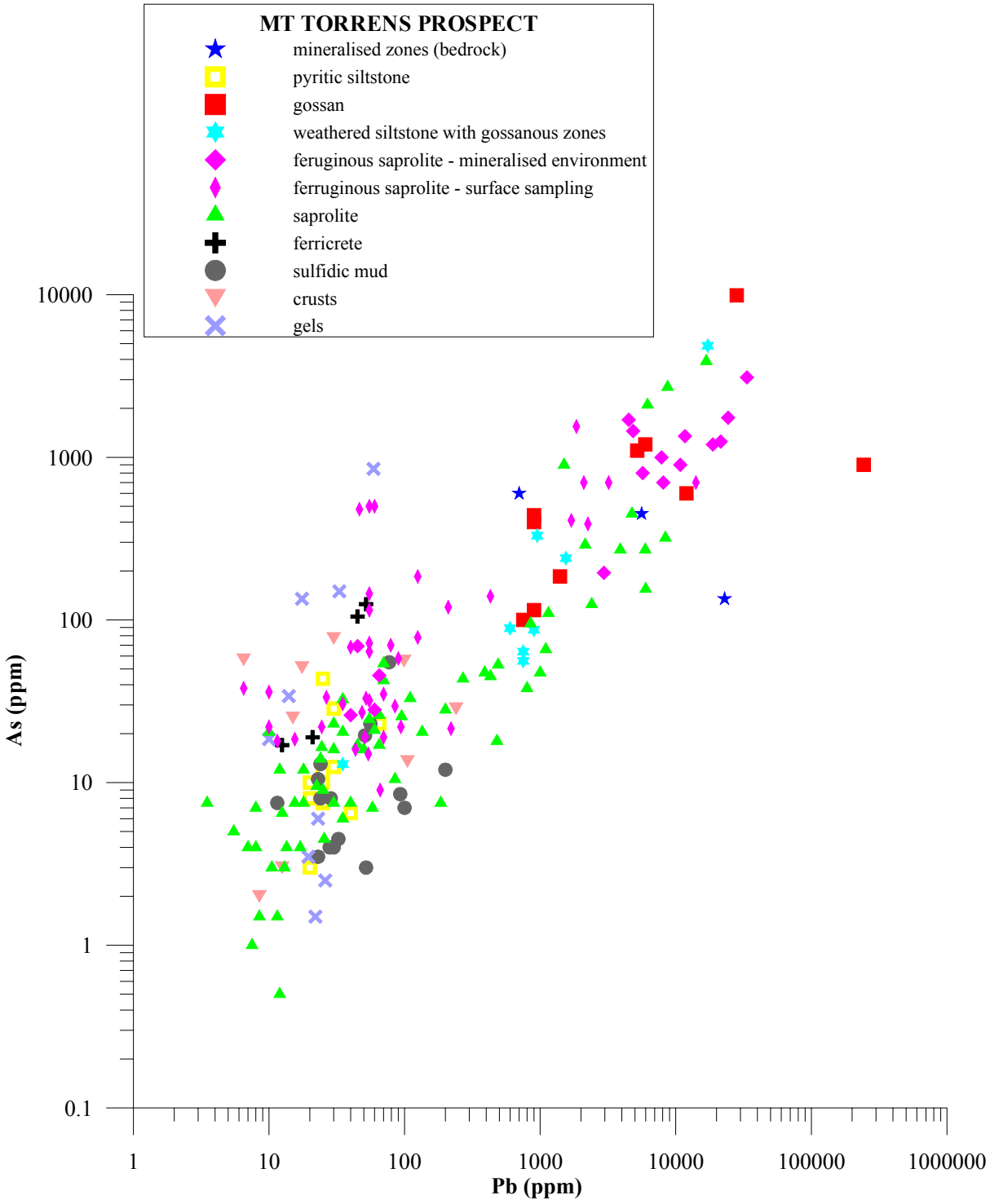

Figure 5.3. Plot of Pb versus As.

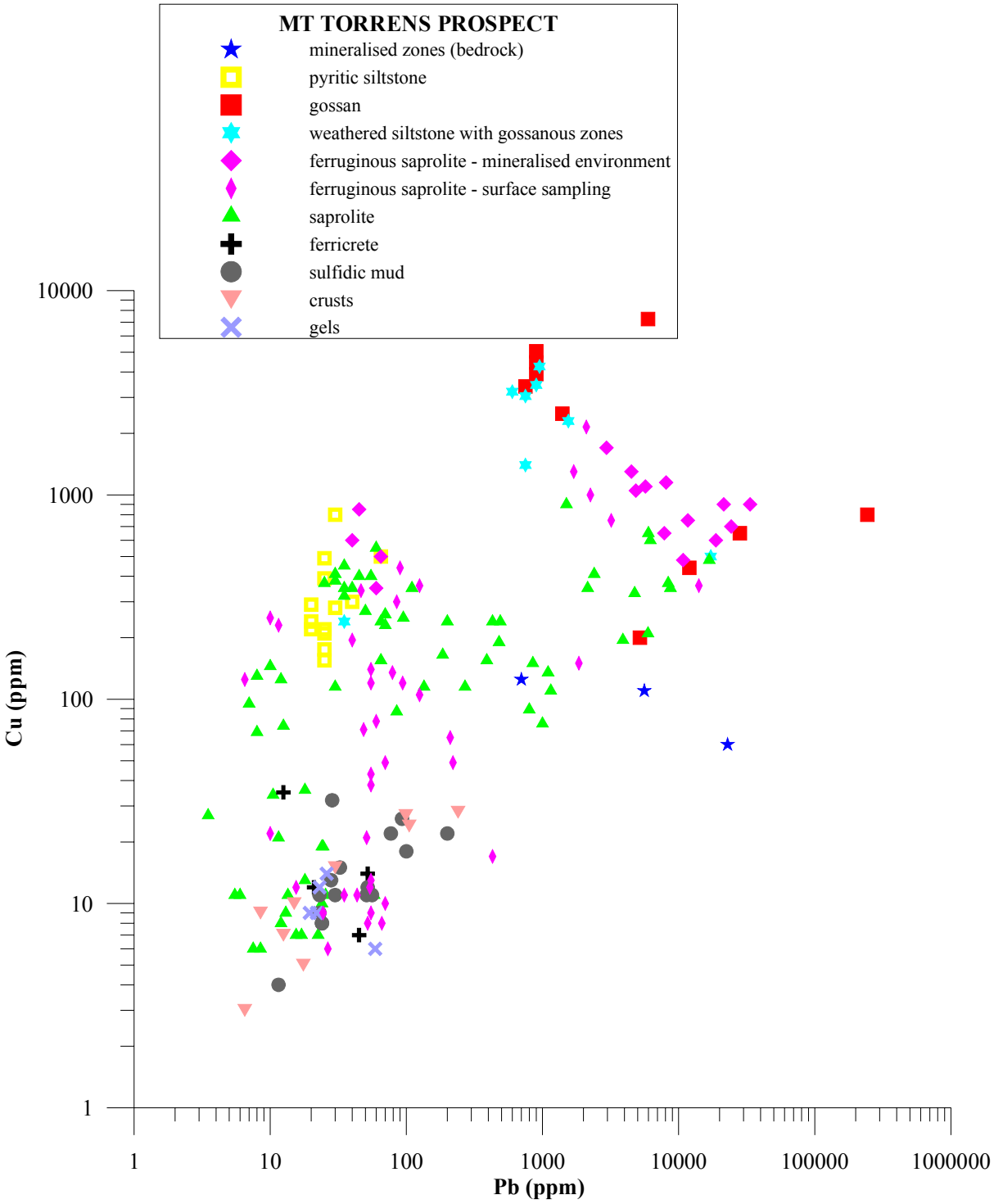

Figure 5.4. Plot of Pb versus Cu.

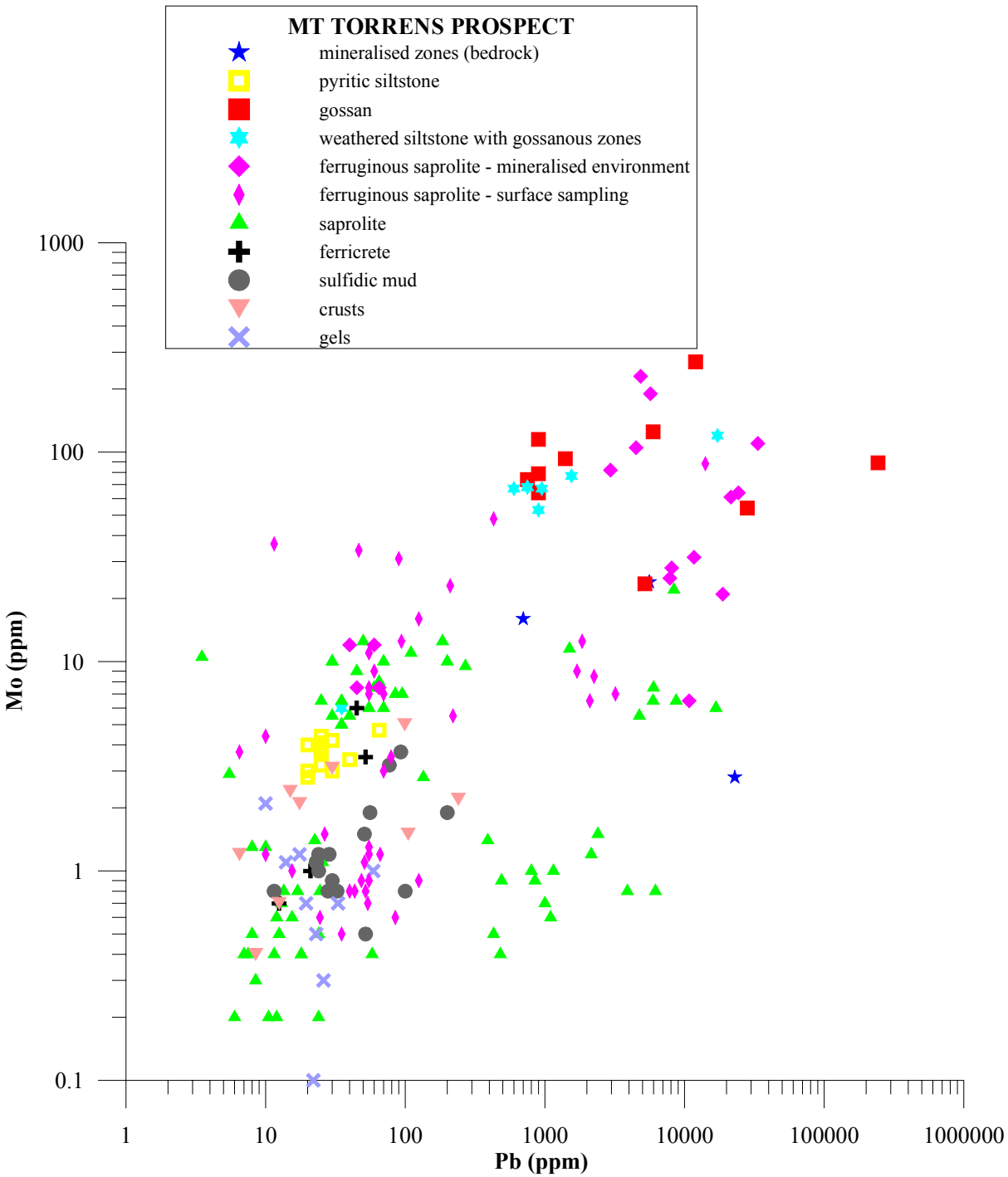

Figure 5.5. Plot of Pb versus Mo.

5.3.3 Geochemical profiles through the Nairne Pyrite Member (MTG2) and gossans (MTG3-4)

The distribution patterns of elements are shown in Appendix 6; selected element profiles are shown in Figures 5.6-5.13. The following general trends are apparent:

(i) Ag, As, Ba, Bi, In, Mo, Pb, Sb and Tl concentrations are higher in gossan and/or weathered metasiltstone than in fresh or weathered Nairne Pyrite Member, reflecting the the greater concentrations of these elements along the mineralised horizon;

(ii) regardless of lithology, Al, Ba, REE, Y, Cr, Cs, Ga, K, Mg, Mn, P, Rb, Sr, Tl, U and Zn concentrations increase with depth, indicating that leaching of these elements has taken place during weathering;

(iii) regardless of lithology, Ag, As, Bi, Cu, Fe, Hf, In, Mo, Se, Th, Ti, V and Zr concentrations decrease with depth; the decreases in Ag, As, Bi, Cu, In, Mo, Se and Th are due to their association with Fe; the greater concentrations of Hf, Ti, V and Zr in regolith are most probably due to residual enrichment following leaching of more mobile components;

(iv) Ca, Cl, Co, Mg, Na, Ni, and S are relatively abundant in fresh bedrock in MTG2, due to the presence of pyrite, scapolite and biotite below the weathering front; the S peak just above the weathering front is due to the presence of jarosite, formed by the oxidation of pyrite; theses elements are relatively strongly depleted above the weathering front due to absence (as a result of weathering) of pyrite, scapolite and biotite;

(v) Ag, Au, Co, Cu, Fe, Mo, Ni, Sn (locally), Te and W concentrations are greater in the gossan than in ferruginous saprolite and saprolite, and may be used to discriminate ferruginous materials derived from mineralisation and from country rocks;

(vi) Al, Hf, K, Nb, P, Rb, Si and V concentrations are less in the gossan than in ferruginous saprolite and saprolite, indicating lesser intrinsic concentrations in the gossan (and unweathered sulfidic zones) than country rocks.

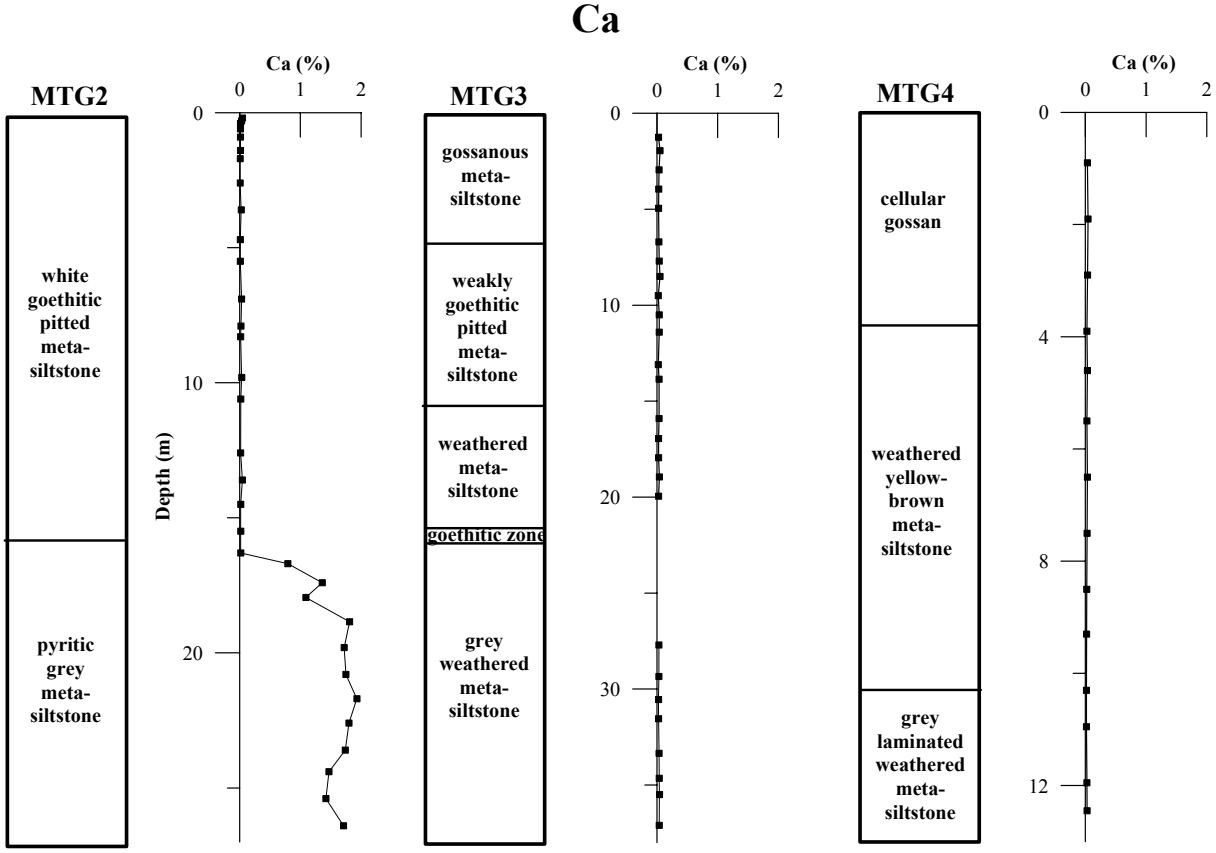

Figure 5.6. Distribution of Ca (%) in regolith and bedrock, MTG2-4.

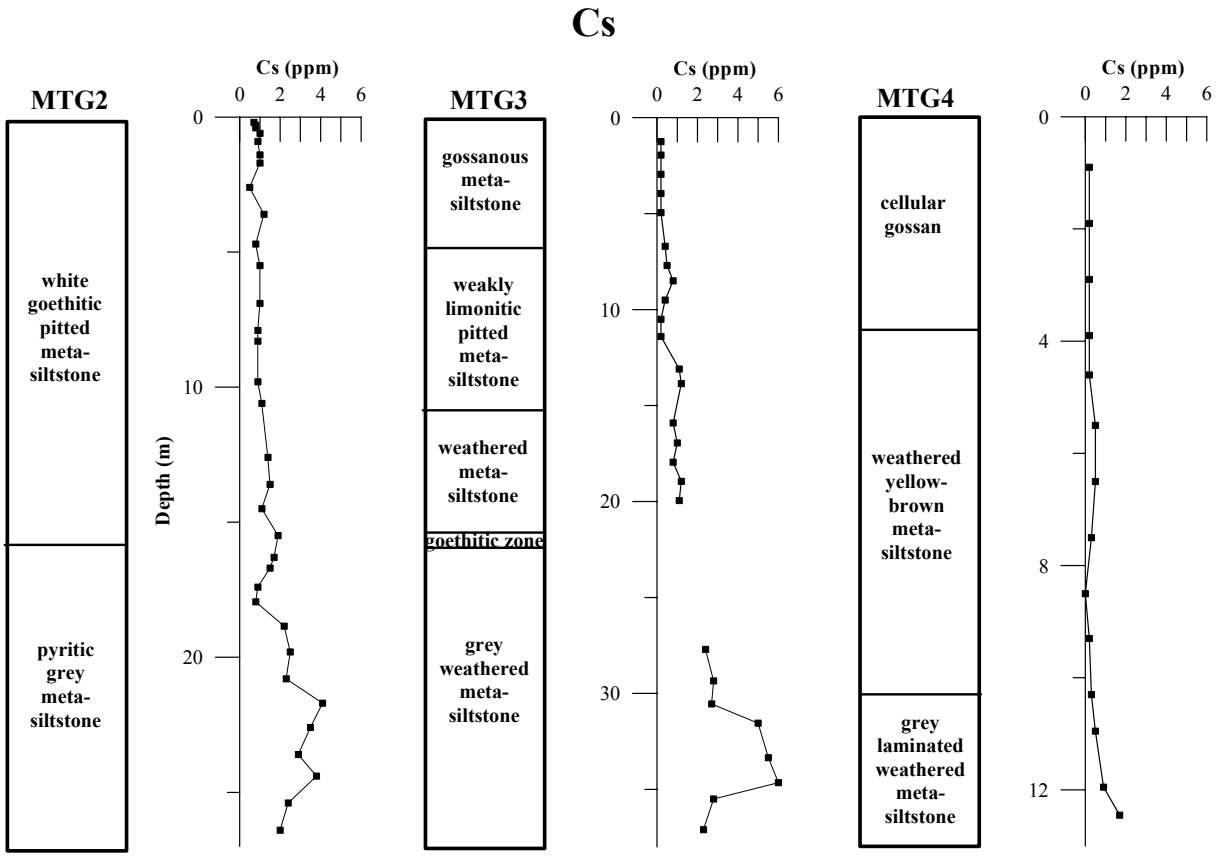

Figure 5.7. Distribution of Cs (ppm) in regolith and bedrock, MTG2-4.

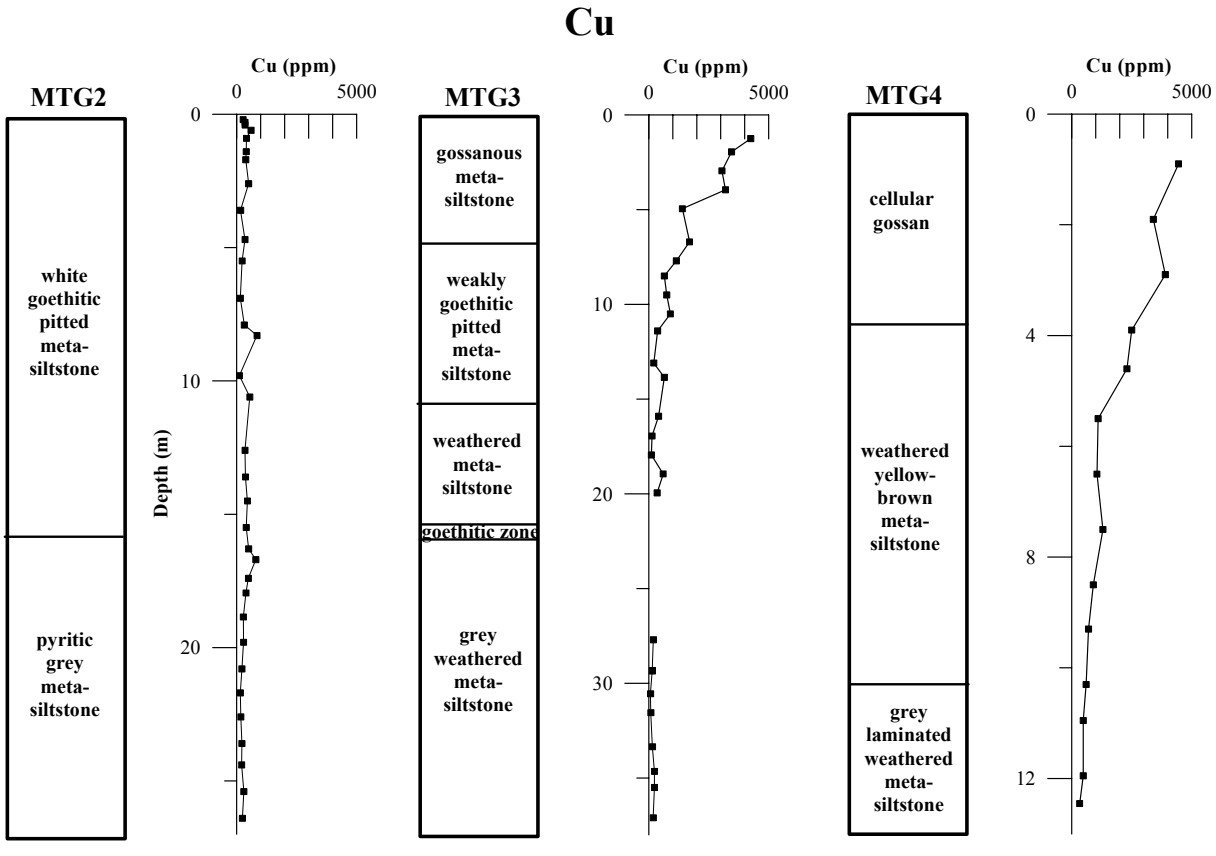

Figure 5.8. Distribution of Cu (ppm) in regolith and bedrock, MTG2-4.

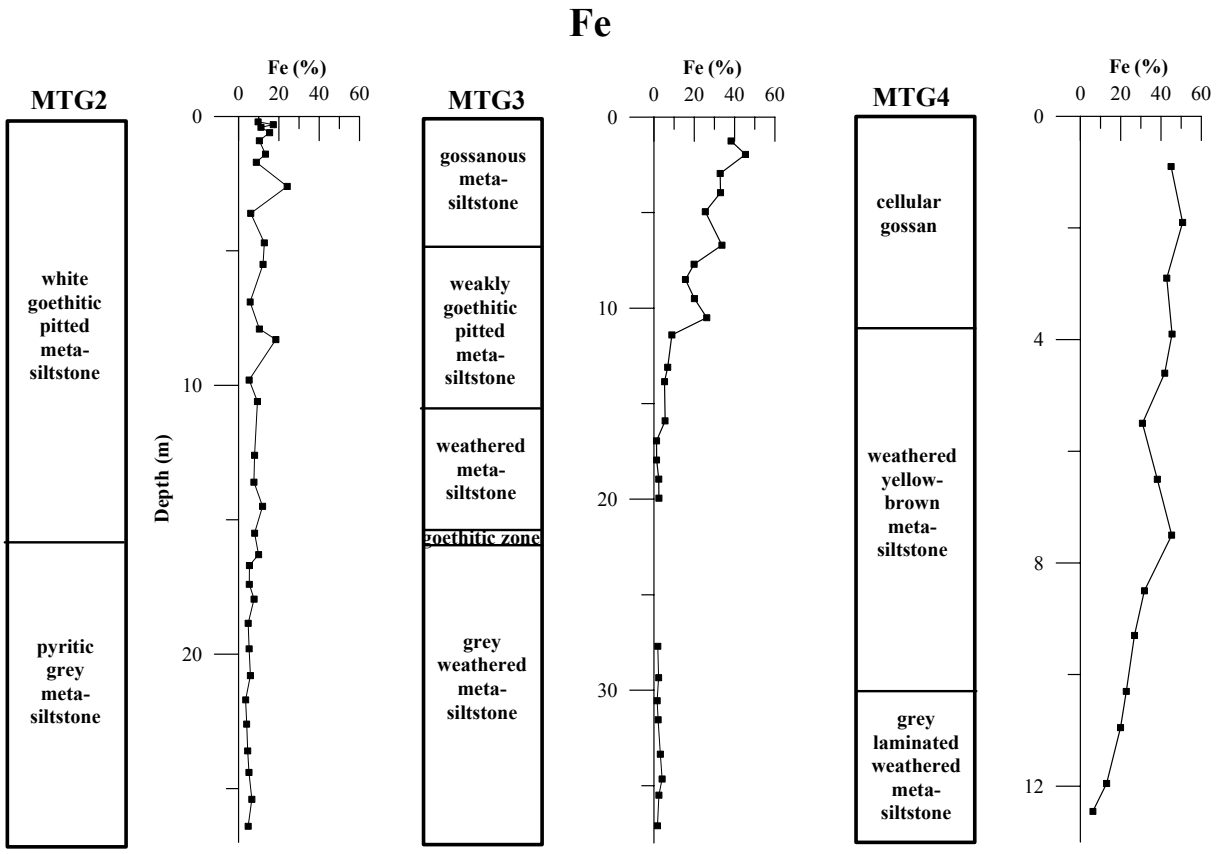

Figure 5.9. Distribution of Fe (%) in regolith and bedrock, MTG2-4.

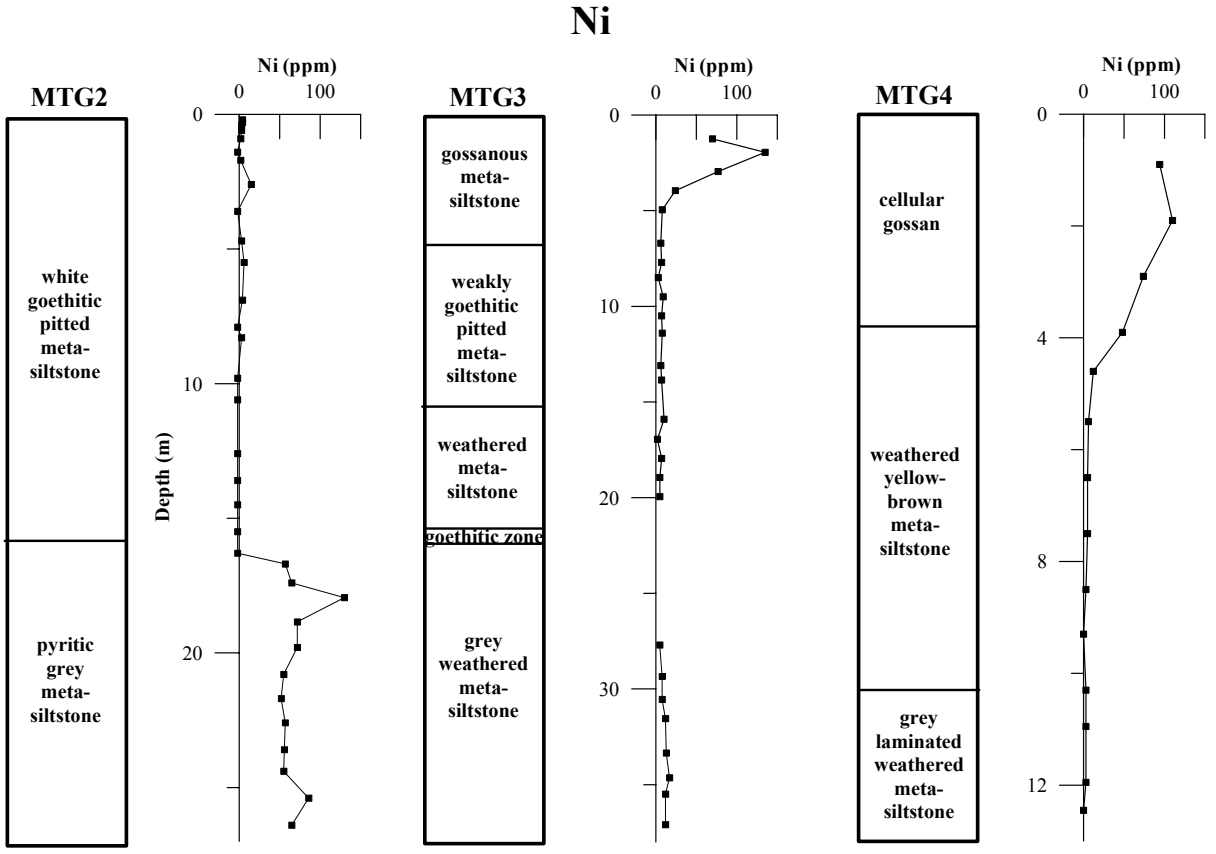

Figure 5.10. Distribution of Ni (ppm) in regolith and bedrock, MTG2-4.

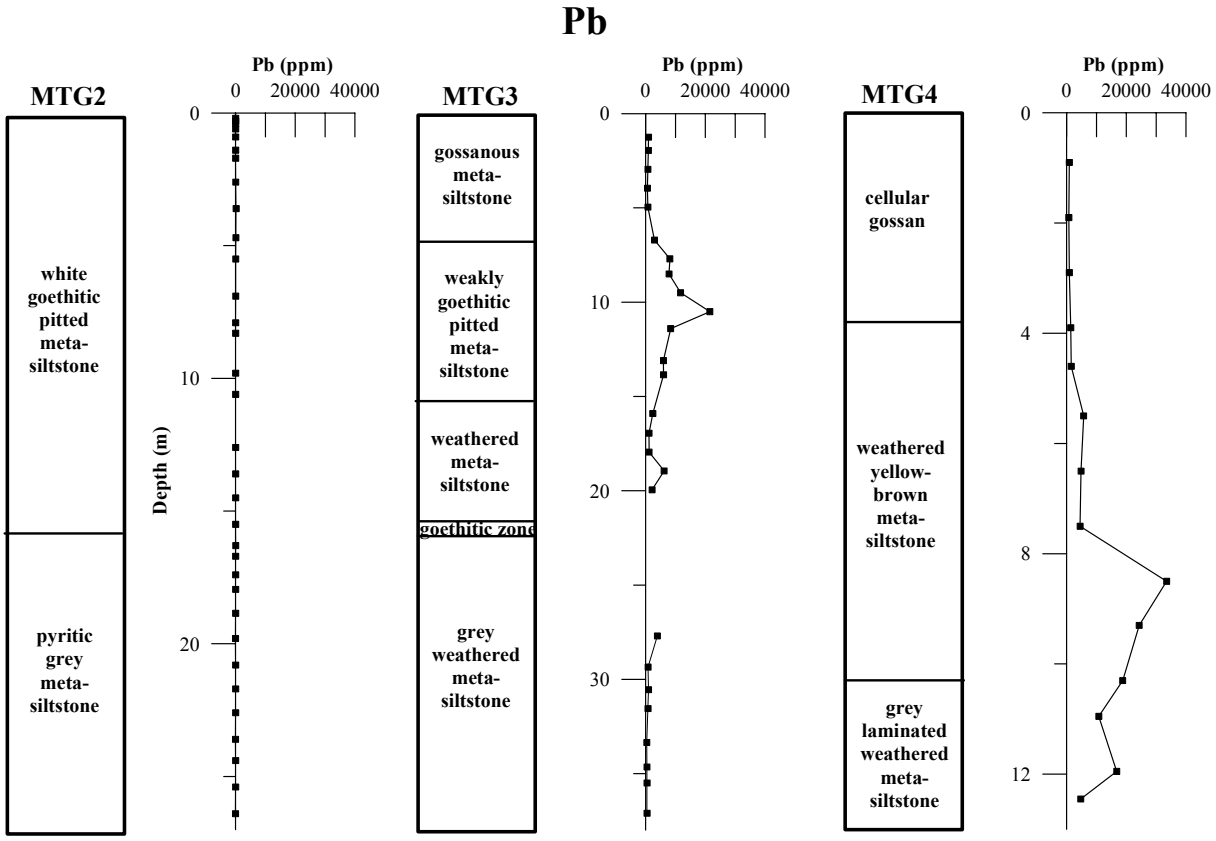

Figure 5.11. Distribution of Pb (ppm) in regolith and bedrock, MTG2-4.

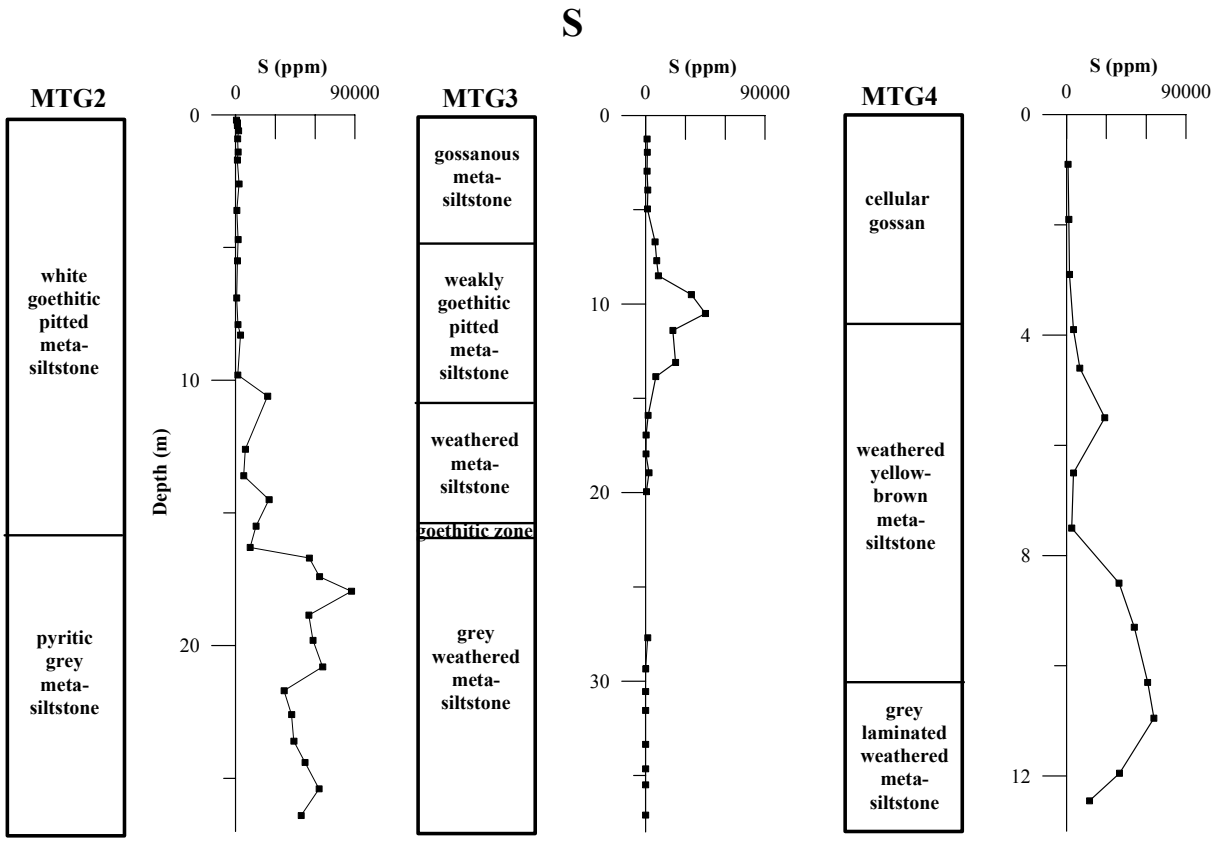

Figure 5.12. Distribution of S (ppm) in regolith and bedrock, MTG2-4.

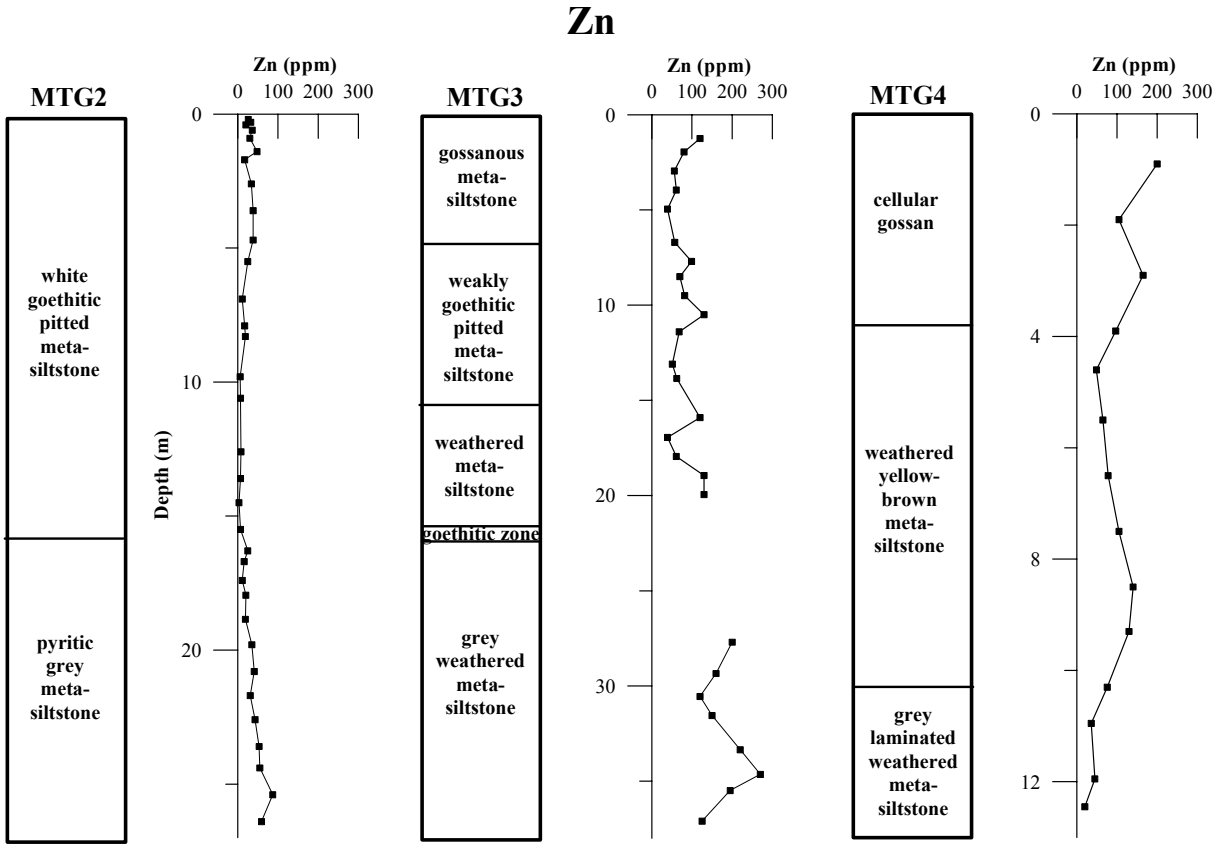

Figure 5.13. Distribution of Zn (ppm) in regolith and bedrock, MTG2-4.

5.3.4 Geochemical dispersion haloes in surface samples

Element distributions in gossan, ferruginous saprolite, sulfidic mud, and Fe- and Al-oxide precipitates (gels) are shown in Appendix 5.

(i) in gossan and ferruginous saprolite, the following elements are found in anomalous concentrations: Ag, As, Au, Ba, Bi, Cd, Cu, Mo, P, Pb, In, S, Sb, Se, Sn, Tl and Zn.

(ii) anomalous concentrations of As, Ba, Bi, Cd, Cu, P, Pb, Sn, Tl and Zn occur in sulfidic materials. The most significant results, in terms of absolute concentrations and location with respect to the mineralised zone, are for Cu, Tl and Zn (Figures 5.14-5.16) in sample MT036.1 from a seep close to outcrops of Tapanappa Formation rocks above the level of Dairy Creek and those seeps along strike of the gossans.

(iii) gels contain anomalous concentrations of As, Ba, Bi, Cd, P, Pb, Sn, Tl and Zn. In particular, the anomalous concentrations of As, Ba, Cd, P, Pb, Sn, Tl and Zn in sample MT055 (Fe oxide gel from a drill hole casing) suggests scavenging of these elements by the gel from groundwater which had circulated through the mineralised zone.

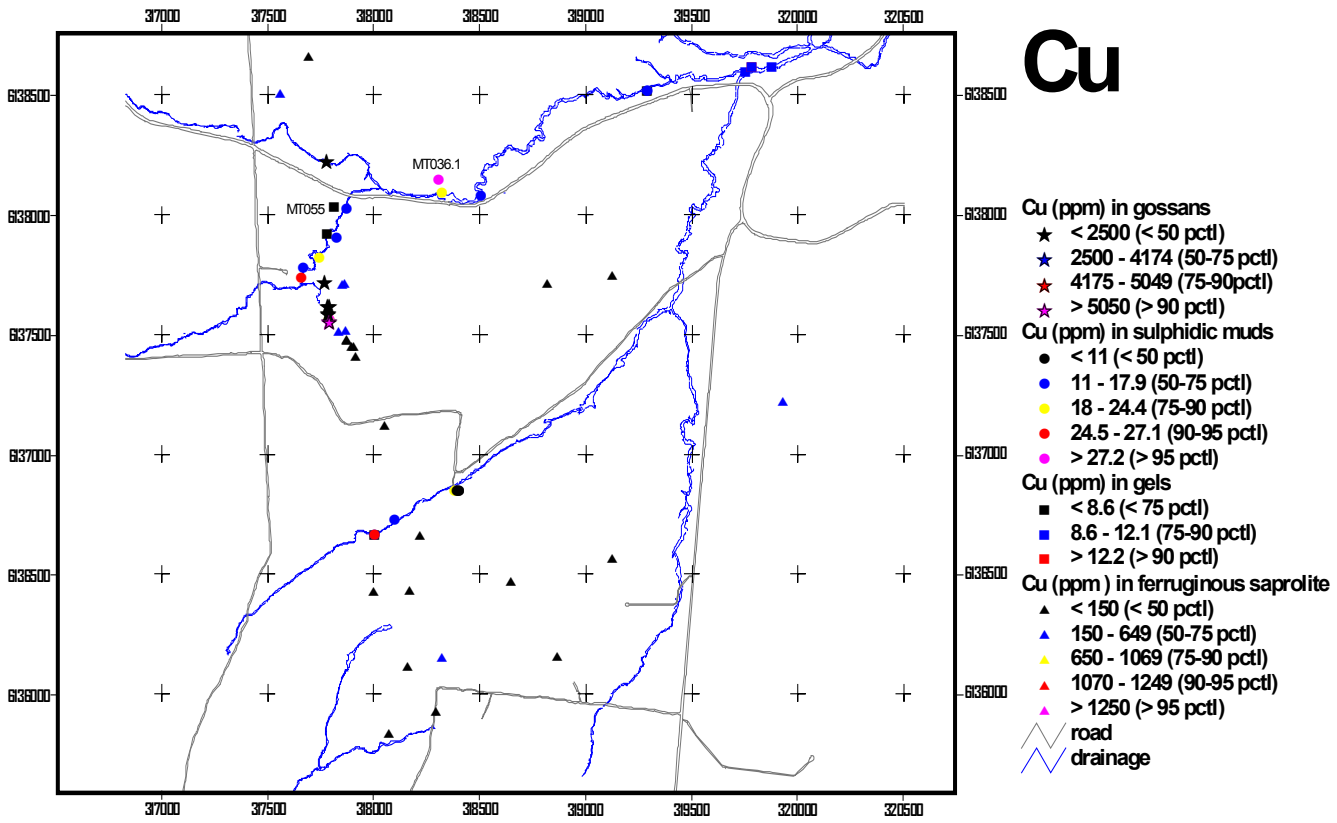

Figure 5.14. Distribution of Cu (ppm) in gossans, sulfidic mud, gels and ferruginous saprolite.

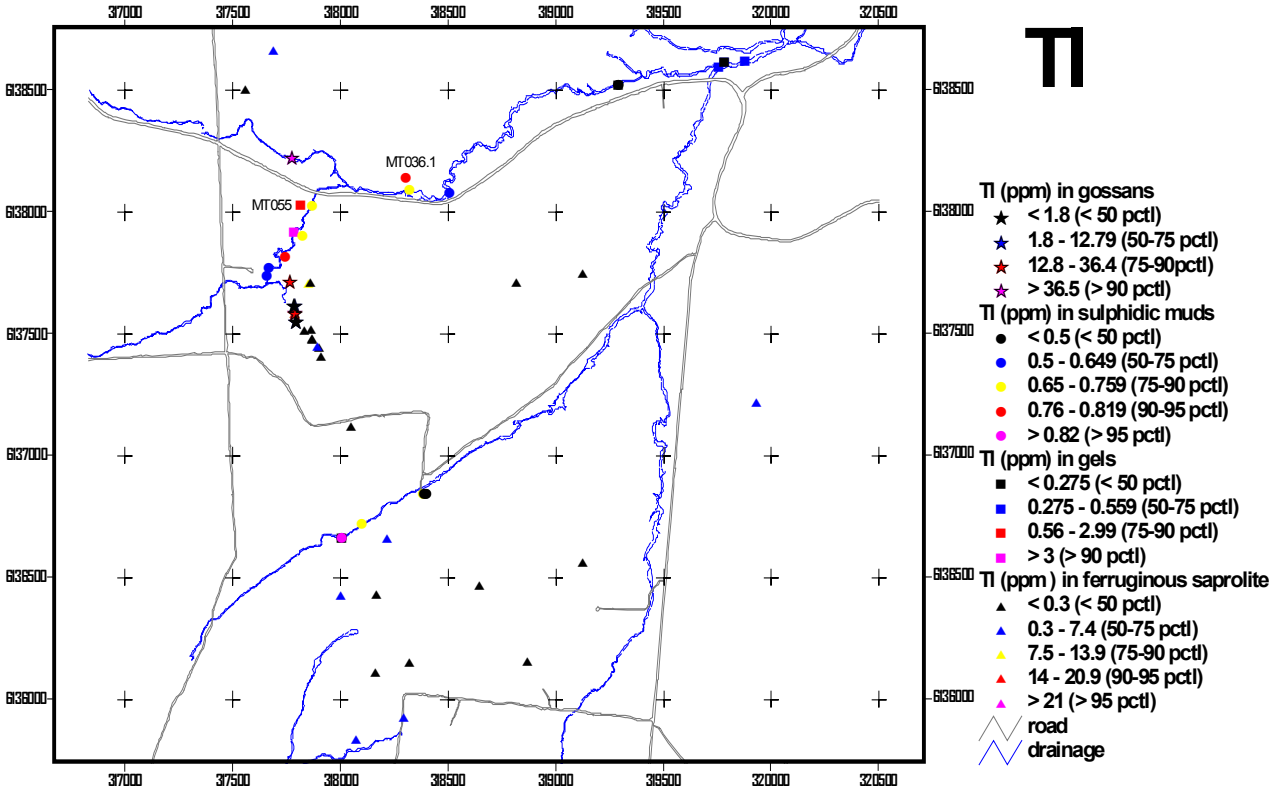

Figure 5.15. Distribution of Tl (ppm) in gossans, sulfidic mud, gels and ferruginous saprolite.

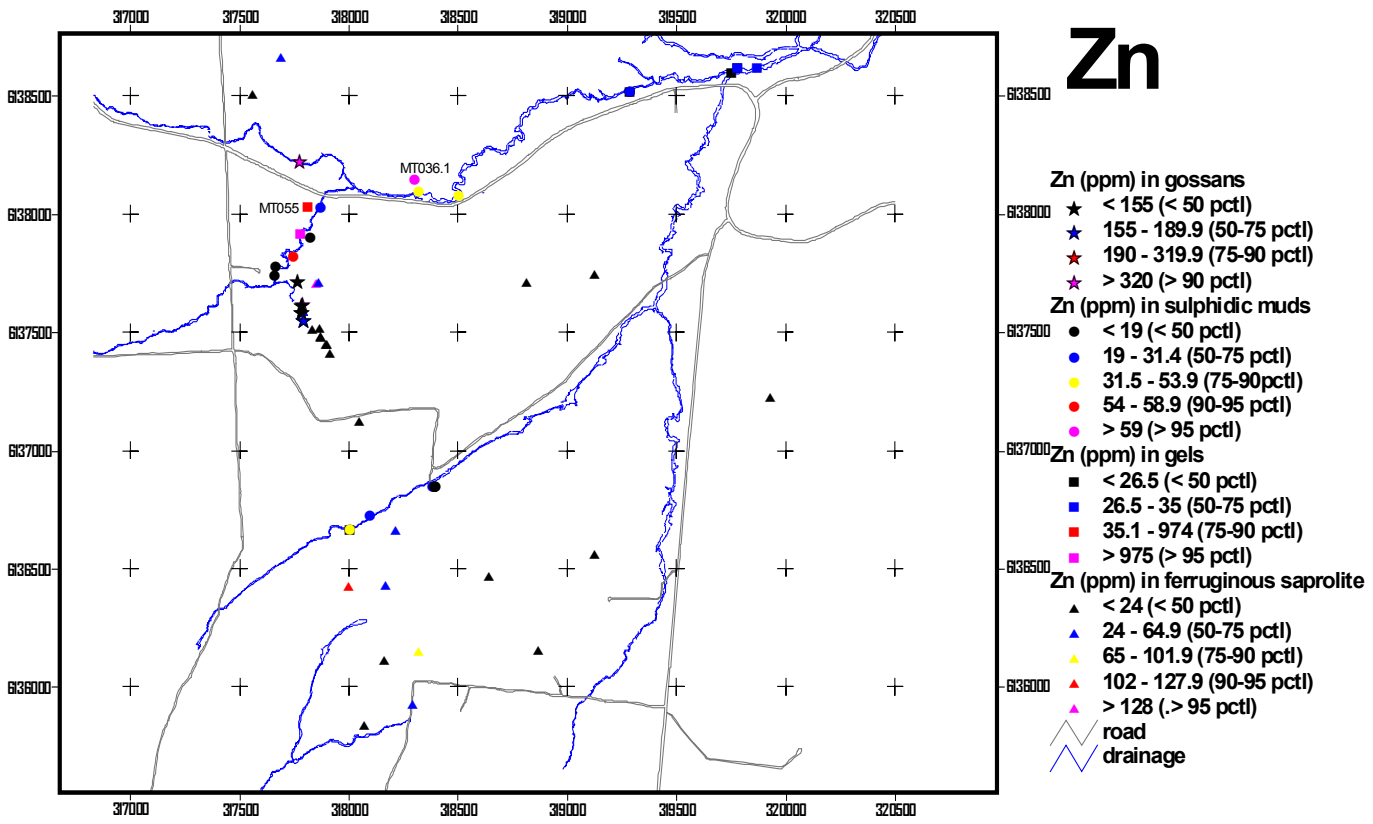

Figure 5.16. Distribution of Zn (ppm) in gossans, sulfidic mud, gels and ferruginous saprolite.

5.3.5 Geochemical signature of sulfidic materials overlying the mineralised zone

Comparison between the composition of black sulfidic materials (Figure 5.17) overlying the mineralised zone (site MT056) and those lateral to mineralisation (site W25; 400 m east) indicates that:

(i) greater concentrations of Al, Bi, Cd, Co, Cr, Cs, Cu, Ga, In, Mo, Nb, Ni, P, Pb, Rb, REE, Se, Sn, Th, Ti, Tl, V, Y and Zn occur in sulfidic materials overlying the mineralised zone;
(ii) greater concentrations of Ba, Ca, Mg, Mn, Na and Sr occur in sulfidic materials lateral to the mineralised zone;
(iii) concentrations of Ag, As, Au, Fe, Hf, K, S, Sb, Se, Te, U and W are similar in both instances.

No comparisons could be made for Cl, LOI, SiO_2 and Zr, since samples from site W25 were not analysed for these.

The concentrations of Bi, Cd, Cu, In, Mo, Pb, Tl and Zn in sulfidic materials at site MT056 reflect the dispersion halo above mineralisation, together with the occurrence of plumbojarosite (Figure 4.34) and plumbogummite. The relatively large concentrations of (i) Ca, Mg, Sr and Mn, (ii) Na, and (iii) Ba reflect the precipitation of magnesian calcite in a slightly alkaline, saline environment (pH 8.0-8.3; Bonifacio et al., 2002), halite and barite respectively in the wetland.

5.3.6 Composition of hardened crusts

Hardened crusts are derived from sulfidic materials through dehydration, oxidation and accumulation of Fe oxides with salts (such as halite, gypsum and calcite) leading to induration. The best studied example (Figure 4.37) is from Guthries (6141500N, 319800E), about 5 km to the northeast of the Herrmanns wetland (Fitzpatrick et al., 1996). The Guthries site is not known to be in a mineralised area, despite anomalous concentrations of Cu, Pb, U, Cd, Co, Ni, Tl and Ge in groundwater (Giblin et al., 1994).

The crust consists of four chemically distinct layers (Figure 5.18):

(i) hard crust, 0-0.3 cm; greatest concentrations of Ca, Cd, Fe, Mg, Na, P, REE, S, U and Zn; lowest concentrations of Ag, Al, Bi, Cr, Cs, Cu, Ga, Hf, K, Mo, Nb, Ni, Pb, Rb, Sb, Sn, Te, Th, Ti, Tl and W;
(ii) grey-brown bleached layer, 0.3-2.4 cm; greatest concentrations of Ag, Cr, Cs, Ti and W;
(iii) layer with orange-brown ferruginous mottling, 2.4-4.4 cm; greatest concentrations of Se;
(iv) grey bleached layer, 4.4-8 cm; greatest concentrations of Al, As, Au, Bi, Cu, Ga, Mn, Mo, Rb and Sn.

The concentrations of Ba, In, SiO_2 and V are similar in each layer.

The composition of each layer in the crust appears to reflect the influence of secondary processes (such as salinisation and precipitation of Fe oxides), as indicated by the concentration of elements such as Ca, Fe, Na and S in the surface layer. It is likely that the distribution of the other elements may also be dependent on the nature of secondary processes. Despite the occurrence of minerals such as schwertmannite and ferrihydrite, there appears to have been no scavenging of elements such as Pb by these Fe-rich minerals, neither in the surface crust nor in the mottled layer. This suggests that schwertmannite and ferrihydrite will only accumulate metals where there is an anomalous source (e.g., mineralisation). Consequently, discrimination between mineralised and barren occurrences is possible, although further work is required.

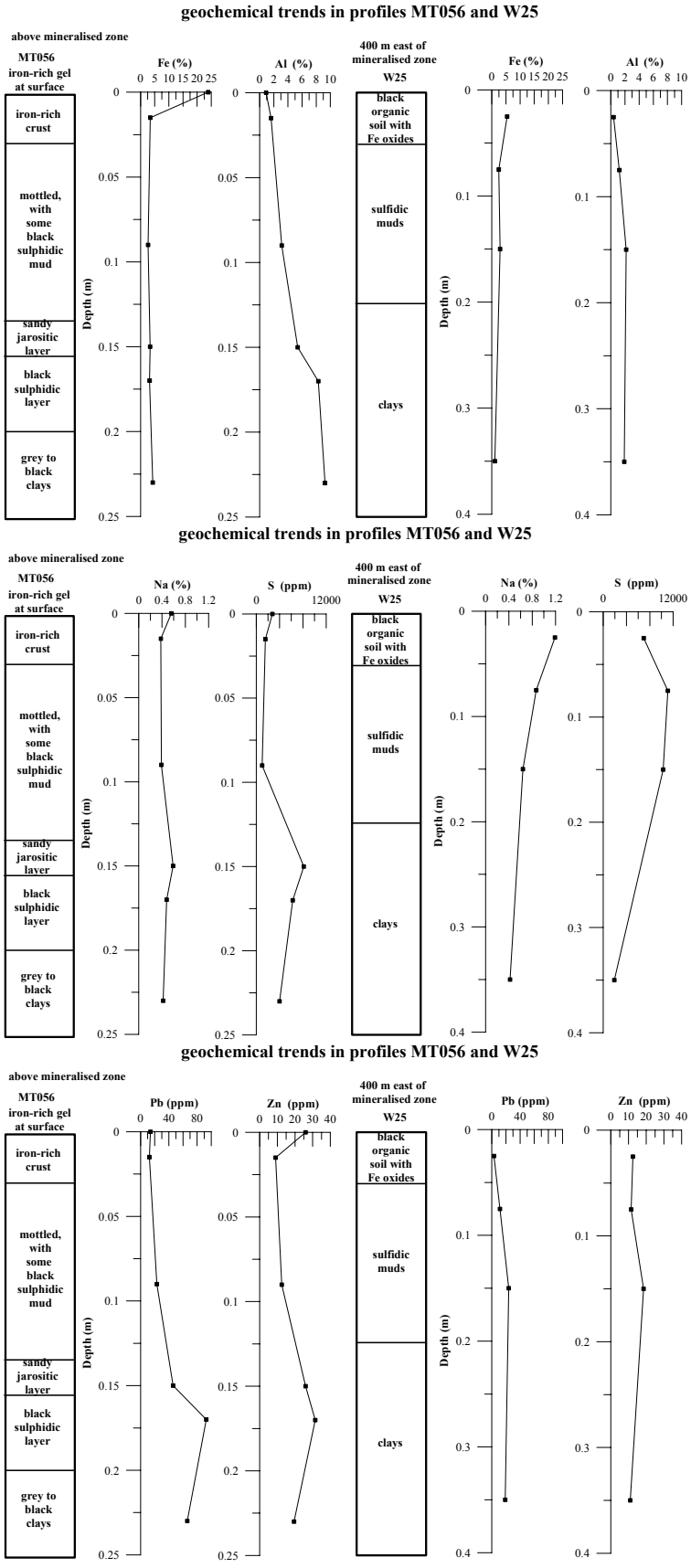

Figure 5.17. Distribution of Fe, Al, Na, S, Pb and Zn in sulfidic muds overlying the mineralised zone (MT056) and lateral to it (W25).

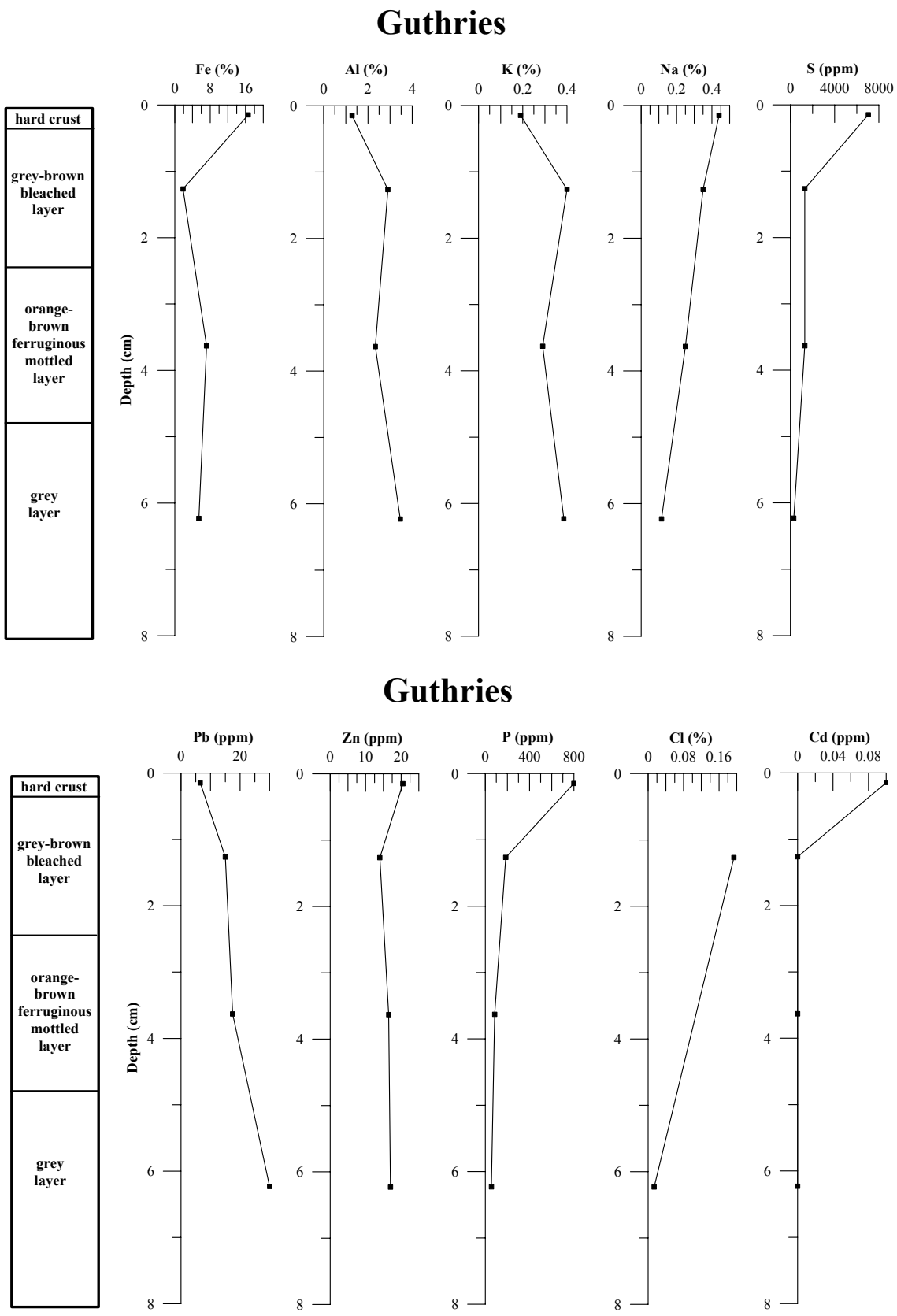

Figure 5.18. Vertical variations in the distribution of selected elements through the crust developed from acid sulfate soil and shown in Figure 4.37, Guthries.

5.3.7 Mass balance calculations for the profile through the Nairne Pyrite Member, diamond drill hole MTG2

Mass balance calculations (using the method of Gresens (1967)) were carried out on the profile extending from fresh bedrock into regolith in diamond drill hole MTG2. The results are shown in Appendix 9; selected results are shown in Figure 5.19. The following trends occur:

(i) elements depleted in the regolith profile relative to fresh bedrock: Al, Ca, Cd, Cl, Co, Cs, In, Mg, Mn, Na, Ni, P, REE (except Ce), S, Sr, U, Y and Zn;
(ii) elements enriched in the regolith profile relative to fresh bedrock: As, Bi, Fe, Hf, Mo, Pb and V;
(iii) elements depleted in the regolith profile relative to fresh bedrock, but enriched around the weathering front: Au, Rb and Tl;
(iv) elements with irregular patterns or no clear average variation: Ag, Ba, Ce, Cr, Cu, Ga, K, Sb, Si, Sn, Te, Th and W; Nb, Se and Ti belong to this group but show distinct near-surface enrichments.

5.3.8 Discussion

The residual nature of the regolith and outcrop of the mineralised zone (as gossan) present no obstacle to conventional sampling (soils, stream sediments, rock chips) and the mineralised zone can be delineated by many elements, e.g., Ag, Bi, Mo, Pb, Sb, Tl (Table 5.1).

The composition of the black sulfidic muds (including sulfuric horizons) and gels suggests that certain elements (As, Ba, Cd, Cu, P, Pb, Sn Tl and Zn) are indicative of mineralisation, due to co-precipitation of these elements from groundwater with Fe sulfides/oxides (Table 5.1). At a prospect scale, a geochemical dispersion halo up to 750 m in width occurs around the mineralised zone, compared to up to 200 m for soils and up to 700 m for stream sediments.

Sulfidic materials (from acid sulfate soils) and Fe and Al oxide gels from seeps are useful sampling media where mineralisation is blind or buried beneath cover. The occurrence of plumbojarosite and plumbogummite in sulfuric horizons may be indicative of underlying Pb mineralisation, as at site MT056.

It is unclear whether hardened crusts are a potentially suitable sampling medium. Further work is required to determine which layer, if any, will provide the best results.

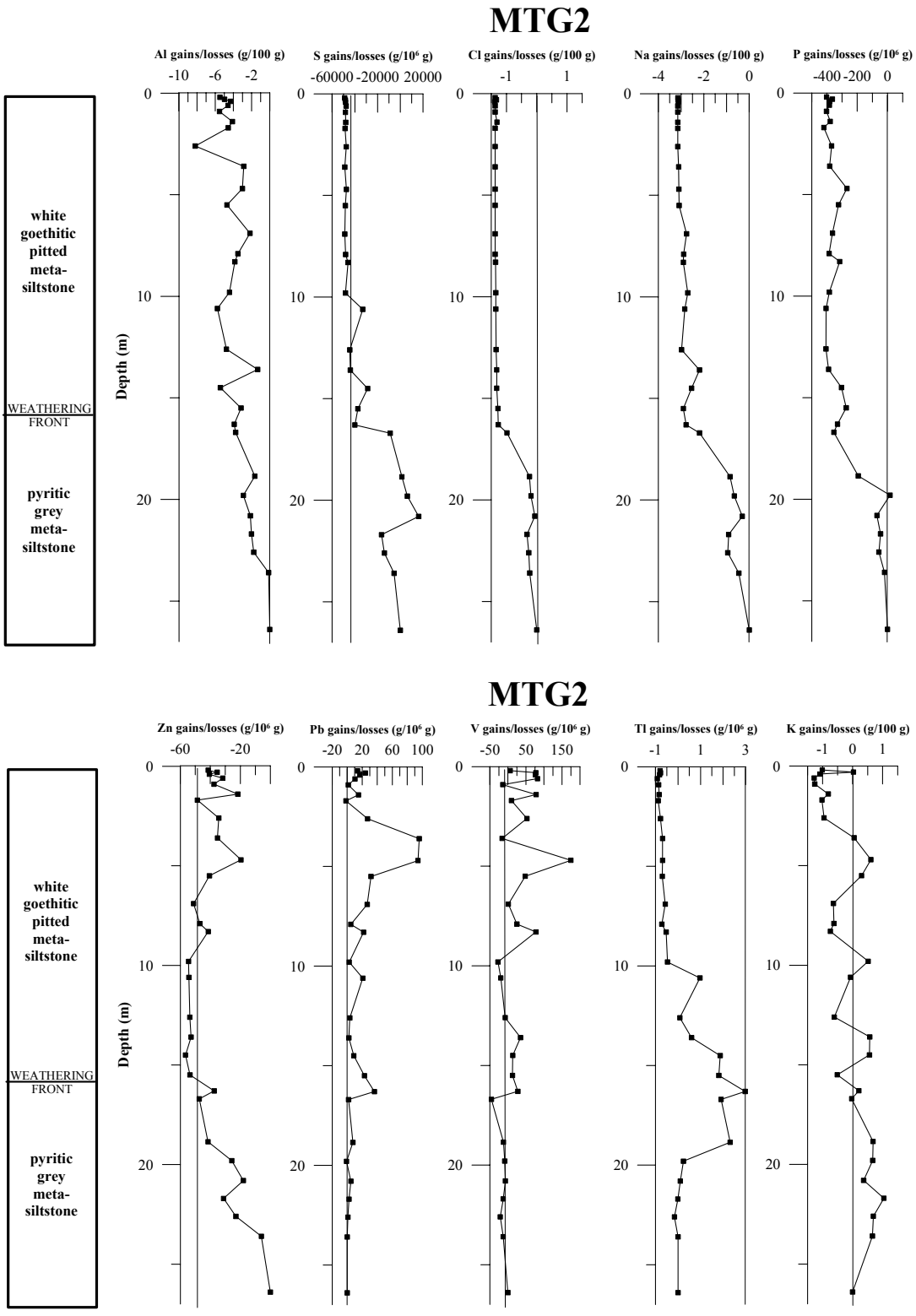

Figure 5.19. Graphical display of mass balance calculations for selected elements, diamond drill hole MTG2.

Table 5.1. Summary of geochemical indicators and dispersion characteristics of various regolith types (Skwarnecki & Fitzpatrick, submitted).

Sample medium	*Indicator elements*	*Analytical methods*	*Detection limits*	*Background (50th percentile)*	*Threshold (90th percentile)*	*Maximum anomaly*	*Dispersion distance (m)*
Primary mineralisation	Ag, Cu, Pb, Zn (As, Bi, Cd, Mn, Mo, Sb, Tl)[1]	probably AAS, digestion unknown (ICP-MS/ICP-OES, mixed acid digest)	Ag 1, Cu 2, Pb 5, Zn 5	Ag <1, Cu 45, Pb 24, Zn 75	Ag <1, Cu 217, Pb 467, Zn 430	Ag 63, Cu 1.7 %, Pb 14.2 %, Zn 7.7 % (As 600, Bi 10, Cd 1950, Mn 4900, Mo 24, Sb 10, Tl 88)[1]	anomalous concentrations restricted to ore zones (<10)
Gossans	Ag, As, Au, Bi, Cu, Mo, Pb, S, Sb, Se, Tl, U, Zn	Au: AAS, graphite furnace, on aqua regia digest; other elements: ICP-MS/ICP-OES, on mixed acid digest	Ag 0.1, As 0.5, Au 1 ppb, Bi 0.1, Cu 2, Mo 0.1, Pb 0.5, S 50, Sb 0.5, Se 0.5, Tl 0.1, U 0.02, Zn 0.5	Ag 39, As 440, Au 8 ppb, Bi 2.8, Cu 2500, Mo 79, Pb 1400, S 1900, Sb 1.25, Se 4, Tl 1.8, U 4.5, Zn 155	Ag 81, As 1200, Au 12.5 ppb, Bi 7.5, Cu 5050, Mo 125, Pb 2.82 %, S 3.72 %, Sb 10, Se 6.5, Tl 36.5, U 13, Zn 320	Ag 100, As 9900, Au 35.5 ppb, Bi 25.5, Cu 7250, Mo 270, Pb 24.3 %, S 6.01 %, Sb 36.5, Se 11.5, Tl 68, U 15.5, Zn 2100	anomalous concentrations restricted to the gossans (<10)
B/C horizon augered soil (bulk fraction)(CRAE)	Cu, Pb, Zn	probably AAS; digestion unknown	Cu 2, Pb 5, Zn 2	Cu 27.5, Pb 29.6, Zn 17.5	Cu 107.5, Pb 278, Zn 70.1	Cu 1220, Pb 1.61 %, Zn 1900	Cu 100, Pb 100, Zn 100
B horizon (<180 μm fraction) soil (ESSO)	As, Cu, Pb, Zn	probably AAS; digestion unknown	As 2, Cu 2, Pb 4, Zn 2	As 6.1, Cu 9.1, Pb 13.5, Zn 11.2	As 17.6, Cu 27.5, Pb 65.2, Zn 47.5	As 240, Cu 195, Pb 3500, Zn 260	As 100, Cu 150, Pb 200, Zn 100
Regional stream sediments (CRAE)	Cu, Pb, Zn	probably AAS; digestion unknown	Cu 2, Pb 20, Zn 5	Cu 7, Pb 28, Zn 15.5	Cu 30, Pb 54, Zn 35	Cu 200, Pb 2100, Zn 450	Cu 300, Pb 700, Zn 300
Groundwater[1]	Cu, Mo, Pb Zn	ICP-MS	Cu 0.2 ppb, Mo 0.2 ppb, Pb 0.2 ppb, Zn 0.2 ppb	insufficient data	insufficient data	Cu 130.6 ppb, Mo 4.2 ppb, Pb 59.9 ppb, Zn 1891 ppb	Cu 1000, Mo 1000, Pb 400, Zn 1000
Sulfidic muds[1] (this study)	As, Ba, Bi, Cd, Cu, P, Pb, Sn, Tl, Zn	ICP-MS/ICP-OES, on mixed acid digest	As 0.5, Ba 5, Bi 0.1, Cd 0.1, Cu 2, P 5, Pb 0.5, Sn 0.1, Tl 0.1, Zn 0.5	As 7.75, Ba 410, Bi 0.23, Cd <0.1, Cu 11, P 165, Pb 30, Sn 1.7, Tl 0.5, Zn 19	As 20.5, Ba 590, Bi 0.55, Cd 0.24, Cu 24, P 370, Pb 95, Sn 4, Tl 0.76, Zn 54	As 55, Ba 800, Bi 1, Cd 0.6, Cu 32, P 550, Pb 200, Sn 12, Tl 0.9, Zn 67	As 100, Ba 600, Bi 600, Cd 100, Cu 600, P 600, Pb 600, Sn 600, Tl 600, Zn 750
Ferruginous saprolite (this study)	Ag, As, Au, Bi, Cu, Mo, Pb, S, Sb, Se, Tl, U, Zn	Au: AAS, graphite furnace, on aqua regia digest; other elements: ICP-MS/ICP-OES, on mixed acid digest	Ag 0.1, As 0.5, Au 1 ppb, Bi 0.1, Cu 2, Mo 0.1, Pb 0.5, S 50, Sb 0.5, Se 0.5, Tl 0.1, U 0.02, Zn 0.5	Ag 0.26, As 70, Au 3.2 ppb, Bi 0.6, Cu 150, Mo 7.1, Pb 67, S 1300, Sb 0.8, Se 2.6, Tl 0.3, U 3, Zn 24	Ag 20, As 1300, Au 10.8 ppb, Bi 11, Cu 1070, Mo 70, Pb 1.12 %, S 4.8 %, Sb 10.1, Se 6.9, Tl 14, U 6.8, Zn 102	Ag 59, As 3100, Au 27.5 ppb, Bi 21.5, Cu 2150, Mo 230, Pb 3.35 %, S 8.04 %, Sb 33, Se 37.5, Tl 56, U 9.5, Zn 360	Ag 50, As 50, Au 50, Bi 30, Cu 50, Mo 60, Pb 50, S 50, Sb 60, Se 60, Tl 50, U, 50, Zn 50
Hardened crusts[1] (this study)	Ag, As, Bi, Mo, Pb, S, Se, Zn	ICP-MS/ICP-OES, on mixed acid digest	Ag 0.1, As 0.5, Bi 0.1, Mo 0.1, Pb 0.5, S 50, Se 0.5, Zn 0.5	Ag 0.22, As 26.5, Bi 0.21, Mo 1.8, Pb 16, S 1375, Se <0.5, Zn 17	Ag 0.5, As 60, Bi 0.6, Mo 3.2, Pb 110, S 7200, Se 1.6, Zn 60	Ag 1.7, As 77, Bi 1.5, Mo 5, Pb 240, S 2.34 %, Se 2.5, Zn 79	insufficient data
Fe and Al oxide gels[1] (this study)	As, Ba, Bi, Cd, P, Pb, Tl, Zn	ICP-MS/ICP-OES, on mixed acid digest	As 0.5, Ba 5, Bi 0.1, Cd 0.1, P 5, Pb 0.5, Tl 0.1, Zn 0.5	As 12, Ba 275, Bi <0.1, Cd 0.45, P 285, Pb 20.5, Tl 0.28, Zn 26.5	As 170, Ba 500, Bi 0.21, Cd 3, P 5000, Pb 35, Tl 2.5, Zn 1000	As 850, Ba 950, Bi 0.4, Cd 21, P 1.47 %, Pb 59, Tl 9.5, Zn 1200	As 250, Ba 50, Bi 70, Cd 70, P 70, Pb 70, Tl 70, Zn 70

all values in ppm except where stated

[1] based on very limited data

6. GEOCHEMICAL DISPERSION MODEL

The following model has been developed to explain the formation of inland acid sulfate soils and mineral precipitates in those catchments, which destroy land and water quality.

The saline groundwater is enriched in sulfate (SO_4^{2-}, Na^+, Mg^{2+}, AsO_4^{2-}, I^- and Cl^-), which can seep up through the soil, concentrates by evaporation and forms various mineral precipitates within and on top of the soil (Figure 6.1a). The combination of rising sulfate-rich groundwater, anaerobic conditions associated with saturated soils, agricultural activity and fractured rocks relatively enriched in Fe, S, Pb and Zn can lead to the formation of saline soils with potential (PASS) and actual acid sulfate (ASS) soil conditions (Fitzpatrick et al., 1996, 2000) and precipitation of anomalous concentrations of ore-related elements such as Pb and Zn. If the soil is wet and contains sufficient organic carbon, anaerobic bacteria use the oxygen associated with the sulfate (SO_4^{2-}) ions during the assimilation of carbon in organic matter. This process produces pyrite (FeS_2) and forms "sulfidic materials". Actual acid sulfate soils result when pugging from animals, drainage works or other disruptions expose the pyrite in the previously saturated soils to oxygen in the air. When this happens, pyrite is oxidised to sulfuric acid and various iron sulfate-rich minerals develop (Figure 6.1b). When sulfuric acid forms, the soil pH can drop from neutral to below 4; locally pH may attain values as low as 2.5 to form a "sulfuric horizon" (Figure 6.1b). The sulfuric acid dissolves the clay particles in soil, causing cations and associated anions (e.g. Na^+, Mg^{2+}, Ca^{2+}, Ba^{2+}, Cl^-, SO_4^{2-}, SiO_4^{4-}), trace elements, and metal ions such as Fe^{3+} and Al^{3+} to be released onto the soil surface and into stream waters (Figure 4.35).

The increased sodicity causes soils to become clogged with clay and mineral precipitates, so that they lose their permeability and groundcover. This prevents the groundwater below from discharging and ponding, with waterlogging extending laterally upslope (Figure 6.1b). Soil around the clogged area eventually erodes, releasing acid, metal ions and salts into waterways and dams; a new area of PASS then develops upslope or adjacent to the original ASS zone. If disturbance continues around the newly created PASS, the area affected continues to expand (Figure 6.1b). If these processes express on the surface of the soil, bare eroded saline scalds surrounding a core of slowly permeable, highly saline, eroded ASS result (Figure 6.1c). These saline landscapes are characterised by slimy red or white ooze and scalds with impermeable iron-rich crusts.

Incorporation of trace elements of economic interest into sulfidic materials renders these a useful sampling medium for mineral exploration. The secondary processes producing ASS redistribute these elements, leading to the precipitation of mineral phases such as plumbojarosite, and produce larger dispersion haloes around mineralised zones.

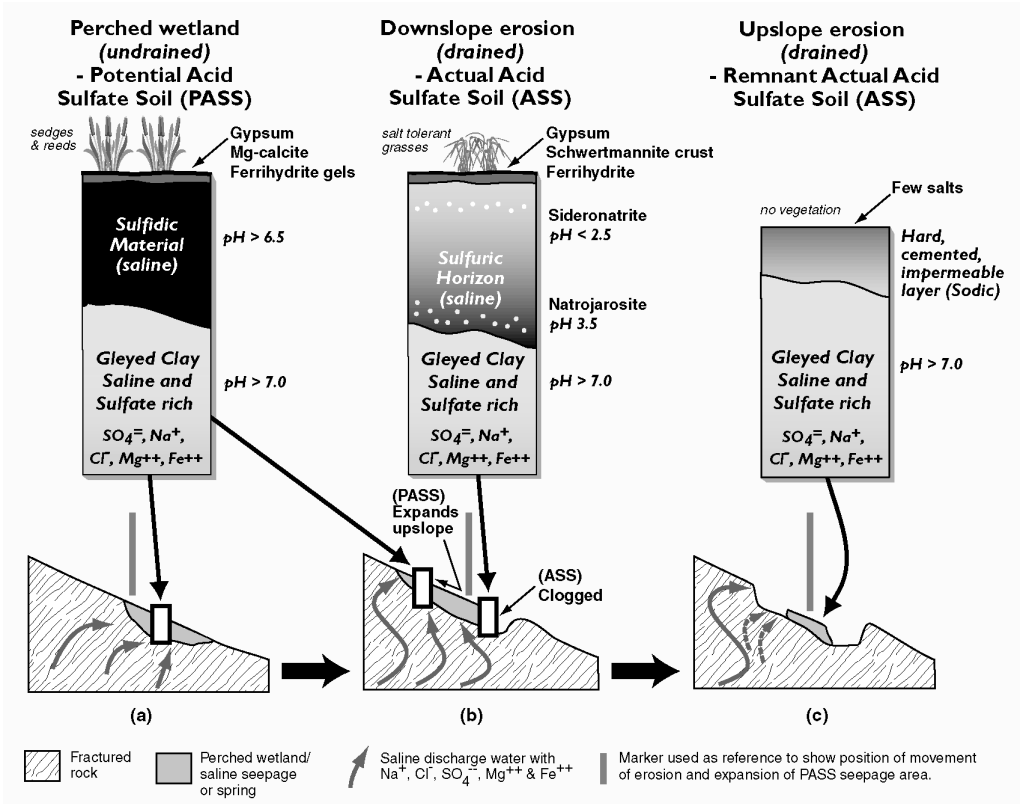

Figure 6.1. Schematic diagram showing the hydrogeochemical processes, which transform saline potential acid sulfate soil (PASS) in a perched wetland to a highly saline actual acid sulfate soils (ASS; modified from Fitzpatrick et al., 2000).

7. CONCLUSIONS

(1) Lead-zinc mineralisation in fresh bedrock is characterised by anomalous Ag, As, Cd, In, Mo, Pb, Sb, Te, Tl and Zn. The gossans also contain anomalous concentrations of these elements (except Cd and Zn, which have been leached), Cu, Se, U and W. Ferruginous saprolite and saprolite along the mineralised horizon are relatively enriched in As, Cu, Mo, Pb and Tl, compared to similar lateral regolith.

(2) The weathering products of sulfidic materials are sulfuric horizons with jarosite mottles, salt efflorescenses (e.g., sideronatrite and tamarugite), and Fe-rich and Al-rich precipitates (gels). Sulfuric horizons above the mineralised zone with secondary plumbojarosite and plumbogummite are characterised by greater Bi, Cd, Cu, In, Mo, Pb, Tl and Zn concentrations than those lateral to the mineralised zone. At a prospect scale, a dispersion halo up to 750 m in width occurs around the mineralisation and is defined by anomalous concentrations of As, Ba, Bi, Cd, Cu, P, Pb, Sn, Tl and Zn in Fe oxide gels and black sulfidic materials (and derived sulfuric horizons).

(3) Future investigations should focus on:

(i) mapping the distribution of acid sulfate soils and characterising their mineralogy and composition;
(ii) regional sampling of seeps, constrained by catchments and areas of known mineralisation, together with background areas with no known mineralisation, to provide a robust evaluation of the technique;

(iii) isotopic (Pb, S) and hydrogeochemical studies to better constrain the processes of acid sulfate soil formation and to provide tracers of the mineralisation, to follow-up the preliminary investigations of Giblin et al. (1994);
(iv) sampling seeps in prospective terrains where there is transported cover to determine whether mineralisation can be detected;
(v) evaluation of coastal acid sulfate soils as a potential sampling medium.

8. ACKNOWLEDGEMENTS

This research could not have been carried out without assistance from the following individuals:

Charles Butt – for his strong support of the project from its inception;
Richard Merry, Eleonora Bonifacio, Henry South – sampling in the field;
Henry South – sample preparation, production of fused borate discs (for XRF);
Greg Rinder and Bob Schuster – scanning diagrams and assistance with production of diagrams;
Stuart McClure – for assistance with the SEM and electron microprobe;
Tim McConachy (CSIRO Exploration & Mining, North Ryde) – pointing out the location of the gossans and general assistance in the field;
Keith Scott (CSIRO Exploration & Mining, North Ryde) – for locating diamond drill core for holes MTG2-4, assistance with sampling, and provision of old polished blocks;
Graham F. Taylor – for providing copies of open-file CRAE reports and general assistance in the field;
Andy Burtt and Justin Gum (PIRSA) – for assistance with the geology of the Kanmantoo and for providing technical information;
CRC LEME, CSIRO Mineral Exploration & mining sector (through Glass Earth), and Pima Mining NL - for providing financial assistance;
Charles Butt and Graham F. Taylor – for their review of the manuscript and suggestions for improvement.

REFERENCES

Belperio, A.P., Preiss, W.V., Fairclough, M.C., Gatehouse, C.G., Gum, J., Hough, J. & Burtt, A. (1998) Tectonic and metallogenic framework of the Cambrian Stansbury Basin – Kanmantoo Trough, South Australia. AGSO Journal of Australian Geology & Geophysics 17, no.3, p.183-200.

Bonifacio, E., Fitzpatrick, R.W., Merry, R.H., McClure, S.G., Raven, M.D. & Skwarnecki, M.S. (2002) Chemical and mineralogical properties of selected soils in the Adelaide Hills (SA). CSIRO Land & Water Technical Report (in preparation).

English, P.W. (1977) Progress report on the Mt Torrens and Pipeline prospects – Kanmantoo E.L. 257, South Australia. South Australia Department of Mines & Energy Open File Envelope No. 2838.

Fitzpatrick, R.W., E. Fritsch and P.G. Self (1996). Interpretation of soil features produced by ancient and modern processes in degraded landscapes: V Development of saline sulfidic features in non-tidal seepage areas. Geoderma 69, 1-29.

Fitzpatrick, R.W., Naidu, R. & Self, P.G. (1992) Iron deposits and microorganisms in saline sulfidic soils with altered soil water regimes in South Australia. Catena Supplement 21, 263-286.

Fitzpatrick, R.W., Raven, M., Self, P.G., McClure, S., Merry, R.H. & Skwarnecki, M.S. (2000) Sideronatrite in acid sulfate soils in the Mt Lofty Ranges: first occurrence, genesis and environmental significance. In: J.A. Adams & A.K. Metherell (eds) – Soil 2000: new horizons for a new century, Australian and New Zealand 2nd Joint Soils Conference, Volume 2, 109-110.

Fitzpatrick, R.W. & Self, P.G. (1997) Iron oxyhydroxides, sulfides and oxyhydroxysulfates as indicators of acid sulfate surface weathering environment. In: K.Auerswald, H. Stanjek & J.M. Bigham (eds) – Soils and environment: soil processes from mineral to landscape scale. Advances in GeoEcology 30, 227-240.

Fritsch, E., and Fitzpatrick, R.W. (1994). Interpretation of soil features produced by ancient and modern processes in degraded landscapes: I. A new method for constructing conceptual soil-water-landscape models. Australian Journal of Soil Research 32, 889-907.

Giblin, A.M., A.R. Carr, A.S. Andrew and D.J. Whitford (1994) Exploration of concealed mineralization: Multi-isotopic studies of groundwaters. AMIRA Project 388. Regional hydrogeochemistry of the Kanmantoo fold belt. CSIRO Exploration and Mining Report 14R. 22 pp.

Gresens, R.L. (1967) Composition-volume relationships of metasomatism. Chemical Geology 2, 47-65.

Scott, K.M., Horne, A.R. & Taylor, G.F. (1979) CSIRO-CRAE collaborative research project on ironstone characterization. 3. Mineralogy of surface and drill core samples from Mount Torrens, South Australia. CSIRO Division of Mineralogy, Restricted Investigation Report 1067.

Sibenaler, X.P. (1975) Geochemical exploration of the Mannum A 1:25 000 sheet. Department of Mines, South Australia, Report Book 75/18.

Skwarnecki, M.S. & Fitzpatrick, R.W. (submitted) Geochemical dispersion at the Mount Torrens prospect, South Australia. In: C.R.M. Butt, M. Cornelius & I.D.M. Robertson (eds) – Regolith expression of Australian ore systems. CRC LEME.

Soil Survey Staff (1999). Soil Taxonomy - a basic system of soil classification for making and interpreting soil surveys, Second Edition. United States Department of Agriculture, Natural Resources Conservation Service, USA Agriculture Handbook No. 436 pp 869.

Sylvester, G.C. (1978a) Preliminary report on gossan evaluation, Mt Torrens prospect, South Australia. CRAE Rept 9326.

Sylvester, G.C. (1978b) S.E.M. mineralogy of samples from profile drilling at Mt Torrens, South Australia. CRAE Rept 9439.

Toteff, S. (1999) Cambrian sediment-hosted exhalative base metal mineralisation, Kanmantoo Trough, South Australia. Geological Survey of South Australia, Report of Investigations 57.